The Need for Aerosol and Cloud Measurements from Space: Essential Contributions from a Rapid Reflight of the Aerosol Polarimetry Sensor

21 July 2011

Editors

Brian Cairns *NASA Goddard Institute for Space Studies*
Michael Mishchenko *NASA Goddard Institute for Space Studies*

Contributors

Andrew Ackerman *NASA Goddard Institute for Space Studies*
Mikhail Alexandrov *Columbia University*
Susanne Bauer *Columbia University*
Bryan Baum *University of Wisconsin/Madison*
Jacek Chowdhary *NASA Goddard Institute for Space Studies*
Peter Colarco *NASA Goddard Space Flight Center*
Oleg Dubovik *Université de Lille 1, CNRS*
Ann Fridlind *NASA Goddard Institute for Space Studies*
Igor Geogdzhayev *Columbia University*
Steven Ghan *Pacific Northwest National Laboratory*
James Hansen *NASA Goddard Institute for Space Studies*
Otto Hasekamp *SRON Netherlands Institute for Space Research*
Andre Hollstein *Free University/Berlin*
Chris Hostetler *NASA Langley Research Center*
Charles M. Ichoku *NASA Goddard Space Flight Center*
Kirk Knobelspiesse *NASA Goddard Institute for Space Studies*
Andrew Lacis *NASA Goddard Institute for Space Studies*
Istvan Laszlo *NOAA/NESDIS*
Li Liu *Columbia University*
Hal Maring *NASA Headquarters*
Ron Miller *NASA Goddard Institute for Space Studies*
Matteo Ottaviani *NASA Goddard Institute for Space Studies*
Carlos Pérez *Columbia University*
Jan Perlwitz *Columbia University*
Jens Redemann *NASA Ames Research Center*
Lorraine Remer *NASA Goddard Space Flight Center*
Thomas Ruhtz *Free University/Berlin*
Knut Stamnes *Stevens Institute of Technology*
Didier Tanré *Université de Lille 1, CNRS*
Larry Travis *NASA Goddard Institute for Space Studies*
Kostas Tsigaridis *Columbia University*
Bastiaan van Diedenhoven *Columbia University*
Apostolos Voulgarakis *Columbia University*
Andrzej P. Wasilewski *Sigma Space Partners*
Ellsworth J. Welton *NASA Goddard Space Flight Center*
Ping Yang *Texas A&M University*
Jianglong Zhang *University of North Dakota*

Contents

Front cover: images of aerosol and cloud fields over the Atlantic Ocean (top) and China (bottom) provided by the NASA Moderate Resolution Imaging Spectroradiometer.

Charge to the APS-2 Science Team and Review Panel

On 4 March 2011, the Aerosol Polarimetry Sensor (APS) was lost as a consequence of the failed launch of the Glory Mission. On 6 March 2011, Dr. Michael Freilich, Director of the Earth Science Division, Science Mission Directorate, NASA Headquarters, directed the Glory APS Science Team to perform a comprehensive study intended to develop and evaluate the science rationale for an APS reflight. This study was to be performed with the help of a panel of outside experts, and its results were to be summarized in the form of a white paper focusing on the following topics:

- What is the current state of the art and the uncertainties associated with estimates of aerosol radiative forcings based on existing satellite data and models?
- What are or will be the critical science questions concerning aerosol effects on the Earth system currently and extending to ~2020?
- What are the limitations of our current and confirmed space-borne aerosol observational capabilities to address these questions?
- Can an APS-2 sensor (a near-carbon copy of the Glory APS) add significantly to the aerosol retrieval capability of current satellite instruments and those expected to be launched before 2015?
- What are the gaps in our knowledge of aerosols that APS-2 would fill?
- What is the key aerosol and cloud information expected to be provided by APS-2 observations that can be used by process models and climate models to improve projections of changes in the Earth system?
- Can formation-flying enhance the ability of APS-2 to address these questions?
- What is the likely impact of postponement of an advanced aerosol polarimetry mission for ~10 years?

This document describes “The real problems to be solved, and how the APS-2 mission will advance the solution, making unique and essential contributions.”

Executive summary

Although the effect of tropospheric aerosols on the Earth system is believed to be nearly comparable to that of the greenhouse gases, it remains poorly quantified and represents one of the largest uncertainties regarding Earth-system change and its anthropogenic component. Addressing this problem requires an advanced space-borne polarimeter providing accurate global measurements of detailed aerosol properties.

Natural and man-made aerosols are essential constituents of the atmosphere affecting many physical and chemical processes as well as global climate and temperature. The Intergovernmental Panel on Climate Change's Fourth Assessment Report (IPCC-4) characterizes the current level of understanding of the direct and indirect aerosol radiative forcings as "medium–low" and "low", respectively. However, more recent studies indicate that the total direct forcing uncertainty can be a factor of $2-4$ greater than the value cited in IPCC-4. They also imply a substantial aerosol indirect forcing via cloud changes. The current uncertainties in the aerosol radiative effects are so large that they preclude definitive climate model evaluation by comparison with observed global temperature change. They also introduce large uncertainties in attributions of causes to observed Earth-system changes, and are in part responsible for differences in Earth-system forecasts. Continued failure to quantify the specific origins of the large aerosol forcings is untenable, as global knowledge of changing aerosol properties is needed to understand the mechanisms of changes in the Earth system.

Providing this critical knowledge was the main objective of the Aerosol Polarimetry Sensor (APS) on-board the Glory Mission authorized by NASA in 2005. The APS team devised a number of unique innovations to realize the requisite aerosol and cloud measurements. While there have been advances in space-based aerosol observation capabilities during the past decade, no other existing or confirmed satellite sensor can provide the measurements needed to significantly improve estimates of the aerosol radiative effects and their anthropogenic components. Pre-flight tests of the Glory APS, extensive sensitivity studies, and analyses of photopolarimetric data collected with an airborne prototype have led to an improved understanding of the expected retrieval capabilities of APS. They strongly indicate that, in conjunction with other ground-, air-, and space-based assets and advanced process and climate models, APS would have met its main objective. If launched successfully, it would have also demonstrated a methodology ideal for future long-term monitoring of atmospheric aerosols and their Earth-system effects.

Recent advances in the Earth-system science have intensified the need for accurate global observations of detailed aerosol properties from space. The unfortunate loss of the Glory APS delays delivery of these critical data. This instrument was conceived to address fundamental aerosol science questions with policy relevance. The science questions remain unanswered, while APS measurements are now viewed as essential in providing the scientific basis for climate policies currently under consideration.

Meeting the science and policy imperatives on the needed time scale can only be accomplished by launching an APS rebuild on a fast-track schedule that capitalizes on the project's assets and innovations and adds value to other space missions.

The critical needs that APS-2 would address include the following:

- global and regional monitoring of essential aerosol properties, including absorption, in clear-sky conditions as well as above and between clouds;
- detailed aerosol information needed for improvement and validation of process and climate models;
- global and regional monitoring of essential cloud properties, with particular sensitivity to cirrus clouds and cloud phase;
- aerosol and cloud data assimilation for operational use and model development;
- essential data for case/analysis type process studies;
- global and regional monitoring of stratospheric aerosols caused by major volcanic eruptions;
- refined aerosol and cloud representations for use by other operational satellite instruments.

The APS-2 Project has developed a rebuild schedule starting in August 2011 that would lead to launch as early as July 2015 and delivery of exploratory aerosol and cloud data products as soon as in the fall of 2015.

1. Introduction: tropospheric aerosols and their Earth-system effects

The state of the Earth system depends upon the delicate balance between incident solar radiation and the response of the atmosphere and surface via absorption, reflection, and re-radiation. Long-term variations in the composition of the atmosphere can disturb this balance and cause global Earth-system changes, thereby affecting local weather patterns that impact the quality of human life.

The composition of the atmosphere is influenced by both natural and anthropogenic factors, such as the byproducts of modern industrial societies. Over the past century the average temperature at the Earth's surface has increased by ~0.8°C (Hansen et al. 2010). Accurately attributing this increase and the concomitant Earth-system change to either natural events or anthropogenic sources is of primary importance to the establishment of scientifically and economically effective policies (Ramaswamy et al. 2001; Hansen et al. 2005; IPCC 2007; Chin et al. 2009a).

Natural and anthropogenic aerosols are important constituents of the atmosphere affecting local and global temperature, biogeochemical processes, and air quality (Ramanathan et al. 2001; Kaufman et al. 2002; Seinfeld and Pandis 2006). Although the radiative effects of tropospheric aerosols are believed to be nearly comparable to those of the greenhouse gases (GHGs) (such as carbon dioxide and methane), they remain poorly quantified and represent the largest uncertainty regarding climate change.

The GHG and aerosol radiative effects are exemplified by Fig. 1 taken from IPCC (2007). The radiative forcing due to the GHGs is well understood and accurately quantified. Its positive sign means that it contributes to global warming. Both at the surface and in the atmosphere, the forcing due to black carbon aerosols, via absorption of solar energy followed by re-radiation of the absorbed energy at infrared (IR) wavelengths, is also

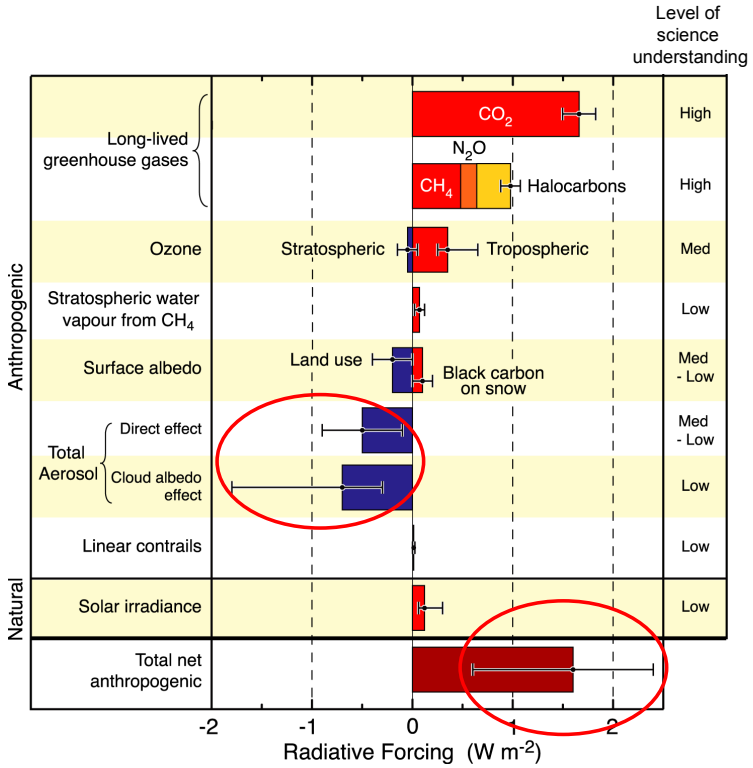

Figure 1. Global average radiative forcing estimates in 2005 together with the assessed level of scientific understanding. The bars show the respective ranges of model results included in the study. The net anthropogenic radiative forcing and its range are also shown (after IPCC 2007).

positive. Nonabsorbing aerosols, such as sulfates, reflect the Sun's radiation back to space and typically cause cooling. In addition to these direct interactions of aerosols with radiation, aerosols also affect radiation indirectly, which is believed to lead to net cooling, by modifying cloud radiative properties and lifetime as well as by modulating precipitation. The estimated magnitude of the total aerosol forcing from Fig. 1 is comparable (but opposite in sign) to that due to the GHGs. However, the spread of the aerosol-forcing model results is large and causes most of the spread in the sum of all climate forcings.

Although IPCC (2007) characterizes the current level of understanding of the direct and indirect aerosol effects as "medium–low" and "low", respectively, recent studies indicate that this assessment may be overly optimistic. For example, Loeb and Su (2010) conclude that the total direct aerosol radiative forcing (DARF) uncertainty from all aerosol parameters combined is $0.5-1.0\ \mathrm{W m^{-2}}$, a factor of $2-4$ greater than the value cited in IPCC-4 (Forster et al. 2007a; Solomon et al. 2007). According to Loeb and Su, DARF uncertainty in clear and cloudy sky (i.e., all-sky) conditions is greater than in clear-sky conditions, even though the global mean clear-sky DARF is more than twice as large as the all-sky DARF. Hansen et al. (2011) claim that most climate models mix heat too efficiently into the deep ocean and as a consequence underestimate the negative forcing by human-made aerosols. Hansen et al. infer the total aerosol radiative forcing to be $-1.6\pm0.3\ \mathrm{W m^{-2}}$, implying substantial aerosol indirect forcing via cloud changes. One should also recognize that fewer than one-third of the model studies included in IPCC-4 incorporated an aerosol indirect effect, and most considered only sulfates. Furthermore, the semi-direct effect (in which the heating by aerosol particles due to absorption of solar radiation results in a decrease of cloud amount; Hansen et al. 1997; Ackerman et al. 2000) is conspicuously absent in Fig. 1.

Hansen et al. (2011) conclude that

> continued failure to quantify the specific origins of the large aerosol forcings is untenable, as knowledge of changing aerosol effects is needed to understand future Earth-system change.

The analyses by Kiehl (2007), Loeb and Su (2010), Lohmann and Ferrachat (2010), and Penner et al. (2011) imply that the current uncertainties in the aerosol radiative forcings are so large that they preclude conclusive climate model evaluation by comparison with observed global temperature change. This also leads to large uncertainties in results that attribute cause to observed Earth-system change, and are in part responsible for differences in projections of future climate change.

The persistent uncertainties in our knowledge of aerosols and their effects must be reduced significantly for uncertainty in climate sensitivity to be adequately constrained (Schwartz 2004). Helping to address this challenging objective was the principal purpose of the APS instrument on-board the NASA Glory Mission (Mishchenko et al. 2007a).

The Glory APS was intended to revolutionize our understanding of tropospheric aerosols by achieving the following key science objectives:

- Determine the global distribution of the optical thickness and microphysical properties of natural and anthropogenic aerosols with substantially improved specificity and accuracy.

- Facilitate more accurate quantification of the aerosol direct and indirect radiative effects by providing key aerosol and cloud information required for the improvement and validation of process models and climate models.
- Provide better aerosol and cloud representations for use in various remote-sensing retrievals, thereby allowing improvements in aerosol and cloud assessments by other operational satellite instruments.

The Glory APS was designed to collect accurate multi-angle photopolarimetric measurements of the Earth along the satellite ground track over a broad visible and near-infrared spectral range, thereby providing aerosol property retrievals to levels of precision and accuracy heretofore unachievable. Furthermore, even though APS is not an imager, its global sampling would be sufficient in order to create the requisite climatology of aerosol and cloud microphysical properties as well as to facilitate process studies and operational data assimilation.

The failure of the Glory launch has prompted a reevaluation of the needs for advanced space-based measurements of aerosol and cloud microphysics. Our knowledge of tropospheric aerosols and our ability to model their properties as well as to measure them from space and *in situ* have evolved since the Glory Mission was authorized in 2005. We will make the case below that these new measurements and modeling studies reinforce the urgent need for the detailed and accurate measurements of aerosol and cloud properties from space that the Glory APS was designed to provide.

2. Aerosol properties required by chemical transport and climate models

During the past decade, significant advances have occurred in modeling atmospheric aerosols and climate. The models that participated in the IPCC's Third Assessment Report (IPCC-3) were developed in the late 1990s and typically included only sulfate aerosols and a fairly coarse resolution. Only the aerosol direct effect was accounted for, with the exceptions of few simplistic indirect effect calculations. The next generation of models that participated in IPCC-4 had finer resolution and included most major aerosol components; in some cases, they also featured more detailed treatments of aerosol indirect effects. However, most models calculated the aerosol indirect effect as a diagnostic only, without allowing aerosols to really affect clouds during the model simulations. This treatment excluded the calculation of the climate feedback of aerosols via the indirect effect. In addition, those models still involved significant simplifications: aerosols were considered externally mixed (i.e., each aerosol component was always pure and did not interact with the others), secondary organic aerosols were not included or were accounted for in a rather crude way, and aerosol size was fixed.

Since IPCC-4, the need for major advances in modeling aerosols and their interactions with radiation, clouds, and climate in general has been identified based on the recognition that aerosols are mixed, dynamically evolving populations and should be treated as such in models. To this end, global model parameterizations have been developed to take into account a number of processes (cf. Fig. 2):

- the complex behavior of semi-volatile secondary (i.e., created from emitted gases)

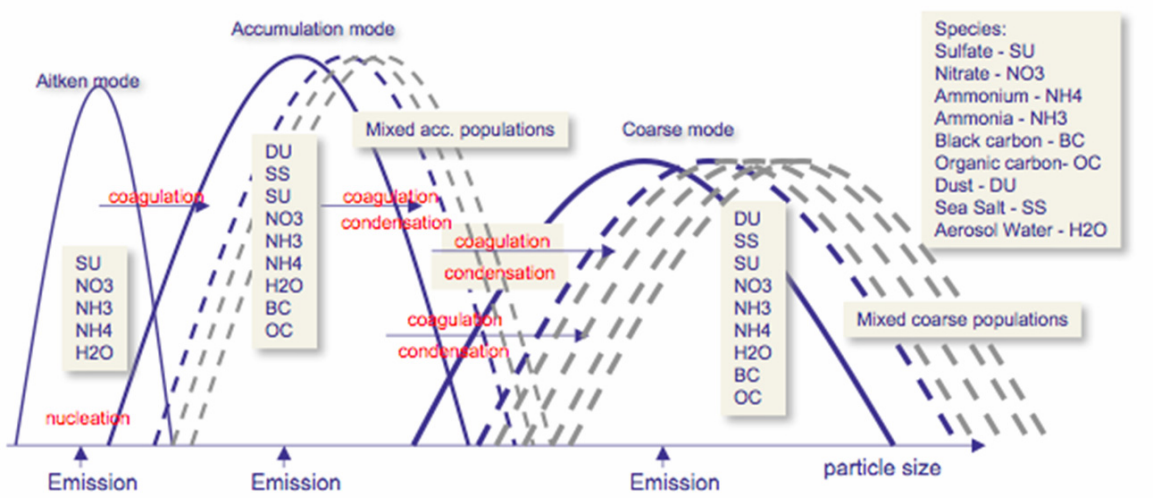

Figure 2. The aerosol microphysical model MATRIX (Bauer et al. 2008).

organic aerosols (e.g., Pankow 1994; Odum et al. 1996; Kanakidou et al. 2000; Chung and Seinfeld 2002; Tsigaridis and Kanakidou 2003);

- the semi-volatile nature of primary (i.e., emitted at the source) organic aerosols (Robinson et al. 2006; Pye and Seinfeld 2010; Jathar et al. 2011);
- the presence of organic compounds in sea-spray (O'Dowd et al. 2004, 2008; Keene et al. 2007; Spracklen et al. 2008; Vignati et al. 2010; Myriokefalitakis et al. 2010; Gantt et al. 2011);
- inorganic aerosol thermodynamics, which includes nitrate aerosol formation (e.g., Metzger et al., 2002; Fountoukis and Nenes 2007);
- the improvement of interactive dust emission schemes by introducing a size resolved parameterization of the dust emission flux physics (Shao et al. 2011) or a subgrid scale variability of surface winds that drive dust emissions (e.g., Cakmur et al. 2004; Miller et al. 2006);
- the aging of dust particles, which are altered by heterogeneous reactions on particles' surfaces through coating with sulfate or nitrate (e.g., Bauer et al. 2007);
- the explicit treatment of aerosol microphysics, which allows for the prognostic calculation of aerosol number, size, mass, and mixing state, as well as their evolution in time and space (e.g., Vignati et al. 2004; Ghan and Zaveri 2007; Bauer et al. 2008; Mann et al. 2010);
- the change of aerosol properties with time, including but not limited to the absorption enhancement due to mixing of black carbon with non-absorbing material (e.g., Bond and Bergstrom 2006; Bauer et al. 2010); the change of aerosol solubility and hygroscopicity, affecting their lifetime and aerosol-cloud interactions (e.g., Petters and Kreidenweis 2007); the aerosol formation in clouds (e.g., Ervens and Volkamer 2010; Myriokefalitakis et al. 2011); and the absorbing fraction of organic aerosols, also called brown carbon (e.g., Ramanathan et al. 2007);
- aerosol effects on formation of ice crystals by homogeneous and heterogeneous nucleation (Liu and Penner 2005; Liu et al. 2007c, 2009; Hoose and Lohmann 2008; DeMott et al. 2010).

The degree to which the above-mentioned processes are included in specific models that

will be used in the IPCC-5 study varies. Still very few global models contain detailed aerosol microphysics, but a significant number of them now include detailed secondary organic aerosol and inorganic thermodynamics parameterizations. It is anticipated that the models that will participate in IPCC-6 will include several of these parameterizations. This will be the time when APS-2 can be expected to be operational.

In order for the models to quantify the present-day aerosol radiative forcing, they should be able to accurately calculate both the aerosol distributions for the pre-industrial and present-day atmospheres, as well as the interactions of aerosols with radiation. To achieve that, a number of key outstanding issues must be addressed, as follows:

- Accurate knowledge of sources of different aerosol species: for both primary and secondary aerosols, their sources are expected to play a major role in defining their global distribution. Emission inventories are important, since they affect aerosol populations either directly, in the case of primary aerosols like sea-salt, dust, black carbon, and organic carbon, or indirectly, in the case of secondary aerosols such as sulfate, nitrate, ammonium, and organic carbon;
- Correct representation of aerosol transport and removal processes: the longer the lifetime of an aerosol population, the longer their effect on radiation and climate. The transport of aerosols and aerosol precursors both horizontally (e.g., dust plumes from the Sahara over the Atlantic Ocean to America; Prospero 1999) and vertically (e.g., in-cloud organic aerosol formation from ground-originated precursors; Sorooshian et al. 2007) influences the way radiation is distributed in the atmosphere. It can alter the top-of-the-atmosphere forcing and vertical distribution of heat as well as affect regional and global climate;
- Detailed and accurate knowledge of aerosol physical properties: wet deposition, the single most important removal process of aerosols from the atmosphere, primarily depends on aerosol hygroscopicity and size. Furthermore, hygroscopicity, in conjunction with aerosol size, affects cloud condensation nuclei, altering cloud formation. Aerosol size also defines the availability of aerosol surface susceptible for heterogeneous reactions, which alters the aerosols' hygroscopicity. Aerosol composition and size affect coagulation and condensation rates, which also lead to changes

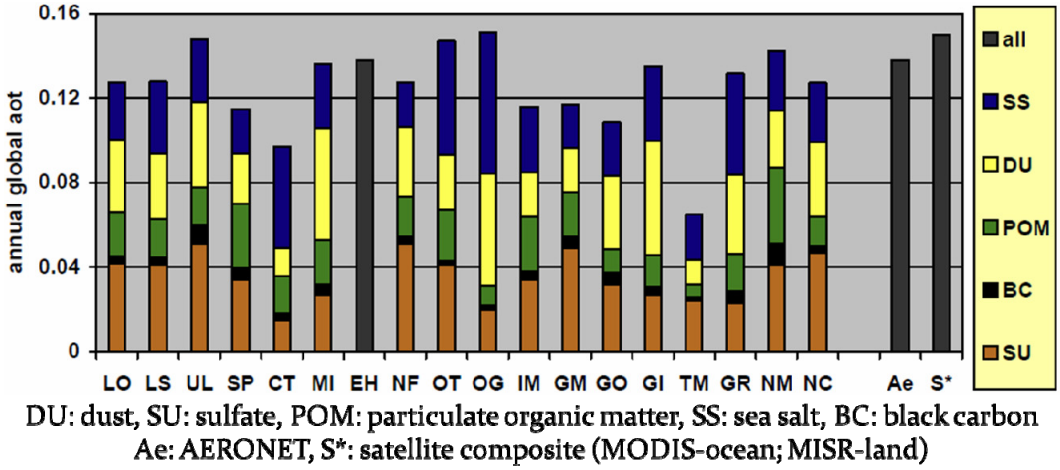

Figure 3. Contribution of different aerosol components to the total aerosol optical thickness, as calculated by different models (Kinne et al. 2006).

in aerosol population and properties, affecting aerosol lifetime and interaction with climate.

- After determining the aerosol spatiotemporal distribution, having sufficient knowledge of their optical properties allows the models to accurately quantify the interaction of aerosols with radiation and, thus, aerosol radiative forcing. The optical properties required for this calculation are functions of aerosol size, composition, shape, mixing state, and radiation wavelength.

Process and climate models do not yet tackle aerosol shape, an important factor determining their optical properties. The vast majority of models assume that aerosols are spherical, a fair assumption under most circumstances, except for two important cases: (i) freshly emitted black carbon particles, which tend to exist in the form of long fractals before eventually collapsing into compact particles that can be approximated by spheres (e.g., Abel et al. 2003; Lewis et al. 2009), and (ii) dust particles exhibiting expressly nonspherical shapes (Reid et al. 2003).

Although substantial knowledge has now been accumulated and included in process and climate models, important uncertainties still hinder our understanding of the effects of aerosols on the Earth system. In most cases, this is due to lack of sufficient data to evaluate, validate, and/or constrain the models.

Globally averaged measurements of column-integrated aerosol optical thickness (AOT) have almost universally been used as an overall gauge of model performance. However, the same global average of the cumulative AOT can be generated by different models for quite different mixtures of aerosol species (Fig. 3). This obviously indicates the urgent need to use detailed microphysical parameters of aerosols for testing, constraining, and improving the models (Schulz et al. 2006). It is especially important to measure aerosol characteristics that can be used to test model parameterizations of various stages of aero-

Table 1. Essential processes and aerosol properties versus current validation/constraint data sources for models

Process/property	Validation/constraint	Process/property	Validation/constraint
Sources (mass/size), load	*In situ* data	Particle shape	Lab, *in situ* data, satellites[2]
Surface concentration, vertical profile	CALIOP,[1,2] *in situ* data	Effective radius, effective variance	AERONET, satellites[2]
Transport, processing	*In situ* data, Lab	Aerosol optical thickness	AERONET, satellites
Dry/wet removal	*In situ* data	Single-scattering albedo	AERONET, satellites[2]
Number concentration, size distribution	AERONET, *in situ* data	Asymmetry parameter	AERONET
Mixing state	*In situ* data, Lab	Refractive index	*In situ* data, Lab

[1]Cloud–Aerosol Lidar with Orthogonal Polarisation
[2]Limited (sometimes qualitative or semi-quantitative) information

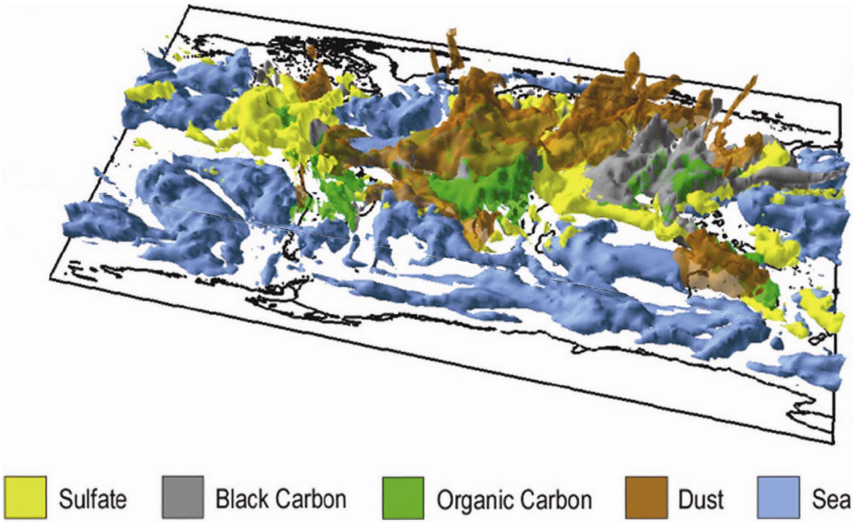

Figure 4. An example of modeling the prevailing aerosol composition on the global scale (Stier 2005). Areas around the borders of different colors have a very mixed aerosol distribution, while no color means very low aerosol load.

sol emission, processing, and transport rather than just the final derivative output in the form of the total AOT (Table 1).

Some of this information is available from ground-based AErosol RObotic NETwork (AERONET) observations (Holben et al. 1998; Dubovik et al. 2002) and has already been used by transport and climate modelers (e.g., Chin et al. 2009b; Colarco et al. 2010). However, the distribution of AERONET stations is highly non-uniform, with virtually no data over the oceans, while the number of AERONET stations is quite inadequate. These factors limit the usefulness of AERONET observations in studies of highly non-uniform and heterogeneous aerosol distributions (cf. Fig. 4). Furthermore, AERONET can provide microphysical aerosol retrievals only in clear-sky conditions. It is, therefore, imperative to have an alternative, space-based means of measuring accurate and detailed aerosol characteristics with uniform, global, and sufficiently dense sampling that extend and improve on the existing characterization of aerosols from space.

3. Summary of aerosol and cloud retrieval requirements

The formulation of a minimum set of retrieval requirements for a space mission is a mandatory and often difficult procedure. Given the great complexity and the multifaceted nature of the aerosol problem considered here, the list of desirable aerosol and cloud properties can be quite long. At the same time, the retrieval capability of any space instrument is inherently limited by the physical nature of the specific measurement methodology and by the varying complexity of actual terrestrial scenes viewed by the instrument. It is, therefore, necessary to seek a balanced approach by ensuring that the final list of retrieval requirements will lead to a significant and necessary improvement in our knowledge of the Earth system while calling for a reasonably affordable and feasible instrument.

There are two general classes of satellite instruments for aerosol and cloud remote sensing. Passive instruments measure the reflected solar or terrestrially emitted thermal radiation. Active instruments rely on an artificial source of illumination, such as a laser or a transmitting antenna. Since passive and active instruments have complementary capabilities, a future comprehensive aerosol–cloud space mission should include instruments of both types. This is planned indeed for the Aerosol–Cloud–Ecosystems (ACE) Decadal

Survey Mission (Earth Science 2007) currently considered for launch after 2020. The following discussion will be limited to passive techniques and will focus on the retrieval strategy and instrument design that help maximize the information content of a passive remote-sensing observation.

The minimum set of retrieval requirements for the Glory APS was formulated and discussed by Mishchenko et al. (2004, 2007a). It is based on the overall objective of creating an advanced global climatology of detailed aerosol and cloud properties that would serve the urgent needs of the modeling and climate communities as discussed in the preceding sections. This set of requirements was largely adopted by the ACE formulation team and is outlined below.

The left-hand panel of Fig. 5 summarizes the overall scientific objectives of a coordinated and systematic approach for dramatically improving our understanding of aerosol Earth-system impacts and environmental interactions (Seinfeld et al. 1996, 2004). To achieve these objectives, advanced models coupled with a comprehensive set of accurate constraints in the form of *in situ* measured and remotely retrieved aerosol and cloud distributions and properties are needed. Accordingly, the right-hand panel of Fig. 5 lists the minimum set of aerosol and cloud parameters required of a passive satellite instrument to facilitate the global quantification of the direct and indirect aerosol effects.

Specifically, aerosol properties essential for constraining the direct forcing include the total column AOT and average column values of the effective radius and effective variance, the real part of the refractive index, and the single-scattering albedo (SSA). The effective radius has the dimension of length and provides a measure of the average particle size, whereas the dimensionless effective variance characterizes the width of the size distribution (Hansen and Travis 1974). Since, apart from the undetectable Aitken mode, the aerosol population is typically bimodal (e.g., Dubovik et al. 2002; Maring et al. 2003), all of these parameters must be determined for each mode. The refractive index must be determined at multiple wavelengths in a wide spectral range, e.g., 400–2200 nm, since this is the only means of constraining aerosol chemical composition from space (Mishchenko et al. 2007a). An integral part of the retrieval procedure must be the detec-

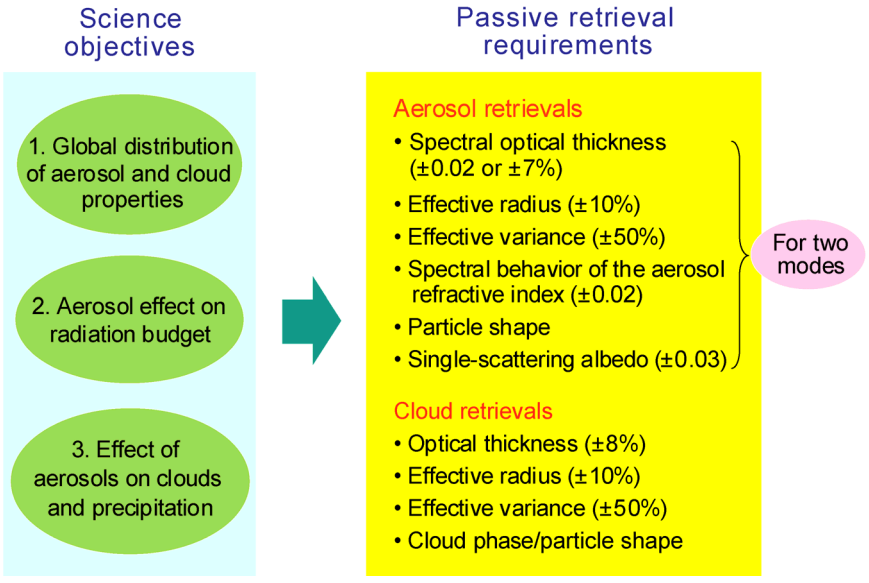

Figure 5. Flowdown of science objectives into specific retrieval requirements for a passive aerosol/cloud satellite instrument.

tion of nonspherical aerosols such as dust-like and soot particles because, if ignored, nonsphericity can significantly affect the results of AOT, refractive index, and size retrievals (e.g., Dubovik et al. 2006).

The aerosol effect on liquid-cloud albedo can be better constrained in models by means of long-term global measurements of the number concentration of aerosol particles, which act as cloud condensation nuclei (CCN), and cloud albedo. Other measurable cloud properties impacted by atmospheric aerosols include cloud droplet size and number concentration and liquid water path (Lohmann and Feichter 2005). Since the droplet generation efficiency of aerosols depends on their size and hygroscopicity, the measurement of aerosol number concentration must be accompanied by the determination of aerosol effective radius and chemical composition.

The respective minimum retrieval requirements (see the right-hand panel of Fig. 5) include the column cloud optical thickness and the average column cloud droplet size distribution as well as the column AOT and the average column values of the effective radius and effective variance of the aerosol size distribution and the real part of the aerosol refractive index for each mode of a bimodal aerosol population. Note that the cloud and aerosol particle number concentrations are derivative rather than retrieved quantities, i.e., are deduced from the column optical thickness and the particle extinction cross section (a function of particle size distribution, refractive index, and shape). The accuracy with which the number concentrations must be determined is very difficult to achieve and necessitates the retrieval of the cloud droplet and aerosol size distributions and the aerosol refractive index with high precision. Assuming rather than retrieving the effective variance of the cloud droplet and aerosol size distributions and the aerosol refractive index can lead to even larger errors in the retrieved number concentrations (Boers et al 2006).

To improve our understanding of aerosol effects on ice clouds and the associated radiative forcing, accurate retrievals of ice cloud optical thickness as well as ice crystal sizes and shapes are needed (Stackhouse and Stephens 1991; Fu 2007; Baran 2009; Baum et al. 2011). Current satellite retrievals of ice cloud optical thickness and particle size encounter difficulties in determining cloud top thermodynamic phase at temperatures between −40°C and 0°C (Nasiri and Kahn 2008) and uncertainties in ice crystal morphology (Zhang et al. 2009a; Baum et al. 2011). Aerosols are known to be a factor controlling ice crystal sizes and ice water paths, although the predominant physical processes remain poorly characterized (e.g., Fridlind et al. 2004; Lohmann and Feichter 2005; Fan et al. 2008; deMott et al. 2010). Estimates of the global distribution of aerosols that are capable of acting as heterogeneous ice nuclei would greatly improve our understanding of aerosol effects on ice-containing clouds. Since ice nuclei are found to be preferentially larger than 0.5 μm in diameter and non-spherical (e.g., Rogers et al. 2001; deMott et al. 2010), accurate retrieval of aerosol size and shape, as well as chemical composition, would provide key constraints on model representation of aerosol effects on cold clouds.

The criteria for specifying the corresponding measurement accuracy requirements detailed in Appendix A are based on the requisite ability to detect plausible changes of the aerosol radiative forcing estimated to be possible during the next 20 years and to determine quantitatively the contribution of this forcing to the planetary energy balance. A significant global mean flux change can be defined as 0.25 $\mathrm{W\,m^{-2}}$ or greater based on the consideration that anticipated increases of GHGs during the next 20 years will cause a forcing of about 1 $\mathrm{W\,m^{-2}}$ (Hansen et al. 1995).

The estimated plausible 20-year change of the global mean AOT is 0.04 (based on projections of SO_2 and black carbon emissions; e.g., Nakićenović and Swart 2000; Pham et al. 2005), whereas the global mean AOT change required to yield the 0.25 Wm^{-2} flux change is 0.01 (Hansen et al. 1995). These numbers justify the proposed threshold accuracy and precision for the AOT measurement.

The accuracy and precision indicated for the aerosol size distribution measurement are dictated in large part by the requirement to determine the aerosol number concentration with a high accuracy facilitating the detection of the effect of increasing CCN concentration on cloud properties (Schwartz and Slingo 1996; Fridlind and Ackerman 2011). The strong dependence of the extinction cross section on the effective radius and effective variance makes the determination of aerosol number concentration very difficult and necessitates high-accuracy retrievals of the size distribution (Mishchenko et al. 1997a; Feingold 2003). Accurate retrievals of the aerosol particle size are also needed to determine the cloud condensation efficiency of aerosols (Rosenfeld 2006).

The SSA accuracy and precision criteria follow from the modeling analysis of the aerosol radiative forcing by Hansen et al. (1997). The measurement accuracy and precision indicated for the real part of the aerosol refractive index are determined by the need to infer aerosol chemical composition based on expected differences between refractive indices typical of relevant chemical species. Chemical speciation is required to identify hygroscopic aerosols, discriminate between natural and anthropogenic aerosol components, and estimate the imaginary part of the refractive index to provide an independent check on the retrieved SSA.

The measurement accuracy and precision for the cloud particle size distribution are dictated by the need to detect a flux change of 0.25 Wm^{-2} or greater (Hansen et al. 1995) as well as detect a change of cloud particle size and number concentration caused by increasing CCN concentrations.

4. Capabilities and limitations of current space-borne aerosol retrievals

Table 2 taken from Yu et al. (2009) summarizes the existing satellite instruments used for aerosol retrievals and the respective data products. The majority of these sensors rely on sunlight as the source of illumination and, thus, belong to the category of passive instruments. As such, they have limited (or no) sensitivity to the vertical distribution of aerosols. Vertically resolved measurements are provided by active instruments such as the Geoscience Laser Altimeter System (GLAS; Spinhirne et al. 2005) and CALIOP (Winker et al. 2010).

Over the past decade, passive satellite retrievals of tropospheric aerosols have become increasingly sophisticated (Kokhanovsky and de Leeuw 2009; Tanré 2010). Until ~2000, the only aerosol climatologies available were those derived from relatively limited Advanced Very High Resolution Radiometer (AVHRR) and Total Ozone Mapping Spectrometer (TOMS) observations (Higurashi and Nakajima 1999; Torres et al. 2002a; Mishchenko et al. 2007b; Zhao et al. 2008). Now there are satellite instruments that measure the angular dependence of reflected radiance and even polarization at multiple wavelengths from ultraviolet (UV) through IR with finer spatial resolution. From these observations, the retrieved aerosol products include not only the AOT at one wavelength, but also spectral AOT values and some information about particle size over both ocean

Table 2. Summary of major satellite measurements currently available for tropospheric aerosol characterization and radiative forcing research

Category	Properties	Sensor/platform	Parameters	Spatial coverage	Temporal coverage
Column-integrated	Loading	AVHRR/NOAA-series	optical depth	~daily coverage of global ocean	1981-present
		TOMS/Nimbus, ADEOS1, EP		~daily coverage of global land and ocean	1979-2001
		POLDER-1, -2, PARASOL			1997-present
		MODIS/Terra, Aqua			2000-present (Terra) 2002-present (Aqua)
		MISR/Terra		~weekly coverage of global land and ocean, including bright desert and nadir sun-glint	2000-present
		OMI/Aura		~daily coverage of global land and ocean	2005-present
	Size, shape	AVHRR/NOAA-series	Ångström exponent	global ocean	1981-present
		POLDER-1, -2, PARASOL	fine-mode fraction, Ångström exponent, non-spherical fraction	global land+ocean	1997-present
		MODIS/Terra, Aqua	fine-mode fraction	global land+ocean (better quality over ocean)	2000-present (Terra) 2002-present (Aqua)
			Ångström exponent		
			effective radius	global ocean	
			asymmetry factor		
		MISR/Terra	Ångström exponent, small, medium, large fractions, non-spherical fraction	global land+ocean	2000-present
	Absorption	TOMS/Nimbus, ADEOS1, EP	absorbing aerosol index, single-scattering albedo, absorbing optical depth	global land+ocean	1979-2001
		OMI/Aura			2005-present
		MISR/Terra	single-scattering albedo (2-4 bins)		2000-present
Vertical-resolved	Loading, size, and shape	GLAS/ICESat	extinction/backscatter	global land+ocean, 16-day repeating cycle, single-nadir measurement	2003-present (~3months/year)
		CALIOP/CALIPSO	extinction/backscatter, color ratio, depolarization ratio		2006-present

and land. In addition, cloud screening has become more robust, and onboard calibration is often available.

The prime examples of such enhanced sensors include the MODerate resolution Imaging Spectroradiometer (MODIS; Kaufman et al. 1997; King et al. 2003; Remer et al.

2008; Levy 2009), the Multi-angle Imaging SpectroRadiometer (MISR; Diner et al. 1998; Martonchik et al. 2002, 2009), POLarization and Directionality of the Earth's Reflectance instrument (POLDER; Tanré et al. 2011), and Ozone Monitoring Instrument (OMI; Torres et al. 2002b). The accuracy of the column AOTs retrieved with MODIS and MISR has been thoroughly assessed (e.g., Ichoku et al. 2005; Remer et al. 2005; Kahn et al. 2005, 2009; Chýlek et al. 2005; Xiao et al. 2009; Mishchenko et al. 2009, 2010; Levy et al. 2010; Shi et al. 2011). According to Yu et al. (2009), it is about 0.05 or 20% of AOT for one standard deviation of all retrievals and is somewhat better over dark water. The retrieved aerosol microphysical properties are often semi-quantitative or even qualitative. Although they may be useful for identification of generically defined aerosol air mass types, their quantitative accuracy generally does not fulfill the requirements summarized in Appendix A (Li et al. 2009).

The most recent studies by Dubovik et al. (2011), Hasekamp et al. (2011), and Tanré et al. (2011) have advanced POLDER to the forefront of passive aerosol retrievals from space. They have demonstrated the benefits of combining multi-spectral and multi-angle measurements of polarization as well as intensity for robust retrievals of complete aerosol properties, including information about aerosol particle sizes, shape, absorption, and composition (via refractive index). Still, some key measurement characteristics of POLDER turn out to be limited (Appendix B), thereby making many retrieval accuracies listed in Appendix A unattainable (see Section 6).

Among the passive satellite instruments scheduled for launch within the next 5 years, the one most suitable for aerosol retrievals is the Visible Infrared Imaging Radiometer Suite (VIIRS) on-board the NPOESS Preparatory Project (NPP) platform. The set and accuracy of VIIRS aerosol products are expected not to exceed those derived from MODIS data.

The above discussion leads to the following conclusion:

Despite significant recent advances in space-borne remote sensing, the existing and near-term expected passive aerosol retrieval capabilities remain inadequate to address the needs of current and anticipated model development.

5. APS-2 measurement strategy and design

The preceding discussion of the state of the art of passive aerosol remote sensing implies that the retrieval of accurate microphysical characteristics of aerosol particles from space remains a very difficult task. The main cause of the problem is the extreme complexity and variability of the atmosphere−surface system and the need to characterize this system by a large number of model parameters, all of which must be retrieved simultaneously. More often than not, the requisite number of unknown model parameters exceeds the number of *independent* (i.e., complementary in terms of their information content) units of data provided by a satellite instrument for a given scene location, thereby making the inverse problem underdetermined (or ill-posed). The retrieval procedure then yields a range of model solutions which are all equally acceptable in that they all reproduce the measurement data equally well within the measurement errors (Mishchenko and Travis 1997; Hasekamp and Landgraf 2005a, 2007). The only way to ameliorate the ill-posed nature of the inverse problem is to increase the number of independent units of data per

scene location until it significantly exceeds the number of unknown model parameters. Then the retrieval procedure based on a minimization technique is likely to become stable and yield a unique solution.

The well-known ways to increase the information content of data provided by a passive instrument measuring the reflected sunlight are the following:

- to measure not only the intensity, I, but also the other Stokes parameters describing the polarization state of the reflected radiation (i.e., Q, U, and V; Hansen and Travis 1974);
- to increase the number of spectral channels and the total spectral range covered;
- to increase the number and range of viewing directions from which a scene location is observed; and
- to improve the measurement accuracy, especially for polarization

(e.g., Mishchenko and Travis 1997). In what follows, we will demonstrate that by combining the above measurement capabilities, APS-2 affords the development of substantially more capable retrieval algorithms. The latter take full advantage of the extreme sensitivity of high-accuracy polarization data to aerosol and cloud particle microphysics and thereby ensure the retrieval of all the quantities listed in the right-hand panel of Fig. 5.

By performing high-accuracy and high-precision measurements of both intensity and polarization over a wide spectral range and at multiple view angles sampling a wide angular range, APS-2 represents a quantum leap in passive detailed aerosol retrievals from space.

APS-2 is designed to offer accurate and stable along-track (Fig. 6) climate measurements over the nominal mission life. As discussed above, the key measurement requirements for the retrieval of aerosol and cloud properties from photopolarimetric data are *high accuracy*, a *broad spectral range*, and observations from *multiple angles*, including a method for reliable and stable *calibration* of the measurements. APS-2 meets all these measurement requirements. The APS-2 design is based on that of the Research Scanning Polarimeter (RSP; Cairns et al. 2003), which has proven the fundamental APS concept with

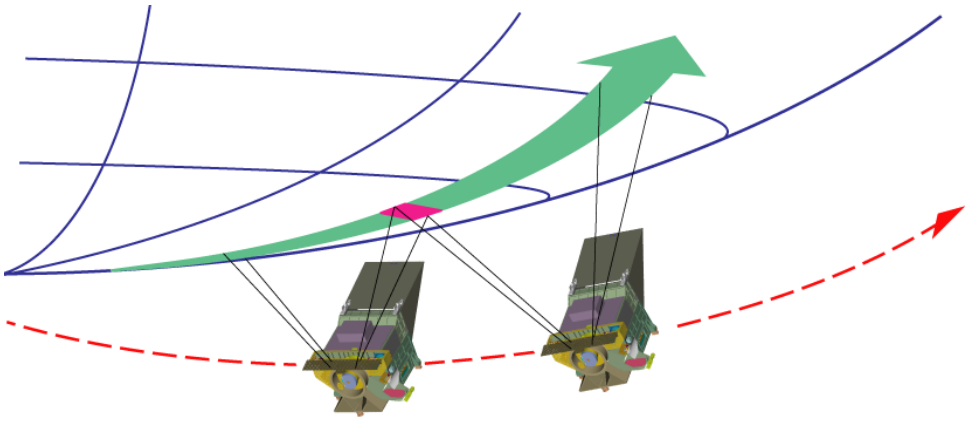

Figure 6. Along-track multi-angle APS-2 measurements via 360° scanning from a sun-synchronous polar-orbiting spacecraft.

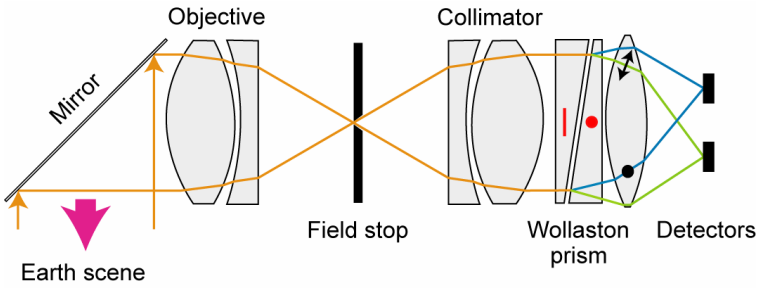

Figure 7. RSP optical approach for polarization measurement adopted for APS-2. Red markings show the orientations of the optical axes of the birefringent crystals forming the Wollaston prism. Orange lines show ray paths undergoing the split into orthogonal polarizations as indicated by the green and blue lines.

better than 0.2% accuracy photopolarimetric data for a range of atmospheric conditions with a diverse range of underlying backgrounds.

The measurement approach required to ensure *high accuracy* in polarimetric observations employs Wollaston prisms to make *simultaneous* measurements of orthogonal intensity components from the same scene (Travis 1992), as illustrated in Fig. 7. The field stop constrains the APS-2 instantaneous field of view (IFOV) to 8 ± 0.4 mrad which, at the nominal A-Train altitude (705 km), would yield a geometric IFOV of 5.6 km at nadir. The spatial field is defined by the relay telescope and is collimated prior to the polarization separation provided by the Wollaston prism. This method guarantees that the measured orthogonal polarization states come from the same scene at the same time and allows the required polarimetric accuracy of better than 0.2% be attained. To measure the Stokes parameters that define the state of linear polarization (I, Q, and U), APS-2 employs a pair of telescopes with one telescope measuring I and Q and the other telescope measuring I and U. This provides a redundant measurement set that increases the reliability of APS-2. APS-2 does not measure the Stokes parameter V since the circular polarization of the reflected sunlight is usually very small and carries virtually no useful information (e.g., Kawata 1978; de Haan et al. 1987).

The *broad spectral range* of APS-2 is provided by dichroic beam splitters and interference filters that define nine spectral channels centered at the wavelengths $\lambda = 413$, 444, 555, 674, 866, 911, 1376, 1603, and 2260 nm, as shown in Fig. 8. Blue enhanced silicon detectors are used in the visible and near-infrared (VNIR) channels, while HgCdTe detec-

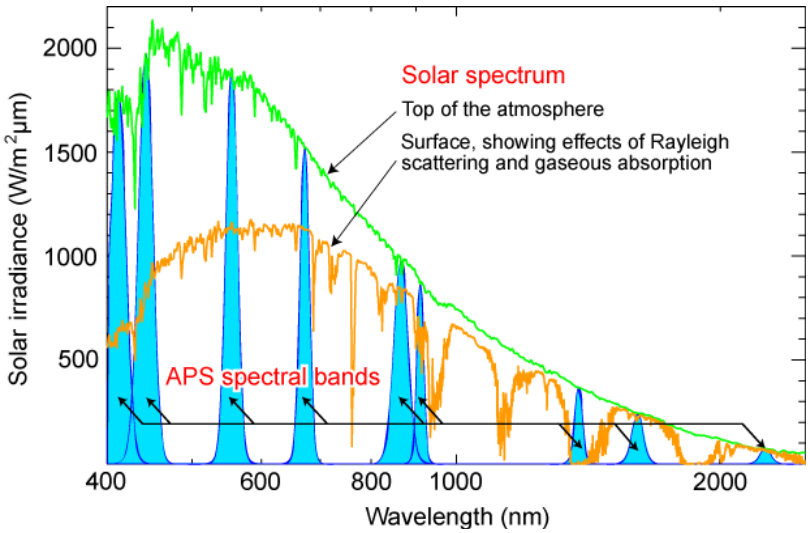

Figure 8. APS-2 spectral bands.

tors, passively cooled to 160 K, are used in the short-wave infrared (SWIR) channels and offer the very high signal-to-noise ratio required to yield a polarimetric accuracy better than ~0.2% for typical clear-sky scenes over dark oceans.

All spectral channels but 1376 nm are free of strong gaseous absorption (Fig. 8). The 1376-nm exception is centered at a major water vapor absorption band and is specifically intended for characterization of thin cirrus clouds and stratospheric aerosols. The locations of the other APS-2 spectral channels are consistent with an optimized aerosol retrieval strategy because they take advantage of several natural circumstances such as the darkness of the ocean at longer wavelengths in the visible and near-infrared, the lower land albedo at shorter visible wavelengths, and the potential for using the 2260-nm band to characterize the land surface contribution at visible wavelengths. The 911-nm band provides a self-contained capability to determine column water vapor amount.

The critical ability to view a scene from *multiple angles* is provided by scanning the APS-2 IFOV along the spacecraft ground track (Fig. 6) with a rotation rate of 40.7 revolutions per minute with angular samples acquired every 8 ± 0.4 mrad, thereby yielding ~250 scattering angles per scene. The polarization-compensated scanner assembly includes a pair of matched mirrors operating in an orthogonal configuration and has been demonstrated to yield instrumental polarization less than 0.05%. From the nominal A-Train altitude, the APS-2 viewing angle range at the earth is $+60°/-80°$ with respect to nadir.

The scanner assembly also allows a set of *calibrators* to be viewed on the side of the scan rotation opposite to the Earth. The APS-2 on-board references provide comprehensive tracking of polarimetric calibration throughout each orbit, while radiometric stability is tracked monthly by observing the Moon to ensure that the aerosol and cloud retrieval products are stable over the period of the mission.

Appendix C summarizes the flowdown of requisite retrieval requirements into APS-2 measurement characteristics. Appendix B compares the measurement characteristics of several relevant satellite instruments and demonstrates that APS-2 is indeed a close prototype of an ultimate passive instrument intended for comprehensive aerosol retrievals.

The relatively large APS-2 IFOV might be viewed as a limitation causing a reduced number of cloud-free pixels suitable for aerosol retrievals. However, there are two important factors supporting this choice of IFOV. First, it provides enough light to ensure the very high polarimetric accuracy of APS-2 while affording a small diameter of light-gathering telescope lenses. Second, there has been growing realization that the dense angular sampling of APS-2 measurements may enable simultaneous retrievals of aerosol and cloud properties in partially cloudy pixels (see Section 7). Then the relatively large APS-2 IFOV becomes an advantage since it provides statistically invariant sampling of cloud fields like the one in Fig. 9. Indeed, although individual small clouds can be expected to change during a 6-min interval nec-

Figure 9. Altocumulus clouds.

essary to scan the full range of viewing geometries, the cloud fraction and thus the radiometric and polarized reflectances of the aerosol–cloud mix captured by the APS-2 IFOV are likely to remain largely the same (Veefkind and Sneep 2007). It is expected that the APS-2 mission will include two cloud cameras (~400 m resolution) which will provide sub-pixel evaluation of the scene complexity and facilitate combined retrievals of aerosol and cloud properties in partially cloudy pixels.

Although the measurement requirements listed above may look quite challenging, extensive pre-flight tests of the actual instrument built by Raytheon for the Glory Mission have demonstrated a remarkable robustness of the APS design (Persh et al. 2010). The technical performance of the Glory APS was found to be fully consistent with original specifications and in many cases exceeded them considerably.

6. Comparative sensitivity analysis of APS-2 and current space-borne aerosol retrieval capabilities

The philosophy behind the APS-2 design described in the preceding section is to avoid the chronically underdetermined nature of many remote sensing instruments. Often this problem is managed by limiting the retrieved aerosol types to those within a previously selected set of models. While this does mean a unique solution is found, it makes it difficult to determine the uncertainty of the retrieved parameters and ultimately introduces a qualitative aspect to the results (e.g., Kokhanovsky et al. 2010).

The amount of information contained within an observation is largely defined by four main characteristics: the number and range of measurement view angles; the number and range of spectral observation bands; sensitivity to polarization state; and measurement accuracy. Current and past missions have individually exploited some of these aspects (Appendix B), but only APS accurately measures polarization state for a large number of view angles at a wide spectral range. The vast amount of information collected by APS-2 for each scene yields aerosol optical and microphysical properties without the need for arbitrary restrictions of aerosol properties based upon previously determined models. Furthermore, quantitative uncertainties can be computed for all retrieved parameters.

The amount of information contained within an observation is determined not just by the number of individual measurements, but also by how variations in aerosol microphysical properties manifest themselves optically. The APS observation strategy utilizes a wide variety of measurement types to capture the diversity of these effects. However, it is difficult to intuitively determine the impact of changing observation characteristics. Fortunately, statistical techniques exist that link the observation design, measurement accuracy, and the sensitivity of aerosol optical effects to the expected retrieval accuracy (Rodgers 2000; Hasekamp and Landgraf 2007). These techniques can be used to efficiently compare the likely retrieval capabilities of different instrument types and the dependence of these capabilities on specific instrument characteristics.

For this study, we performed a comparison of expected retrieval accuracy for APS-2 to two other types of instruments currently in orbit. While more details can be found in Appendix D, Fig. 10 provides a representative example. Specifically, we predicted the retrieval uncertainty for various instruments for about fifty types of aerosols over an ocean, whereby ten aerosol parameters, as well as surface characteristics, are retrieved simultaneously. These results were compared to the accuracy requirements in Appendix A, which should be met if an observation is to improve significantly the treatment of

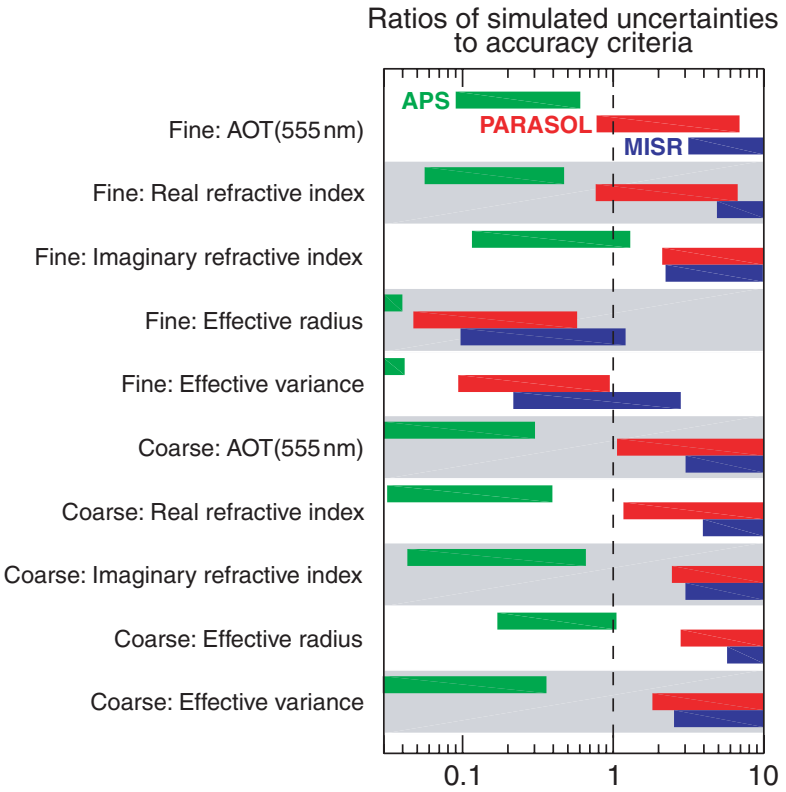

Figure 10. Relative assessment of expected instrument retrieval accuracies for aerosol simulations over an ocean. The ranges of simulated accuracies, normalized by the retrieval requirements described in Mishchenko et al. (2004), are shown for each retrieval parameter and instrument type. Values to the left of the dashed vertical line meet the retrieval requirements, while those to the right exceed them. Note that these results are for retrievals where there is no prior knowledge of the aerosol properties. In practice many algorithms utilize aerosol models and therefore assume a lower uncertainty. Very large ratio values indicate a lack of sensitivity to that parameter without prior information.

aerosols in process and climate models. APS-2 is, indeed, capable of meeting these requirements for aerosol properties for two different aerosol size modes. Currently existing instruments, on the other hand, are only capable of meeting the criteria for the parameters that describe the size of the sub-micron aerosol mode. This is the case even though the MISR, and Polarization and Anisotropy of Reflectances for Atmospheric Sciences coupled with Observations from a Lidar (PARASOL) instruments both have different technical characteristics (Appendix B). For example, MISR observes a scene at nine different viewing angles, but is not sensitive to polarization and has only four spectral channels covering a rather narrow wavelength range. PARASOL observes each scene at up to 16 viewing angles, has a slightly wider spectral range than MISR, and is sensitive to polarization. This generally improves the information content available in a retrieval, especially for sub-micron aerosols. However, the accuracy criteria are still not met.

An instrument like APS-2, which combines *all* of these technical characteristics to have a wide spectral range, many more view angle measurements, and sensitivity to polarization an order of magnitude more accurate than PARASOL, successfully meets the majority of requisite retrieval accuracy criteria.

Appendix D provides a description of the methodology used and a detailed discussion of the results obtained for aerosol retrievals over ocean and land surfaces. While this analysis cannot be used to predict specific retrieval accuracies for a given instrument in all cases, it can be used to compare quantitatively the *relative performance* of different instrument types. This analysis shows the far greater information content of APS-2 observations compared to its predecessors. Because of this, the APS-2 retrieval algorithm would not need to assume aerosol microphysical properties like MISR or MODIS retrieval algorithms. It would therefore not be subject to the unquantifiable uncertainties that are the consequence of that approach, such as described in Ichoku et al. (2003) for MODIS and Kahn et al. (2007) for MISR. Indeed, this analysis transcends retrieval methodology and purely represents the accuracy potential of a specific instrument design. The results of Appendix D demonstrate that APS-2 would have far more potential to meet aerosol accuracy retrieval criteria than any instrument currently in orbit.

7. Summary of APS-2 aerosol retrieval algorithms

The APS-2 aerosol retrieval algorithms build on the existing work on ground-based and satellite-based remote sensing using multi-angular, multi-spectral and polarimetric observations (Dubovik and King 2000; Stamnes et al. 2003; Hasekamp and Landgraf 2005a, 2007; Spurr et al. 2007; Dubovik et al. 2011; Hasekamp et al. 2011). Algorithms use a statistical optimization to find a maximum likelihood match between modeled radiation fields and the observations, considering uncertainties in both (Edie et al. 1971; Priestley 1981; Rodgers 2000). Effective use of this type of retrieval approach requires significant data redundancy which is provided by APS-2 observations at 200 view angles (if the observations are limited to $\pm 50°$ from nadir to limit pixel growth) and 8 spectral bands (413, 444, 555, 674, 866, 1376, 1602, and 2260 nm for aerosols) of the Stokes parameters I, Q and U. Although not all the observations are independent, and the 1376-nm spectral band only serves as a means to estimate the contribution of thin cirrus (Meyer and Platnick 2010; Ottaviani et al. 2011) or stratospheric aerosols to the observations, having 4800 measurements for a scene makes APS-2 observations more akin to AERONET observations than to other satellite instruments. This is why the APS-2 observations can be used to determine the optical thickness, size, complex refractive index, and SSA of a bimodal aerosol size distribution over ocean (Chowdhary et al. 2002, 2005, 2011) and land (Waquet et al. 2009a; Cairns et al. 2009b; Knobelspiesse 2011a) surfaces as well as above clouds (Waquet et al. 2009b; Knobelspiesse et al. 2011b).

One of the issues in applying an optimal estimation scheme to satellite observations, particularly for observations in the solar spectrum where scattering is significant, is the significant complexity of performing a multi-variable inversion (Dubovik et al. 2011). This places a substantial burden on efficiently calculating the state of the radiation field for a given distribution of aerosols and clouds, and also how the radiation field varies as a function of changes in the aerosol and cloud field (i.e., the functional derivative of the radiation field with respect to the atmospheric state, or Jacobian) since this is essential for optimal estimation (Ortega 1988; Dubovik and King 2000; Rodgers 2000).

There are a number of factors that now make use of optimal estimation schemes feasible for satellite data sets. Recent increases in the size of computer memory allow the use of tables in a modified form where the reflected radiance is simulated for many hundreds (~1200) of fine and coarse mode aerosol models together with the Jacobians for

every microphysical model table entry and for variations in optical thickness and surface parameters. The fine and coarse mode aerosols are then combined using a simple mixing approximation (Wang and Gordon 1994). Tables in this form provide a simulation of the radiation field and its Jacobians and as such can be used in an optimal estimation scheme (e.g., Dubovik et al. 2011; Hasekamp et al. 2011) in just the same way as the usual forward model calculations. Errors caused by the mixing approximation and interpolation between the table entries are corrected by taking the results from applying the optimal estimation technique to a search of the tables as the starting point in a second optimal estimation using a complete radiation model. The advantage of this technique is that the tables can be used to find a rough approximation of the aerosol parameters quickly, while the more computationally expensive complete radiative transfer model is only used to refine the solution. The radiative transfer model that is used, which provides an analytical calculation of all Jacobians in a single calculation (Hasekamp and Landgraf 2005b; Spurr et al. 2007; Cairns et al. 2009b), limits the computational burden of forward model calculations.

In order to apply optimal estimation schemes, a complete model of the surface-atmosphere system is needed and the surface, or cloud (for aerosols above cloud), or broken cloud is an important aspect of that system. We therefore summarize here the approaches taken for modeling ocean, land, and overcast cloud surfaces for aerosol retrievals. We also describe the methodology for aerosol retrievals in broken cloud scenes that is used for RSP observations. The same methods will be used in the analysis of APS-2 observations. We also briefly discuss the spatial and temporal sampling differences between ground track only, but comprehensive, APS-2 retrievals and less comprehensive imaging sensors.

Ocean models. Over the ocean, the contribution of upwelling radiation at wavelengths shorter than 865 nm must be either known or simultaneously retrieved with the aerosol properties for radiance only measurements (Stamnes et al. 2003; Spurr et al. 2007). Theoretical analyses show that polarized radiances are much less sensitive to ocean color than radiances, but the ocean body contribution cannot be neglected (Chowdhary et al. 2011). The contribution to polarized and unpolarized upwelling radiation from the ocean body can be parameterized on Chlorophyll-*a* concentration for Case I, open ocean, waters. This theoretical analysis has been verified by low altitude airborne observations during the Chesapeake Lighthouse Airborne Measurements for Satellites (CLAMS) and the Megacity Initiative: Local and Global Research Observations (MILAGRO) field experiments (Chowdhary et al. 2006, 2011; see also Appendix E). The APS-2 aerosol retrieval algorithms over ocean provide the Chlorophyll-*a* concentration and the wind speed that are used to estimate the ocean surface reflectance.

Land models. For retrievals over land the surface bidirectional reflectance distribution function (BRDF) is modeled using the AMBRALS kernel model (Wanner et al. 1997). This model has been used for the MODIS land surface product (Schaaf et al. 2002) and for the modeling of RSP observations (Knobelspiesse et al. 2008). The polarized reflectance of the surface has been found to have very weak spectral variations (Bréon et al. 1995; Waquet et al. 2009c; Litvinov et al. 2010), except for view angles close to backscatter. Away from backscatter the angular dependence of the polarized reflectance is similar to Fresnel reflectance from an isotropic distribution of facets (Vanderbilt and Grant 1985; Rondeaux and Herman 1991; Bréon et al. 1995) and is therefore primarily

dependant on the real component of the surface material refractive index, but insensitive to the imaginary component. The real component of the refractive index for most surface materials shows weak variations across the spectral range of the APS-2 bands, which explains the observations of Bréon et al. (1995), Waquet et al. (2009c), and Litvinov et al. (2010). Various alternative parameterizations have been suggested where the polarized Fresnel reflectance is modified by some factor that is introduced based on observations (Nadal and Bréon 1999; Maignan et al. 2009). Although there are limitations to all such models (Litvinov et al. 2010), the APS-2 algorithms use simple soil and vegetation models (Bréon et al. 1995) that are modified by shadowing (Saunders 1967; Waquet et al. 2009c). This model eliminates unphysical values of the albedo that are unacceptable in exact radiative transfer calculations and reduces the polarized reflectance at high view angles in a manner similar to that observed (Waquet et al. 2009c). The APS-2 aerosol retrieval algorithms over land therefore provide the parameters of the AMBRALS kernel model and the polarized reflectance model that are used to estimate the land surface reflectance.

Cloud models. It has recently been noted that multi-angle polarimetric observations provide substantial sensitivity to aerosols above clouds (Waquet et al. 2009b) particularly to fine, or accumulation mode aerosols (Knobelspiesse et al. 2011a). The reason for this is that such aerosols generate substantial polarization at side scattering angles ($\sim 70° - 130°$) whereas light reflected by clouds is only significantly polarized over the angular range from $135° - 180°$ which includes all of the rainbow and glory features. Furthermore, polarized cloud reflectance is insensitive to cloud optical thicknesses greater than two, which means that this parameter does not need to be determined (Goloub et al. 1994).

In order to use polarized reflectances in aerosol retrievals, it is sufficient to retrieve the cloud droplet size distribution for any clouds with optical thicknesses greater than $2 - 3$ (saturated regime) since this completely determines the polarized reflectance of the cloud for overcast cloud scenes. It is important to note that optical thickness variations within an overcast scene do not affect the polarized reflectance as long as the cloud is in the saturated regime. Since it is the structure of the rainbow that is used to determine the droplet size distribution, this retrieval does not require solving the vector radiative transfer calculations, is robust against three-dimensional (3D) radiative transfer effects (see examples in Appendix E), and is not affected by the underlying surface properties.

Once the droplet size distribution is determined, a table of calculations based on cloud droplet effective radius and effective variance is used to provide a lower boundary condition for an optimal estimate of aerosol properties. This means that on-line cloud calculations are not required as part of the optimal estimation scheme. In order to use the unpolarized reflectance, which can provide additional constraints on aerosol absorption (see Appendix E), it is necessary to also determine the scaled cloud optical thickness (King 1987). All visible−near IR spectral bands are used as part of the determination of cloud optical thickness in the iterative retrieval with the retrieved droplet size distribution model. However over land observations at 413 and 444 nm dominate the cloud optical thickness estimate because uncertainties in surface albedo are lower (Hsu et al. 2004). Over both land and ocean the cloud as a lower boundary condition is provided from a table and only the cloud optical thickness is allowed to vary in the optimal estimate of the aerosol products. The SWIR bands at 1603 and 2260 nm are not used in this aerosol above cloud retrieval scheme since the radiances observed in these bands are determined

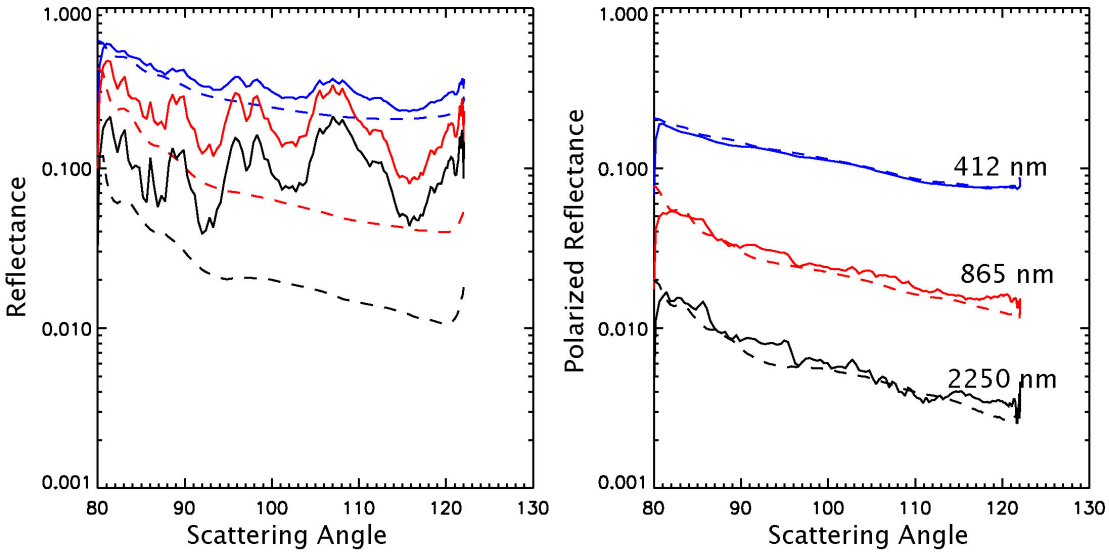

Figure 11. This figure shows RSP measurements over the Gulf of Mexico during CRYSTAL-FACE at 412, 865, and 2250 nm, where solid curves are for a cloud contaminated scene and dashed curves are for a nearby clear-sky scene. In the left-hand panel reflectance observations are shown, while the right-hand panel shows polarized reflectance observations. The variation in reflectance with scattering angle is caused by attitude variations of the Proteus aircraft during data acquisition, which means that different parts of the cloud field are seen at different scattering angles. The lack of sensitivity of the polarized reflectance to the presence of clouds over the scattering angle range from 80°–120° is apparent in the right-hand panel.

by cloud droplet sizes at a different depth within cloud (Platnick 2000) and are far more sensitive to within pixel optical thickness variations and 3D effects (Zuidema and Evans 1998; Marshak et al. 2006; Kato and Marshak 2009).

Broken clouds. The APS-2 instrument will fly with cloud cameras (~400-m resolution) that provide a sub-pixel evaluation of the scene used to constrain the retrieval algorithm approach. Recent analyses suggest that it is possible to retrieve aerosols in the presence of sub-pixel cloud contamination if multi-spectral, multi-angular observations are available (Hasekamp 2010). Additional examples are provided in Appendix E. It is certainly the case that limited cloud contamination (<10%) of an APS-2 scene does not have the same consequences as for a radiometric measurement that cannot differentiate between the small particle (aerosol) and large particle (cloud) sources of the observed radiance as can be seen in Fig. 11 where the presence of clouds only has a weak effect on the polarized reflectance. However, the combined retrieval of aerosol and cloud properties in scenes that have substantial cloud contamination is a recent addition to the capabilities that have been identified as possible with APS-2 (Hasekamp 2010). The cloud camera observations are therefore used to estimate a cloud optical thickness for each 400-m pixel (particle size is estimated from the APS-2 polarized reflectance size retrieval). The radiance contributions from the clouds are then incorporated into the standard optimal estimation scheme with appropriate adjustment of measurement uncertainties for the known effects of clouds on nearby clear-sky radiances and, to a lesser extent, polarized radiances. This approach to handling partial cloud cover has substantial advantages over the approach currently used by operational imagers. Indeed, the retrieval of accumulation mode size and absorption from radiance measurements in the shorter wavelength bands

becomes impossible within a large-scale fair weather cumulus field because cloud illumination of the clear sky areas dominates the unpolarized observations and has a pronounced blue spectral signature (Marshak et al. 2008).

Examples of RSP aerosol retrievals over ocean, land, and overcast clouds are given in Appendix E.

Sampling. As noted above, the APS-2 observations provide thousands of measurements for every ground pixel allowing greater retrieval capabilities than is possible with the comparatively limited set of measurements per pixel available from other satellite sensors (Dubovik et al. 2011). The APS-2 observations are therefore akin to the AERONET ground observations and complementary to them. AERONET provides a complete sampling of the diurnal cycle with limited spatial sampling whereas the APS-2 observations provide limited diurnal sampling with complete and uniform global sampling. Cloud contamination biases are comparable since both have similar effective sampling domains with a ~10 km diameter. In both cases the value of the observations is the capability to provide a comprehensive and accurate aerosol retrieval. The AERONET capability to provide accurate AOTs even with limited sampling has been used in the evaluation of assimilation models (Zhang et al. 2008; Zhang and Reid 2009; Benedetti et al. 2009). The retrievals of microphysical variables (complex refractive index) from AERONET have also been used to reassess existing climatological information about the optical properties of aerosol components (Sinyuk et al. 2003; Kinne et al. 2006; Schulz et al. 2006) and the appropriate refractive indices for black carbon in global models (Stier et al. 2007). Retrievals of aerosol spectral complex refractive indices are also invaluable in evaluating the mixing state of aerosols (Schuster et al. 2005; Russell et al. 2010), which is required in the evaluation of current and future global aerosol models (e.g., Ghan and Schwarz 2007; Bauer et al. 2008). The APS-2 observations are therefore expected to provide a revolutionary increase in the global coverage of detailed aerosol and cloud retrievals that substantially improves our existing understanding of the spatial distribution and composition of aerosols.

A detailed assessment of the APS-2 sampling of the most variable aerosol characteristic, AOT, is given in Appendix F.

8. Key aerosol information provided by APS-2

Forecasting the Earth system and its climate requires correct boundary value (forcings) and an accurate model (feedbacks). The largest uncertainty in the boundary value is the aerosol radiative forcing (Hansen et al. 1998; Solomon et al. 2007). Moreover, the sensitivity of mid and high Northern latitude climate to local forcings is much stronger than the use of a global mean radiative forcing would suggest (Shindell and Faluvegi 2009). Since the aerosol radiative forcing is indeed regionally concentrated, the effects of aerosols, compared with those of well-mixed GHGs, are significantly underestimated by using a global mean forcing. This is an issue when trying to separate aerosol and well-mixed GHG effects through patterns of temperature change (Hegerl et al. 2007). Current economic development in South and East Asia means that changes in the aerosol radiative forcing in mid and high latitudes are likely to be substantial both short-term and long-term. Numerous recent studies indicate that the current uncertainties in the aerosol forcing limit our ability to evaluate climate models by comparison with observed global

temperature change (Knutti et al. 2002; Smith et al. 2002; Schwartz et al. 2007; Forster et al. 2007b).

APS-2 generates key data for both the direct evaluation of the DARF and the evaluation of process and climate models that are essential tools for the prediction of Earth-system change and the evaluation of approaches to the mitigation of climate change.

It provides not only a detailed quantitative gauge of model performance, but also can offer essential information about the reasons why models agree or disagree with measurements. A major advantage of APS-2 over existing capabilities is that it yields size-resolved aerosol properties by retrieving the effective radii and variances and the fraction of non-spherical particles in each of two particle size modes. This information, along with the spectrally resolved complex refractive index, is sufficient for the calculation of the optical properties of aerosols that are required for the determination of the surface and top-of-the-atmosphere radiative effects of aerosols. The value of such retrievals for model evaluation is that simulations of aerosol size distributions can be tested and it is possible to identify where chemical composition predictions (Fig. 2) are compatible, or incompatible, with observations. Available satellite products (cumulative AOT) test whether the model conversions of the total mass of all the different aerosol components to a scattering cross-section are acceptable, and current models have considerable skill in matching such observations (Schulz et al. 2006). The APS-2 capability moves the validation of model performance to a more relevant (Roesler and Penner 2010) and challenging evaluation of the mixing state of the aerosols for which there is currently little agreement among global models (Schulz et al. 2006). Table 1 summarizes the key processes and aerosol properties included in models, as well as the means of validation that exist today. With the exception of aerosol sources, APS-2 can provide information for all processes and properties in climate models. Furthermore it can do so not only for a single size bin or a generic fine/coarse mode characterization, but rather for the actual bimodal size distribution.

Examples of how this information can be used by modelers include the following:

- Verification of which regions exhibit significant enhancement of aerosol absorption due to black carbon coating and the identification and quantification globally of the presence of brown carbon.
- A recently emerged area of research is dust mineralogy. It is well known that different dust sources in various regions around the world have different mineralogical composition (Koven and Fung 2006), with each mineral having different optical properties. Future developments are expected to include this information in standard model simulations. For example, it has already been included in the development version of the GISS modelE climate model (Perlwitz et al., in preparation). Having satellite information for the spectral effective refractive index in dust-dominated regions will provide important constraints on how the dust mineralogy changes.
- Although particle shapes other than spheres have not been taken into account in global climate models yet, having information on the aerosol shape on the global scale is a useful tool for identifying regions in which this assumption may be incorrect. This analysis can include areas where dust is an important contributor to AOT and areas where fresh emissions of black carbon occur, which are highly non-spherical. Persistent biomass burning occurs in various regions, but mainly in the

tropics and the temperate and boreal forests; by studying the plumes that can extend several hundreds or even thousands of kilometers downwind, the aging of black carbon can be evaluated, as well as the amount of time that it takes for the fractal-shaped particles to collapse into more spherical structures.

- One of the most challenging tasks for the modeler is to identify ground-based stations that are representative of large regions (of the order of 100 km or larger) in order to be able to validate a model with grid cells as large as a few hundred kilometers at the equator. Although APS-2 observations cannot fill completely a whole model grid, they can prove very useful in understanding how homogeneous a model's grid is. Size distribution information over large areas is only available from very limited aircraft measurements, and not all measurement stations are unaffected by local sources. Having a satellite that provides aerosol information along gridbox slices provides an understanding of the degree of homogeneity (or inhomogeneity) of a given gridbox, as well as whether the ground-based measurements (when co-located with the satellite overpasses) are indeed representative of a large region, or are dominated by local sources.

While AERONET already provides some of the aforementioned information for a limited and spatially inhomogeneous sample, APS-2 will be a key addition by providing global space-borne retrievals with the sensitivity to aerosol refractive index, shape, and absorption that is essential to improving our knowledge of the effects of aerosols. Each APS-2 ground pixel can be treated by models as a sampling "station" generating a vast amount of data to test the validity of the simulated number/mass relations and composition. These "stations" (Fig. 12) will provide a dense sampling of the entire globe except for the poles and will offer very robust results since all measurements will be made with the same instrument and processed with the same retrieval algorithms. The APS-2 "stations network" will be equivalent to more than 1,000 AERONET networks and will offer a sampling density that has a maximal spacing of ~1.5° in longitude at the equator for a typical sun-synchronous orbit, with substantially denser sampling at higher latitudes. The revisit time is roughly sixteen days and is dependent on the details of the orbit that would be selected for an APS-2 re-flight (see Section 12). Finally, APS-2 will provide information on aerosol properties above clouds with particular sensitivity to absorbing aerosols, which AERONET cannot do. This information will be key in obtaining more accurate global assessments of the all-sky DARF and the semi-direct effect.

Note that, apart from affecting climate, the modification of radiation by aerosols also has major implications for atmospheric chemistry (Bian et al. 2003; Martin et al. 2003; Tie et al. 2005). Absorption and scattering affect the amount of light available in various parts of the atmosphere for the breakdown of gas molecules (photolysis). The information provided by APS-2 (SSA, refractive index, effective radius and effective variance for two aerosol modes) will help improve the representation of aerosol optical properties that are needed for photolysis calculations in models (e.g., Wild et al. 2000; Tie et al. 2005). The more accurate representation of photolysis can significantly improve the models' ability to capture the variability of important gases (e.g., Voulgarakis et al. 2009), something that can subsequently be evaluated by comparisons of model results with measurements from other satellite instruments. Apart from contributing to more accurate atmospheric chemistry simulations, a better-constrained representation of photolysis will also improve the ability of models to simulate important climate forcing agents, such as ozone, meth-

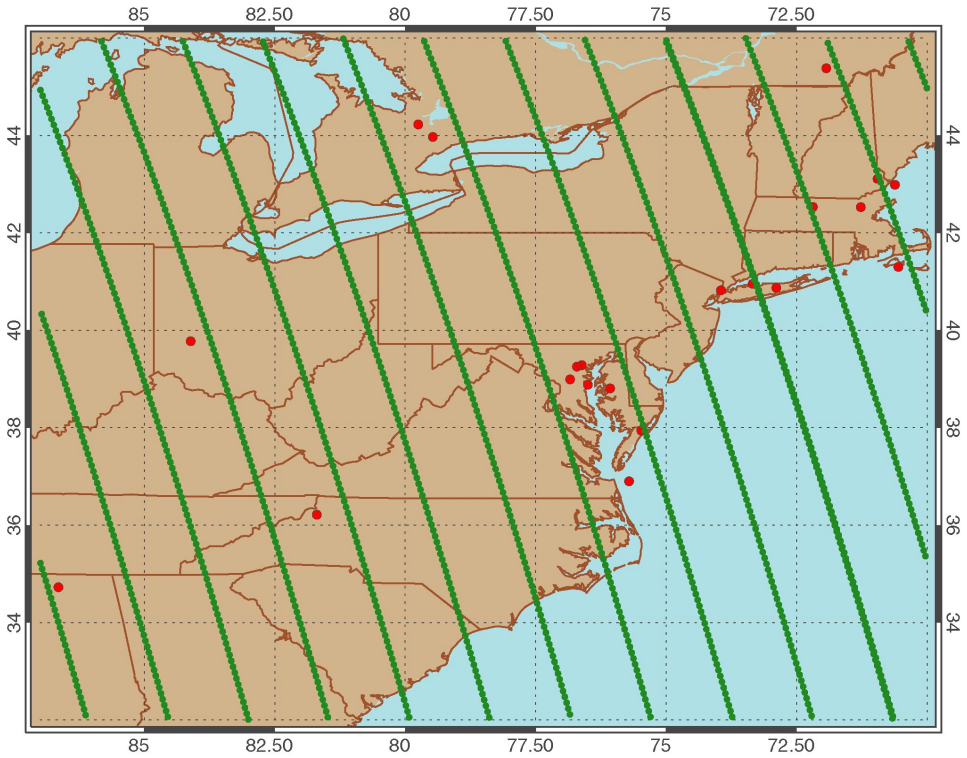

Figure 12. Comparison of the spatial scales of a typical 2° × 2.5° climate model grid (dashed lines), AERONET measurements from currently active stations (red dots), and APS-2 ground tracks corresponding to adjacent A-train orbits (green dotted lines).

ane, and sulfate aerosols, which are all strongly affected by tropospheric oxidation processes, which depend on photolysis.

9. Summary of APS-2 cloud retrieval algorithms and data products

Cloud feedbacks are among the principal sources of uncertainty in assessing the climate sensitivity of the Earth (Stephens 2005; Bony and Dufresne 2006; Soden and Held 2006; Solomon et al. 2007). The sign of the net cloud radiative forcing (i.e., whether clouds act to warm or cool the planet in a global sense) depends on cloud optical thickness and height, as well as on the thermodynamic phase and size/shape distributions of the cloud particles (Baker 1997; Liou 2002). Aerosols can alter cloud macro- and micro-physical properties, and thereby the global net cloud radiative forcing, through indirect effects (Chen and Penner 2005; Lohmann and Feichter 2005), although there are physical reasons to believe that existing global model results can overestimate some of such effects (Stevens and Feingold 2009). For instance recent simulations that embed a cloud-resolving model (CRM) in each vertical column of a global model found much smaller aerosol indirect effects than were simulated in the host model without a CRM (Wang et al. 2011). This can in part be explained by the fact that a CRM implicitly includes some of the buffering effects (Stevens and Feingold 2009) that reduce the strength of aerosol–cloud interactions. However there are still substantial uncertainties in the modeling of the global indirect effect of aerosols on climate.

Absorbing aerosols can also exert semi-direct effects on clouds by heating the atmosphere or reducing surface insolation and may decrease cloud cover (Ackerman et al. 2000; Koren et al. 2004, 2008; Penner et al. 2003; Fan et al. 2008) or increase cloud cover (Johnson 2005; Feingold et al. 2005; McFarquhar and Wang 2006; Brioude et al. 2009) depending on the cloud type, the vertical location of the aerosol layer with respect to the cloud layer, and the surface conditions (Koch and Del Genio 2010).

While the primary objective of the APS-2 instrument is the retrieval of accurate aerosol parameters, this sensor is also uniquely capable of providing information about cloud thermodynamic phase (ice, water, or a combination of the two), the shape and size distributions of the cloud particles, and cloud optical thickness.

Although the daily sampling of APS-2 is limited, it is expected to provide unique and important observational targets for studies of cloud processes and indirect aerosol effects since virtually all cloud types will be sampled sufficiently.

The anticipated APS-2 cloud retrieval procedures are based on those applied to the POLDER and MODIS satellite instruments and the airborne RSP instrument. Owing to the collection of multi-spectral, multi-angle polarization observations APS-2 would allow for the following advances:

- improved ability, compared to POLDER and MISR, to infer the morphology (surface texture and overall shape) of ice particles in optically thick ice clouds globally;
- a specialized, polarization sensitive channel at 1376-nm that will have an unprecedented sensitivity to the morphology (surface texture and overall shape) of ice particles in optically thin cirrus (including sub-visible, optical thickness <0.1; Ottaviani et al. 2011) which are a ubiquitous and important component of the tropical upper troposphere (Lee et al. 2009);
- unambiguous sensitivity to the presence of liquid water at temperatures below 0°C using the difference in the polarization features of ice and water clouds in the rainbow region;
- retrievals of the effective radius and variance of the drop size distribution near cloud top using the structure of rainbow polarization features that are not significantly affected by 3D radiative transfer effects or uncertainties in surface reflection;
- retrievals of cloud-top pressure using the Rayleigh scattering contribution to polarized reflectance at multiple wavelengths;
- retrievals of cloud-base pressure for stratiform clouds over the ocean using the differential increase in absorption between unpolarized and polarized light leading to estimates of droplet number concentration (derived from droplet size, optical thickness and cloud pressure thickness) and liquid water path (derived from cloud pressure thickness, droplet number concentration, and effective variance).

Unlike liquid cloud droplets, ice particles are non-spherical and can have a roughened surface. The size of the particles is the primary determinant of the SSA (Hansen and Travis 1974; Mitchell 2002; Platnick et al. 2003) while the shape, particularly aspect ratio, and microscopic surface roughness control the asymmetry parameter (Liou 2002; Fu 2007; Yang and Fu 2009; Baran 2009; Baum et al. 2010). A fundamental question that remains to be addressed is what ice particle properties should be assumed in the operational retrievals of ice size (Zhang et al. 2009a; Baum et al. 2011) and also how accurate

are the ice properties either assumed or predicted in climate and cloud-resolving models that remain poorly constrained by observations. Images of ice crystals obtained from *in situ* probes generally indicate the presence of myriad complex particles, often highly aggregated, or with irregular shapes (Baran 2009). The infrequent occurrence of halos and sundogs in cirrus together with measurements from nephelometers (Garrett et al. 2003; Gayet et al. 2011) and other *in situ* probes (e.g., Small Ice Detector-3; Ulanowski et al. 2006; Kaye et al. 2008) suggest that ice particles generally do not have smooth crystalline surfaces. A concern with the historical record from *in situ* probes is the effects of crystal shattering (Field et al. 2006; Korolev et al. 2011), although improved *in situ* probe design and analysis techniques are now allowing such effects to be mitigated at least in particle size measurements (Jensen et al. 2009; Lawson et al. 2010; Lawson 2011). Additional concerns with existing *in situ* measurements are their necessarily limited spatial availability, ambiguity in the classification of habit, and inability to resolve microscopic surface roughness. The use of multi-angle polarized reflectance measurements is therefore complementary to *in situ* measurements and invaluable in building a global picture of the shape and roughening of cloud ice particles (Chepfer et al. 2001; Knap et al. 2005; Baran and Labonnote 2006).

APS-2 will improve our understanding of ice clouds by establishing the relationships between ice crystal morphology and cloud type, particle size, and cloud top temperature. Its increased spectral sampling and angular resolution, compared with POLDER, will allow the inference of ice crystal size, shape, and roughness for virtually every APS field-of-view that contains ice clouds. Another improvement in the APS-2 observations over those available from POLDER is the inclusion of a 1376 nm band (Gao et al. 1993), similar to that on MODIS (Meyer and Platnick 2010), which is relatively insensitive to surface reflectance and low altitude water clouds and permits the detection of thin and sub-visible cirrus with optical thicknesses down to a few hundredths, as well as the retrieval of ice crystal morphology for such clouds (Ottaviani et al. 2011). Although sub-visible cirrus necessarily have little impact at solar wavelengths, they do affect outgoing longwave radiation (McFarquhar et al. 2000; Hartman et al. 2001) and appear to play a significant role in the heat balance of the tropical tropopause and dehydration of the stratosphere (Jensen et al. 1996a,b; Holton and Gettelman 2001; Dinh et al. 2010).

The dependence of the thermodynamic phase of clouds on temperature for different climate regimes is a valuable observational target for the evaluation of both climate and cloud-resolving models because the temperature level at which glaciation occurs influences every aspect of the radiative and dynamical behavior of cold clouds (Fowler et al. 1996; Baker 1997). On a more fundamental level, accurate determination of the cloud thermodynamic phase partitioning, that is, whether clouds are composed of liquid or ice particles or a combination of both, is essential for the retrieval of other cloud properties such as particle size and shape.

APS-2 will be capable of inferring the presence of liquid water at temperatures below 0°C by exploiting the difference in the polarization features of ice and water clouds in the rainbow region, as demonstrated using POLDER (Goloub et al. 2000; Riedi et al. 2010). The signal of the rainbow in polarized reflectance is determined by the relative amount of scattering on ice and liquid particles. In the case of an ice layer above liquid cloud, polarization measurements contain information that can be used to determine the ice optical thickness above the liquid layer (Riedi et al. 2010). APS-2 measurements will improve

our understanding of cloud glaciation processes and their dependence on climate regime and aerosol loading, among other factors. The phase determination from APS-2 is expected to be better than that from POLDER owing to the finer angular resolution within the rainbow region and the higher accuracy of APS-2 measurements.

Existing passive instruments such as MODIS, AVHRR, or VIIRS provide cloud thermodynamic phase based on IR measurements or a combination of solar and IR measurements (Platnick et al. 2003; Pavolonis et al. 2005). However, the MODIS Collection 5 IR thermodynamic phase retrievals have significant limitations (Nasiri and Kahn 2008; Cho et al. 2009) primarily in the ability to discriminate between ice and water clouds at temperatures between −40°C and 0°C. Polarized lidar measurements such as those from CALIOP generally use thresholds of lidar depolarization and backscatter to determine cloud phase. However, results from this technique are significantly affected by uncertainties in, e.g., ice crystal back-scattering and depolarization properties, ice crystal orientation, and the possible presence of aerosol (Hu et al. 2007; Sassen and Zhu 2009; van Diedenhoven et al. 2011). The APS-2 cloud phase retrievals will therefore improve the climatological data on the transition of clouds from water to ice as temperature decreases and, if flown in formation with the Aqua, Cloud–Aerosol and Infrared Pathfinder Satellite Observation (CALIPSO), NPP, or EarthCARE satellites, can be used to improve operational IR, solar/IR, and polarized lidar methods for phase discrimination.

The shortwave albedo of liquid water clouds is determined by their liquid water path and the size distribution of cloud drops, which can both be significantly affected by aerosols (Lohmann and Feichter 2005; Levin and Cotton 2008). Perhaps the most obvious effect of aerosols on clouds is the change in cloud droplet sizes in ship tracks (Coakley et al. 1987). Such observations provide a valuable test of our ability to use remote sensing (Coakley and Walsh 2002; Segrin et al. 2007) and large-eddy simulation models (Ackerman et al. 2003) to better understand the behavior of boundary-layer clouds. The global co-variation of AOT, cloud droplet size, and cloud fraction retrieved from satellite observations has been used as an observational target to test aerosol effects in general circulation models (Lohmann and Lesins 2002; Quaas and Boucher 2005; Menon et al. 2008), although the significance of aerosol effects on clouds in such analyses is uncertain (Quaas et al. 2010). The width of the cloud droplet size distribution may also be affected by aerosols and its impact on global indirect radiative forcing has been shown in highly idealized estimates to be significant (Rotstayn and Liu 2003, 2009; Peng and Lohmann 2003). Moreover, the evidence for aerosol effects on the width of the droplet size distribution is ambiguous (Liu and Daum 2002; Pawlowska et al. 2006; Zhao et al. 2006); modeling studies indicate a broad range of such effects (Lu and Seinfeld 2006) as well as effects of the droplet size distribution width on clouds (Xie and Liu 2011). Accurate determination of cloud top droplet size distributions by satellites would therefore provide a valuable observational target for testing simulations by large-scale models that include droplet size distribution effects.

Multispectral measurements in absorbing and non-absorbing bands are generally used to simultaneously retrieve the cloud droplet effective radius and optical thickness (King 1987; Nakajima and King 1990; Nakajima et al. 1991; Platnick et al. 2003). These parameters can then be mapped to a droplet number concentration and cloud layer thickness if an adiabatic cloud profile can be assumed (Bennartz 2007). However, the apparently different sensitivity of adiabatic and non-adiabatic clouds to aerosol effects (Kim et al.

2008) makes the use of such an assumption in analyses of aerosol indirect effects problematic. The main issue for droplet size retrievals of this type is that for partially cloudy scenes, leakage of light out of the sides of the clouds tends to cause a high bias in the size retrievals (Marshak et al. 2006; Zinner and Mayer 2006; Zinner et al. 2010; Zhang et al. 2011). Polarimetric observations made by POLDER can also be used to determine the droplet size distribution at cloud top (Bréon and Goloub 1998) but only for homogeneous clouds decks of ~100 km in size because of the poor angular sampling at smaller spatial scales.

The high angular resolution of APS-2 observations of the polarization of reflected light in the rainbow region (at scattering angles between 135° and 165°) allows unique retrievals of the droplet size distribution, including its width, for every ground pixel (see Appendix E) and will therefore provide a valuable complement to existing observations. Polarimetric retrievals of droplet size depend on the rich angular structure of single scattering by spherical droplets which is not affected by the leakage of light out of cloud sides, other 3D cloud effects, or aerosols above clouds (Waquet et al. 2009b; Knobelspiesse et al. 2011a; Hasekamp 2010). Furthermore, such retrievals are just as accurate over land or ocean surfaces and over a much wider range of cloud optical thicknesses than is the case for existing measurements. The APS-2 instrument will also provide continuity with existing and future measurements through its spectral bands at 1603 and 2260 nm to which the usual absorbing/non-absorbing droplet size retrievals can be applied. Retrievals using the radiances for these bands are sensitive to droplet sizes deeper in the cloud than the polarimetric size retrievals (Platnick 2000; Zhang et al. 2011), which provides some limited sensitivity to vertical variations in cloud particle size.

To use the cloud retrievals in evaluating the radiative effects of clouds, it is essential to know the altitude at which the cloud is located. For APS-2 this is accomplished by using polarized reflectance observations in short wave ($\lambda < 500$ nm) spectral bands that provide a direct measure of cloud top height by using Rayleigh scattering as a barometer (Goloub et al. 1994). In addition, observations in the spectral band at 911 nm permit water vapor above cloud to be estimated using attenuation of the polarized reflectance in the rainbow at 911 nm compared to that at 866 nm because the rainbow features are generated at cloud top. The water vapor amount within the cloud can then be estimated separately by using the unpolarized reflectance observations that are sensitive to the full depth of the cloud. The within-cloud water vapor amount is proportional to the product of the cloud pressure thickness and the water vapor mixing ratio. The cloud pressure thickness can therefore be derived by assuming that the cloud layer has a saturated water vapor mixing ratio. The saturated mixing ratio could possibly be calculated from the cloud top temperature observed by an operational imager (e.g., MODIS or VIIRS) or can be estimated from a forecast model.

Once the cloud pressure thickness is determined, it can be combined with the droplet size and optical thickness retrievals to determine the cloud droplet number concentration that does not depend on adiabaticity assumptions, which may be substantially in error (Painemal and Zuidema 2011). The droplet number concentration is a particularly valuable observational product for testing models because it provides a more direct indication of aerosol effects on clouds than changes in cloud droplet size (Brenguier et al. 2003). Estimates from APS-2, which will be independent of adiabatic assumptions, will therefore provide a valuable complement to other approaches (Boers et al. 2006; Bennartz

2007; Hu et al. 2007) for the remote estimation of droplet number concentration. Additionally, combining estimates of cloud thickness, cloud droplet concentration, and effective variance will allow for an estimate of cloud liquid water path that does not require assuming a vertically uniform cloud (Stephens et al. 1978) or an adiabatic liquid water profile (Wood and Hartmann 2006).

10. Use of APS-2 products in assimilation models

AOT fields with global coverage generated by MODIS have been found to provide substantial benefits in aerosol assimilation and forecasting (Zhang et al. 2008; Benedetti et al. 2009; Morcrette et al. 2009). Data with limited horizontal coverage such as the data from CALIPSO can still be valuable for assimilation systems and can improve global aerosol transport modeling and prediction because of their unique resolution of vertical variability (Sekiyama et al. 2010; Zhang et al. 2011). The spatial sampling provided by APS-2 will be similar to that of CALIPSO, and so its unique products that constrain mixing state through the retrieval of real and imaginary refractive indices (e.g., Schuster et al. 2005) and its accurate AOT and size retrievals are expected to be of value for assimilation purposes and forecast models if the retrievals are provided in near real time. It is through constraining the mixing state of aerosols in global prediction models (Liu et al. 2007a,b) that APS-2 data would have its largest impact on air quality forecasts that currently use AOT as a constraint on surface concentrations of particulates (Engel-Cox et al. 2004; Al-Saadi et al. 2005; Hoff et al. 2009; Zhang et al. 2009b).

One of the primary issues for the effective assimilation of aerosol data is the correction of biases and the provision of a reliable assessment of retrieval uncertainties (Shi et al. 2011). It is therefore essential for the assimilation of APS-2 level 2 products that a pixel level assessment of errors in the retrievals is provided. The inclusion of error estimates is planned for the APS-2 products that will be generated using an optimal estimation scheme (Cairns et al. 2009a; Dubovik et al. 2011; Hasekamp et al. 2011). This scheme includes an assessment of retrieval errors and model validity (retrieval quality) as part of the retrieval process (Rodgers 2000) for each retrieval. Although APS-2 data with significant latency (~days) may be of interest for the assessment of model performance and reanalysis applications, the data need to be processed and made available in near real time in order to be used in aerosol forecast models. The APS-2 satellite options all have resources (power, bandwidth, processing power) that can provide a direct broadcast capability that would facilitate the provision of APS-2 products within 24 h of data acquisition. The APS-2 pixel size of 5.6 km from a 705 km altitude means that there will be cloud contamination, particularly in broken cloud fields. However, the polarized signal generated by fine-mode aerosols is very distinct from the signal caused by clouds, which makes the fine-mode aerosol retrieval valid even in the presence of clouds (Hasekamp 2010; see also Appendix E). This is an important aspect of APS-2 retrievals, if they are to be used for assimilation, and will minimize scene dependent biases (Zhang and Reid 2009).

11. Validation strategy

In this section we discuss validation of APS-2 results, by which we mean the acquisition of independent observations, or measurements, that provide a clearly quantifiable meas-

ure of the accuracy and/or precision of the APS-2 products. There are two levels of validation of the products from APS-2: the radiance (level 1) products and geophysical (level 2) retrieval products. It is clear that level 1 products must be validated first to have a clear understanding of the radiometric and polarimetric accuracy and precision of the APS-2 observations that are the inputs to the level 2 retrievals (Cairns and Geogdzhayev 2010). However, validation of level 1 products must be an ongoing activity throughout the period of the mission to provide a continuous and independent guarantee of the quality of the observations that are being made. Validation of level 2 products is more complex than for level 1 products, given the wide range of geophysical retrievals that will be provided by APS-2, and must explore a significant sample of climate regimes to evaluate the validity of the APS-2 algorithms and their associated error estimates.

Level 1 validation. The primary method for validating the APS-2 level 1 products will be a direct radiance based cross-calibration (Slater et al. 1996) with an airborne simulator mounted on one of the NASA ER-2 aircraft. The RSP instruments that have been used to test APS-2 retrieval algorithms and develop robust models of the surface polarized BRDF also serve as airborne simulators of the APS-2 observations with close matches to the spectral bands at 413, 555, 674, 866, 1603, and 2260 nm. The RSP instruments have National Institute of Standards and Technology (NIST) traceable radiometric calibration that will be repeated before each deployment, and they can be polarimetrically recalibrated before and after each validation flight. Stability of the RSP instruments is better than 1% per year for radiometric observations and 0.1% per year for polarimetric observations. One RSP instrument is currently being integrated onto the NASA ER-2 with test flights scheduled at the end of August 2011. The RSP instrument has previously been flown in a similar environment (–100°C at over 17 km altitude) on the Scaled Composites Inc. Proteus aircraft during the CRYSTAL-FACE field experiment. The IFOV of the RSP instrument is 14 mrad and has a ground pixel size of 250 m at a 19 km altitude, which is smaller than the 5.6 km ground pixel size of APS-2 from a 705 km orbit. Large targets are therefore required for radiance based cross calibrations. The ideal targets are clear skies over the ocean to validate the low end of the radiometric scale and cirrus anvils, or stratocumulus cloud decks to validate the high end of the radiometric scale. The expected accuracy of the transfer of radiometric calibration for sensors with different IFOVs is 2% (Slater et al. 1996). Validation of the other bands will rely on spectral interpolation using the physical models provided by the aerosol and cloud retrievals with a focus on clear sky ocean scenes, water cloud scenes, and ice cloud scenes for validation of the 444, 911, and 1376 nm bands, respectively.

Level 2 validation. The APS-2 aerosol retrieval products requiring validation are the AOT, size distribution parameters (effective radius and effective variance for a fine and a coarse mode), and complex refractive index together with the optical parameters (spectrally varying SSA, scattering cross section, backscatter fraction, etc.) that depend on the microphysical retrievals. The primary issue for validation of the ground track only retrievals obtained by an APS-2 sensor is collecting an adequate sample of validation measurements that are obtained close enough in space and time. The only effective way to accomplish this is through the use of airborne measurements obtained by flying along the satellite ground track ±30 min from overpass time.

An RSP instrument has been integrated onto the NASA LaRC UC12 and flown in conjunction with the High Spectral Resolution Lidar (HSRL). The HSRL provides a di-

rect measure of extinction and therefore AOT at 532 nm (Hair et al. 2008). Flying both instruments at an altitude (8.5 km) for which most of the aerosol and molecular scattering is below the aircraft allows for the direct validation of the APS-2 AOT product at 532 nm along the APS-2 ground track, under most conditions. In addition, the lidar intensive observables (backscatter Ångström exponent, lidar ratio, depolarization at 532 and 1064 nm) provide a test of the retrieved aerosol microphysical model. Measurements from a platform of this type can also provide ongoing validation of the level 1 APS-2 products although with increased transfer uncertainty (~1%–2%) compared with ER-2 observations. The increased transfer uncertainty is caused by having a lower altitude and potential contamination by thin cirrus, which would be limited to optical thicknesses of less than 0.01 when using screening with the APS-2 1376 nm band. Measurements with RSP and HSRL on the same platform also allow for algorithmic validation throughout the course of a day, not just at overpass time, because the APS-2 algorithms can be applied to the RSP observations.

Validation of the spectral AOT, across the solar spectrum, can be performed by airborne upward looking sun (AATS-14; Redemann et al. 2009) or sun/sky (4STAR; Dunagan et al. 2011) photometers. In the case of the 4STAR instrument, AERONET type sky radiance retrievals that can be used to estimate the column size distribution and complex refractive index are feasible. These upward looking photometers typically fly on a platform that also makes aerosol *in situ* observations (CIRPAS Twin Otter, DoE G-1, NASA P-3) which can provide the most direct and accurate measurements of aerosol size distribution (scanning mobility and aerosol particle sizers) and absorption (Moosmüller et al. 2009) that can be used to validate these APS-2 products. The only *in situ* measurement that has sufficient sensitivity to real refractive index to act as a direct validation of the APS-2 product is a polar nephelometer, which measures the polarized phase function of the aerosols to infer the refractive index. An instrument of this type is scheduled to fly on the NASA LaRC B200 platform, which is being outfitted as an aerosol *in situ* observation platform, in the summer of 2011. In addition to the polar nephelometer, the B200 will fly a suite of instruments to measure aerosol number concentration, size, scattering (integrating nephelometer), absorption (Particle Soot/Absorption Photometer), effects of humidity on the aerosol scattering coefficient, and cloud properties. It is worth noting that requiring consistency between *in situ* size measurements and measurements of scattering and absorption cross sections can also provide constraints on complex refractive indices if the polar nephelometer were not to be available, or as a check on its measurements (Virkkula et al. 2006; Petzold et al. 2009).

The APS-2 cloud retrieval products requiring validation are the optical thickness, size distribution parameters, cloud boundaries, and number concentration of droplets. These products can all be validated in liquid water clouds using an *in situ* probe such as the Cloud, Aerosol and Precipitation Spectrometer (CAPS; Baumgardner et al. 2001) that is part of the NASA LaRC B200 *in situ* payload. Measurements of this kind were made on the CIRPAS Twin Otter during the CSTRIPE and RACORO field experiments (Vogelmann et al. 2011) and were used to validate the cloud retrieval products from the RSP (see Appendix E).

Ideally, for validation, the *in situ* measurement platform would fly at the same time as the high altitude UC12 deploying RSP and HSRL so that the *in situ* measurements can be obtained at the altitude, or altitudes, where the bulk of the aerosol burden is located,

thereby maximizing the efficiency of data collection. Although there are other more comprehensive aerosol and cloud *in situ* measurement capabilities (NASA P3, DoE G-1, NASA DC-8, CIRPAS Twin Otter) the NASA LaRC UC12 and B200 offer a combination of remote sensing and *in situ* measurements that can be flown from NASA LaRC sufficiently frequently to obtain statistics for both clear and cloudy scenes that will be adequate to validate the APS-2 products. We therefore regard measurements of this kind as the primary form of validation with larger field campaigns providing a smaller statistical sample with much more complete measurements (e.g., visible/UV absorption, aerosol speciation/composition, CCN).

Validation of ice cloud optical thickness, particle size, shape and roughness, and cloud top pressure will be primarily through participation in large-scale field experiments since specialized aircraft are usually required to reach the altitude of cirrus clouds. Ice cloud particle sizes can be validated using observations from *in situ* sensors, which mitigate ice crystal shattering artifacts, such as the 2D-S instrument (Lawson et al. 2010). Aspect ratios are also measured *in situ* by the cloud particle imager (CPI; Korolev and Isaac 2003). However, these measurements are uncertain due to ice shattering and sampling problems. Also the aspect ratios estimated from CPI images are of the complete crystal, whereas radiative properties and microphysical parameters are mainly determined by the aspect ratios of individual components of complex ice crystals (e.g., the individual bullets of a rosette). Ice crystal roughness is not measured directly by any *in situ* probe, and only a measurement of the ice crystal asymmetry parameter (Gerber 2000) or measurements of scattered light (Ulanowski et al. 2006; Gayet et al. 2011) would provide a validation of this retrieval product.

12. Scientific assessment of orbit options

The technical assessment for the flight of an APS-2 has identified five mission options. We note that if options 4 or 5 were to be selected then it would, in principle, be possible to fly in formation with the European Space Agency (ESA) EarthCARE mission. Therefore, a discussion of the benefits of formation flying with that mission is included in this section.

The options are:

1. Launch into a nominal sun-synchronous (97.4° inclination) orbit at 500 km altitude with no propulsion system to provide control of local crossing time.
2. Launch into a nominal sun-synchronous (97.6° inclination) orbit at 550 km altitude with no propulsion system to provide control of local crossing time.
3. Launch into a nominal sun-synchronous (97.6° inclination) orbit at 550 km altitude with a cold-gas propulsion system to correct for launch injection dispersions and provide control of local crossing time.
4. Launch directly into a sun-synchronous (98.7° inclination) 824 km altitude orbit with a propulsion subsystem to allow for formation flying with NPP.
5. Launch into a 640 km orbit and raise the orbital altitude to 705 km using a propulsion subsystem to allow for formation flying with the A-Train platforms. Include sufficient propellant to allow for a subsequent orbit raise to the NPP orbit.

The first three options that are nominally sun-synchronous, preclude formation flying and have similar scientific value. Launch vehicle dispersions mean that the injection orbits of the first two options are not guaranteed to be circular and may precess in terms of the local time of the equator crossing. The magnitude of these effects based on a worst case (3σ orbital injection dispersions) analysis is ~45 min/year, which means that for an initial injection local crossing time of 13:30 the spatial extent of the available data would be decreasing from launch on with an increasing bias to the summer hemisphere and extremely limited coverage after three years. These mission options allow the primary scientific requirements of an APS-2 mission to be met since the accurate retrieval of aerosol and cloud radiative properties is met by an APS instrument on its own and the value of the retrievals lies in their accuracy. However option 3 to maintain the local crossing time has the substantial advantage that data coverage is uniform throughout the mission and the length of the mission is not compromised.

The fourth option, to formation fly with NPP, has as its focus coordinated measurements with VIIRS and Cross-track Infrared Sounder (CrIS) with the APS-2 satellite flying within 2–3 min of NPP. The VIIRS instrument is expected to have a similar, although somewhat more limited, capability to MODIS. The co-ordination of APS-2 measurements with an imager of this kind allows the use of APS-2 retrievals to improve on the assumptions used in the VIIRS aerosol and cloud algorithms and can also be used to cross-validate VIIRS ocean color retrievals given the close match between the APS-2 and VIIRS ocean color spectral bands. The VIIRS cloud masking capability can also be used to supplement the cloud masking of APS-2 measurements with onboard cloud cameras. CrIS measurements are of interest because of their strong sensitivity to the opacity of dust layers and their height with little sensitivity to biomass burning, or pollution, aerosols that often coexist with dust. The TROPOspheric Monitoring Instrument (TROPOMI; De Vries et al. 2007)) spacecraft is also expected to be flying in formation around 5 minutes behind NPP, and this updated version of the OMI instrument will have the capability to detect UV absorbing aerosols and to retrieve substances such as sulfur dioxide, formaldehyde, nitrogen dioxide, and carbon monoxide that serve as tracers of pollution. For example, formaldehyde–aerosol correlations can provide information on secondary aerosol formation, while SO_2–aerosol correlations can be indicative of anthropogenic influences on aerosols (e.g., Veefkind et al. 2011). However, the primary value of collocating TROPOMI measurements of aerosols with those from APS-2 would be their sensitivity to UV absorption and the oxygen A-band observations that are available on this version of OMI and are sensitive to the vertical distribution of aerosols. These capabilities compliment the APS-2 estimates of absorption that run from the visible to the deep blue. Contrasts between retrievals from both instruments will allow significant issues regarding the relative magnitudes of absorption by organic, or brown, and black carbon to be addressed.

The fifth option, to formation fly within 2–3 min of the Aqua satellite in the A-Train, allows coordinated observations with CALIOP on the CALIPSO satellite, the MODIS and Atmospheric Infrared Sounder (AIRS) instruments on the Aqua satellite, and the OMI and Tropospheric Emission Spectrometer (TES) instruments on the Aura satellite. The additional capability to orbit raise to formation fly with NPP eliminates the risks associated with A-Train instruments failing shortly before, or early in, an APS-2 mission but allows the unique capabilities provided by a lidar to be exploited if they are available. The CALIOP lidar provides, at the most basic level, profiles of attenuated backscatter

and depolarization. These measurements can be used to distribute aerosol opacity in the vertical, thereby reducing uncertainties in the APS-2 retrievals of aerosol absorption. Although APS-2 can provide the height of the top of the aerosol layer, it would also be valuable to have information on whether aerosols exist in single or multiple layers, such as the mixed biomass burning and dust plumes that are present over Africa and the tropical Atlantic each summer. This would allow the aerosol retrieval algorithms to correct for biases (Kalashnikova et al. 2011) caused by the assumption of a single aerosol layer. In addition, the combination of lidar depolarization at cloud top with APS-2 cloud top size distribution retrievals provides a direct, and independent measure of cloud droplet number concentration that is of particular value for the identification of aerosol indirect effects (Hu et al. 2007). The value of coordinated measurements with MODIS is similar to that provided by VIIRS, but with a better ocean color capability, while the aerosol retrievals from OMI and the retrievals of pollutants such as formaldehyde from OMI and CO from TES serve the same purpose as outlined for option 4.

The last two options could also permit flying APS-2 in formation with ESA's EarthCARE mission, which is planned for launch in 2015 into a polar sun-synchronous orbit at a 410-km altitude, with a local crossing time around 2 pm. This mission includes an atmospheric lidar, which would provide similar benefits as CALIOP. It also carries a multispectral imager, somewhat similar to MODIS and VIIRS albeit lacking the short-wavelength bands needed for aerosol and ocean color retrievals, and a cloud profiling radar.

Summary. Formation-flying with a lidar-carrying satellite can provide extremely useful information on where aerosols exist in the atmospheric column that has substantial value in understanding their effects on clouds and allows the profile of radiative heating caused by aerosols to be estimated. The only concern with formation flying in the A-Train is that the CALIPSO mission may no longer be in the A-Train by the time an APS-2 is launched because of lack of propellant to maintain station keeping beyond the 2016 A-Train inclination maneuver (Ferrier et al. 2010). It is highly probable that MODIS Aqua will be capable of providing cloud detection/masking and properties beyond 2018 but ocean color and aerosol retrieval quality beyond 2016 is likely to degrade (Platnick and Xiong 2011). The issue with formation flying with EarthCARE is that the mission may not have launched by the time an APS-2 mission is launched and will only have a short lifetime because of its low altitude orbit.

Formation flying an APS-2 mission with NPP has significant benefits, and it is expected that the instrument suite would still be performing well by the time an APS-2 was launched. An APS-2 flying on its own with cloud cameras to provide cloud clearing can provide the primary aerosol products that are required for a better estimate of the radiative effects of aerosols and, with the availability of a propulsion system, could provide data for an extended period (5–10 years). An APS-2 mission without a propulsion system has a 99% probability of lasting 3 years if successfully launched but is not likely to have an extended life because of launch dispersions causing a precession of the orbit.

13. APS-2 delivers critical information for policy makers

Among NASA's major objectives is the study of the Earth system from space to advance scientific understanding and meet societal needs. To address this charge and to respond to

the Decadal Survey vision of an integrated Earth science program that emphasizes both scientific advance and societal benefits, one must consider the role of atmospheric aerosol observations in the development and implementation of national policies to address the challenges of regional and global Earth-system changes.

When originally approved, the Glory APS was an aerosol-science priority with clear relevance to future national policy. Today, APS-2 measurements remain a high-priority aerosol and climate science need and have risen in both relevancy and urgency to national policy. It is now widely acknowledged that lack of understanding of the role of aerosols in the Earth system limits the degree to which climate sensitivity (i.e., warming at the surface from a doubling of CO_2) can be inferred observationally. Aerosol emissions from fossil fuel use in China, India, and other rapidly developing countries have grown dramatically in the past decade, and there are increasingly large uncertainties in their contributions to the buildup of atmospheric aerosol and its climate and ecological effects.

By providing unprecedented capability to discriminate between natural and man-made aerosols globally, APS-2 is uniquely positioned to yield essential information on the anthropogenic component of Earth-system changes.

For instance, APS-2 observations could contribute to fossil fuel use verification and quantification efforts by providing specific regional information on aerosol emissions derived from fossil fuel inventories and, especially, on their short- and long-term trends. As the US government considers mechanisms to address climate change through limiting fossil fuel use, reliable and independent global measurements of man-made atmospheric aerosol will fulfill critical policy needs.

14. Conclusions

Advances in Earth-system science have intensified the need for accurate global observations of detailed aerosol properties from space. The unfortunate loss of the Glory APS delays delivery of much of these critical data. This instrument was conceived to address fundamental aerosol science questions with policy relevance. The science questions remain unanswered and have since grown in complexity, as APS measurements are now viewed as essential in providing the scientific basis for evolving national climate policies.

There have been substantial advances in space-based aerosol observation capabilities during the past decade. However, no other existing or confirmed satellite sensor can provide the measurements needed to significantly improve estimates of the aerosol effects on the Earth system and their anthropogenic components.

Recent sensitivity studies and analyses of RSP and POLDER data have yielded a much improved understanding of the expected retrieval capabilities of APS. They reinforced the criticality of many design features of APS and demonstrated its potential ability to yield important aerosol information in partially and even completely cloudy pixels. Furthermore, it has become clear that APS can provide key information about liquid-water, cirrus, and mixed-phase clouds as well as about stratospheric aerosols in the case of a major volcanic eruption during the life-time of the instrument. The accumulated body of evidence confirms that, in conjunction with other ground-, air-, and space-based assets and advanced process and climate models, the Glory APS would have met its main objectives. If launched successfully, it would have also demonstrated a methodology

ideal for future long-term monitoring of atmospheric aerosols and their effects on the Earth system and climate.

Meeting the outstanding and near-future science and policy imperatives on the needed time scale can only be accomplished by launching an APS rebuild on a fast-track schedule that capitalizes on the project's assets and innovations and adds value to other missions. Importantly, extensive pre-flight tests of the Glory APS have demonstrated a remarkable robustness of its design. The actual performance of the Glory APS was found to be fully consistent with original technical specifications and in many cases exceeded them considerably. This provides a strong argument in favor of rebuilding and reflying a near-carbon copy of the Glory APS.

APS-2 is uniquely designed to achieve the following critical science objectives with policy relevance:

- provide long-term global and regional monitoring of essential aerosol properties in clear-sky conditions as well as above and between clouds;
- provide detailed aerosol information needed for improvement and validation of process and climate models;
- provide long-term global and regional monitoring of essential cloud properties;
- provide long-term global and regional monitoring of stratospheric aerosols caused by major volcanic eruptions;
- provide refined aerosol and cloud representations for use in various remote-sensing retrievals, thereby allowing improvements in aerosol and cloud assessments by other operational satellite instruments.

At the direction from NASA HQ, the Glory APS team performed a quick assessment to determine what it would take to replace the APS capabilities. They found that the fastest approach would be to produce and launch a build-to-print copy of the instrument. With a start date in August 2011, a carbon copy of APS could be ready for launch in about 30 months. With a July 2015 launch date, the APS-2 science team could begin delivering an aerosol–cloud data product in the fall of 2015.

APS-2 has the requisite characteristics to be the vanguard aerosol–cloud satellite instrument for the period 2015–2020. It would add critically important information and make a bridge to advanced aerosol–cloud missions of the future.

References

Abel, S. J., J. M. Haywood, E. J. Highwood, J. Li, and P. R. Buseck, 2003: Evolution of biomass burning aerosol properties from an agricultural fire in southern Africa. *Geophys. Res. Lett.* **30**, 1783.

Ackerman, A. S., O. B. Toon, D. E. Stevens, A. J. Heymsfield, V. Ramanathan, and E. J. Welton, 2000: Reduction of tropical cloudiness by soot. *Science* **288**, 1042–1047.

Ackerman, A. S., O. B. Toon, D. E. Stevens, and J. A. Coakley, Jr., 2003: Enhancement of cloud cover and suppression of nocturnal drizzle in stratocumulus polluted by haze. *Geophys. Res. Lett.* **30**, 1381.

Ackerman, A. S., M. P. Kirkpatrick, D. E. Stevens, and O. B. Toon, 2004: The impact of humidity above stratiform clouds on indirect aerosol climate forcing. *Nature* **432**, 1014–1017.

Al-Saadi, J., J. Szykman, R. B. Pierce, C. Kittaka, D. Neil, D. A. Chu, L. Remer, L. Gumley, E. Prins, L.Weinstock, C. MacDonald, R. Wayland, F. Dimmick, and J. Fishman, 2005: Improving national air quality forecasts with satellite aerosol observations. *Bull. Amer. Meteorol. Soc.* **86**, 1249–1261.

Baker, M., 1997: Cloud microphysics and climate: tropospheric processes. *Science* **276**, 1072–1078.

Baran, A. J., and L. C. Labonnote, 2006: On the reflection and polarisation properties of ice cloud. *J. Quant. Spectrosc. Radiat. Transfer* **100**, 41–54.

Baran, A. J., 2009*:* A review of the light scattering properties of cirrus*. J. Quant. Spectrosc. Radiat. Transfer* **110**, 1239–1260.

Bauer, S. E., D. Koch, N. Unger, S. M. Metzger, D. T. Shindell, and D. G. Streets, 2007: Nitrate aerosols today and in 2030: a global simulation including aerosols and tropospheric ozone. *Atmos. Chem. Phys.* **7**, 5043–5059.

Bauer, S. E., D. L. Wright, D. Koch, E. R. Lewis, R. McGraw, L.-S. Chang, S. E. Schwartz, and R. Ruedy, 2008: MATRIX (Multiconfiguration Aerosol TRacker of mIXing state): an aerosol microphysical module for global atmospheric models. *Atmos. Chem. Phys*. **8**, 6003–6035.

Bauer, S. E., S. Menon, D. Koch, T. C. Bond, and K. Tsigaridis, 2010: A global modeling study on carbonaceous aerosol microphysical characteristics and radiative effects. *Atmos. Chem. Phys.* **10**, 7439–7456.

Baum, B. A., P. Yang, Y.-X. Hu , and Q. Feng, 2010: The impact of ice particle roughness on the scattering phase matrix. *J. Quant. Spectrosc. Radiant. Transfer* **111**, 2534–2549.

Baum, B. A., P. Yang, A. J. Heymsfield, C. Schmitt, Y. Xie, A. Bansemer, Y.-X. Hu, and Z. Zhang, 2011: Improvements to shortwave bulk scattering and absorption models for the remote sensing of ice clouds. *J. Appl. Meteorol. Climatol.* **50**, 1037–1056.

Baumgardner, D., H. Jonsson, W. Dawson, D. O'Connor, and R. Newton, 2001: The cloud, aerosol and precipitation spectrometer (CAPS): A new instrument for cloud investigations. *Atmos. Res*. **59**, 251–264.

Benedetti, A., J.-J. Morcrette, O. Boucher, A. Dethof, R. J. Engelen, M. Fisher, H. Flentje, N. Huneeus, L. Jones, J. W. Kaiser, S. Kinne, A. Mangold, M. Razinger, A. J. Simmons, and M. Suttie, 2009: Aerosol analysis and forecast in the European Centre for Medium-Range Weather Forecasts Integrated Forecast System: 2. Data assimilation. *J. Geophys. Res*. **114**, D13205.

Bennartz, R. 2007: Global assessment of marine boundary layer cloud droplet number concentration from satellite. *J. Geophys. Res.* **112**, D02201.

Bergstrom, R. W., K. S. Schmidt, O. Coddington, P. Pilewskie, H. Guan, J. Livingston, J. Redemann, and P. B. Russell, 2010: Aerosol spectral absorption in the Mexico City area: results from airborne measurements during MILAGRO/INTEX B. *Atmos. Chem. Phys.* **10**, 6333–6343.

Bian, H., M. J. Prather, and T. Takemure, 2003: Tropospheric aerosol impacts on trace gas budgets through photolysis. *J. Geophys. Res.* **108**, 4242.

Boers, R., J. R. Acarreta, and J. L. Gras, 2006: Satellite monitoring of the first indirect aerosol effect:

retrieval of the droplet concentration of water clouds. *J. Geophys. Res*. **111,** D22208.

Bond, T. C., and R. W. Bergstrom, 2006: Light absorption by carbonaceous particles: an investigative review. *Aerosol Sci. Technol.* **40**, 27–67.

Bony, S., and J.-L. Dufresne, 2006: Marine boundary layer clouds at the heart of tropical cloud feedback uncertainties in climate models. *Geophys. Res. Lett.* **32**, 20806.

Brenguier, J.-L., T. Bourrianne, A. A. Coelho, J. Isbert, R. Peytavi, D. Trevarin, and P. Weschler, 1998: Improvements of droplet size distribution measurements with the Fast-FSSP (Forward Scattering Spectrometer Probe). *J. Atmos. Oceanic Technol.* **15**, 1077–1090.

Brenguier, J.-L., H. Pawlowska, and L. Schüller, 2003: Cloud microphysical and radiative properties for parameterization and satellite monitoring of the indirect effect of aerosol on climate. *J. Geophys. Res.* **108**, 8632.

Bréon, F.-M., and B. Dubrulle, 2004: Horizontally oriented plates in clouds. *J. Atmos.Sci.* **61**, 2888–2898.

Bréon, F. M., and P. Goloub, 1998: Cloud droplet effective radius from spaceborne polarization measurements. *Geophys. Res. Lett.* **25**, 1879–1882.

Bréon, F. M., D. Tanré, P. Lecomte, and M. Herman, 1995: Polarized reflectance of bare soils and vegetation: measurements and models. *IEEE Trans. Geosci. Remote Sens.* **33**, 487–499.

Brioude, J., O. R. Cooper, G. Feingold, M. Trainer, S. R. Freitas, D. Kowal, J. K. Ayers, E. Prins, P. Minnis, S. A. McKeen, G. J. Frost, and E.-Y. Hsie, 2009: Effect of biomass burning on marine stratocumulus clouds off the California coast. *Atmos. Chem. Phys.* **9**, 8841–8856.

Bruegge, C. J., N. L. Chrien, R. R. Ando, D. J. Diner, W. A. Abdou, M. C. Helmlinger, S. H. Pilorz, and K. J. Thome, 2002: Early validation of the Multi-angle Imaging SpectroRadiometer (MISR) radiometric scale. *IEEE Trans. Geosci. Remote Sens.* **40**, 1477–1492.

Bruegge, C. J., D. J. Diner, R. A. Kahn, N. Chrien, M. C. Helmlinger, B. J. Gaitley, W. A. Abdou, 2007: The MISR radiometric calibration process. *Remote Sens. Environ.* **107**, 2–11.

Cairns, B., and I. Geogdzhayev, 2010: Aerosol Polarimetry Sensor calibration theoretic basis document (glory.giss.nasa.gov/aps/docs/APS_ATBD_CALIBRATE_CCB.pdf).

Cairns, B., E. E. Russell, J. D. LaVeigne, and P. MW. Tennant, 2003: Research scanning polarimeter and airborne usage for remote sensing of aerosols. *Proc. SPIE* **5158**, 33–44.

Cairns, B., A. A. Lacis, B. E. Carlson, K. Knobelspiesse, M. Alexandrov, 2009a: Inversion of multi-angle radiation measurements. In *International Conference on Mathematics, Computational Methods & Reactor Physics,* Saratoga, NY.

Cairns, B., F. Waquet, K. Knobelspiesse, J. Chowdhary, and J. L. Deuzé, 2009b: Polarimetric remote sensing of aerosols over land surfaces. In Kokhanovsky, A. A., and G. de Leeuw, Eds., *Satellite Aerosol Remote Sensing Over Land*. Springer, Chichester, UK, pp. 295–325.

Cakmur, R. V., R. L. Miller, and O. Torres, 2004: Incorporating the effect of small-scale circulations upon dust emission in an atmospheric general circulation model. *J. Geophys. Re*s. **109**, D07201.

Chen, Y., and J. E. Penner, 2005: Uncertainty analysis for estimates of the first indirect aerosol effect. *Atmos. Chem. Phys.* **5**, 2935–2948.

Chepfer, H., G. Brogniez, P. Goloub, F. Bréon, and P. Flamant, 1999: Observations of horizontally oriented ice crystals in cirrus clouds with POLDER-1/ADEOS-1. *J. Quant. Spectrosc. Radiat. Transfer* **63**, 521–543.

Chepfer, H., P. Goloub, J. Riedi, J. De Haan, J. Hovenier, and P. Flamant, 2001: Ice crystal shapes in cirrus clouds derived from POLDER/ADEOS-1. *J. Geophys. Res*. **106**, 7955–7966.

Chin, M., R. A. Kahn, and S. E. Schwartz, Eds., 2009a: *Atmospheric Aerosol Properties and Climate Impacts*. U.S. Climate Change Science Program, Washington, DC.

Chin, M., T. Diehl, O. Dubovik, T. F. Eck, B. N. Holben, A. Sinyuk, and D. G. Streets, 2009b: Light absorption by pollution, dust and biomass burning aerosols: A global model study and evaluation

with AERONET data. *Ann. Geophys.* **27**, 3439–3464.

Cho, H.-M., S. L. Nasiri, and P. Yang, 2009: Application of CALIOP measurements to the evaluation of cloud phase derived from MODIS infrared channels. *J. Appl. Meteorol. Climatol.* **48**, 2169–2180.

Chowdhary, J., B. Cairns, and L. D. Travis, 2002: Case studies of aerosol retrievals over the ocean from multiangle, multispectral photopolarimetric remote sensing data. *J. Atmos. Sci.* **59**, 383–397.

Chowdhary, J., B. Cairns, M. I. Mishchenko, P. V. Hobbs, G. F. Cota, J. Redemann, K. Rutledge, B. N. Holben, and E. Russell, 2005: Retrieval of aerosol scattering and absorption properties from photopolarimetric observations over the ocean during the CLAMS experiment. *J. Atmos. Sci.* **62**, 1093–1118.

Chowdhary, J., B. Cairns, and L. Travis, 2006: Contribution of water-leaving radiances to multiangle, multispectral polarimetric observations over the open ocean: bio-optical model results for case 1 waters. *Appl. Opt.* **45**, 5542–5567.

Chowdhary, J., B. Cairns, F. Waquet, K. Knobelspiesse, M. Ottaviani, J. Redemann, L. Travis, and M. Mishchenko, 2011: Sensitivity of multiangle, multispectral polarimetric remote sensing over open ocean to water-leaving radiance: analyses of RSP data acquired during the MILAGRO campaign. *Remote Sens. Environ.*, in revision.

Chung, S. H., and J. H. Seinfeld, 2002: Global distribution and climate forcing of carbonaceous aerosols. *J. Geophys. Res.* **107**, 4407.

Chung, C. E., V. Ramanathan, D. Kim, and I. A. Podgorny, 2005: Global anthropogenic aerosol direct forcing derived from satellite and ground-based observations. *J. Geophys. Res.* **110**, D24207.

Chýlek, P., B. G. Henderson, and G. Lesins, 2005: Aerosol optical depth retrieval over the NASA Stennis Space Center: MTI, MODIS, and AERONET. *IEEE Trans. Geosci. Remote Sens.* **43**, 1978–1983.

Clarke, A., C. McNaughton, V. Kapustin, Y. Shinozuka, S. Howell, J. Dibb, J. Zhou, B. Anderson, V. Brekhovskikh, and H. Turner, 2007: Biomass burning and pollution aerosol over North America: organic components and their influence on spectral optical properties and humidification response. *J. Geophys. Res*. **112**, D12S18.

Coakley, J. A., Jr., R. L. Bernstein, and P. A. Durkee, 1987: Effect of ship-stack effluents on cloud reflectivity. *Science* **237,** 1020–1022.

Coakley, J. A., Jr., and C. D. Walsh, 2002: Limits to the aerosol indirect radiative effect derived from observations of ship tracks. *J. Atmos. Sci*. **59**, 668– 680.

Coddington, O., P. Pilewskie, J. Redemann, S. Platnick, P. Russell, K. Schmidt, W. Gore, J. Livingston, G. Wind, and T. Vukicevic, 2010: Examining the impact of overlying aerosols on the retrieval of cloud optical properties from passive remote sensing. *J. Geophys. Res.* **115**, D10211.

Colarco, P., A. daSilva, M. Chin, and T. Diehl, 2010: Online simulations of global aerosol distributions in the NASA GEOS-4 model and comparisons to satellite and ground-based aerosol optical depth *J. Geophys. Res.* **115**, D14207.

Coulson, K. L., 1988: *Polarization and Intensity of Light in the Atmosphere*. Deepak Publishing, Hampton, VA.

Cox, C., and W. Munk, 1954: Measurement of the roughness of the sea surface from photographs of the sun's glitter. *J. Opt. Soc. Am.* **44**, 838–850.

De Graaf, M., P. Stammes, and I. Aben 2007: Analysis of reflectance spectra of UV-absorbing aerosol scenes measured by SCIAMACHY. *J. Geophys. Res*. **112**, D02206.

De Haan, J. F., P. B. Bosma, and J. W. Hovenier, 1987: The adding method for multiple scattering calculations of polarized light. *Astron. Astrophys.* **183**, 371–391.

De Vries, J., E. C. Laan, R. V. M. Hoogeveen, R. T. Jongma, I. Aben, H. Visser, E. Boslooper, H. Saari, M. Dobber, P. Veefkind, Q. Kleipool, and P. F. Levelt, 2007: TROPOMI: solar backscatter satellite instrument for air quality and climate. *Proc. SPIE* **6744**, 674409.

DeMott, P. J., A. J. Prenni, X. Liu, S. M. Kreidenweis, M. D. Petters, C. H. Twohy, M. S. Richardson, T. Eidhammer, and D. C. Rogers, 2010: Predicting global atmospheric ice nuclei distributions and their impacts on climate. *Proc. Natl. Acad. Sci. USA* **107**, 11217–11222.

Diner, D., J. Beckert, T. Reilly, C. J. Bruegge, J. E. Conel, R. A. Kahn, J. V. Martonchik, T. P. Ackerman, R. Davies, S. A. W. Gerstl, H. R. Gordon, J.-P. Muller, R. B. Myneni, P. J. Sellers, B. Pinty, and M. M. Verstraete, 1998: Multiangle Imaging SptectrRadiometer (MISR) description and experiment overview. *IEEE Trans. Geosci. Remote Sens.* **36**, 1072–1087.

Dinh, T. P., D. R. Durran, and T. P. Ackerman, 2010: Maintenance of tropical tropopause layer cirrus. *J. Geophys. Res.* **115**, D02104.

Dubovik, O., and M. D. King, 2000: A flexible inversion algorithm for retrieval of aerosol optical properties from Sun and sky radiance measurements. *J. Geophys. Res.* **105**, 20673–20696.

Dubovik, O., B. Holben, T. F. Eck, A. Smirnov, Y. J. Kaufman, M. D. King, D. Tanré, and I. Slutsker 2002: Variability of absorption and optical properties of key aerosol types observed in worldwide locations. *J. Atmos. Sci*. **59**, 590–608.

Dubovik, O., A. Sinyuk, T. Lapyonok, B. N. Holben, M. Mishchenko, P. Yang, T. F. Eck, H. Volten, O. Muñoz, B. Veihelmann, W. J. van der Zande, J.-F. Leon, M. Sorokin, and I. Slutsker, 2006: Application of spheroid models to account for aerosol particle nonsphericity in remote sensing of desert dust. *J. Geophys. Res.* **111**, D11208.

Dubovik, O., M. Herman, A. Holdak, T. Lapyonok, D. Tanré, J. L. Deuzé, F. Ducos, A. Sinyuk, and A. Lopatin, 2011: Statistically optimized inversion algorithm for enhanced retrieval of aerosol properties from spectral multi-angle polarimetric satellite observations. *Atmos. Meas. Tech.* **4**, 975–1018.

Dunagan, S., R. Johnson, J. Zavaleta, R. Walker, C. Chang, P. Russell, B. Schmid, C. Flynn, J. Redemann, and J. Livingston, 2011: 4STAR spectrometer for sky-scanning sun-tracking atmospheric research: instrument technology development. 34th International Symposium on Remote Sensing of Environment, Sydney, Australia, 10–15 April 2011.

Earth Science, 2007: *Earth Science and Applications from Space: National Imperatives for the Next Decade and Beyond*. National Academies Press, Washington, DC.

Edie, W. T., D. Dryard, F. E. James, M. Roos, and B. Sadoulet, 1971: *Statistical Methods in Experimental Physics*. North Holland, New York.

Emde, C., and B. Mayer, 2007: Simulation of solar radiation during a total eclipse: a challenge for radiative transfer. *Atmos. Chem. Phys*. **7**, 2259–2270.

Emde, C., R. Buras, B. Mayer, and M. Blumthaler, 2010: The impact of aerosols on polarized sky radiance: model development, validation, and applications. *Atmos. Chem. Phys*. **10**, 383–396.

Engel-Cox, J. A., C. H. Holloman, B. W. Coutant, and R. M. Hoff, 2004: Qualitative and quantitative evaluation of MODIS satellite sensor data for regional and urban scale air quality. *Atmos. Environ.* **38**, 2495−2509.

Ervens, B., and R. Volkamer, 2010: Glyoxal processing by aerosol multiphase chemistry: towards a kinetic modeling framework of secondary organic aerosol formation in aqueous particles. *Atmos. Chem. Phys.* **10**, 8219–8244.

Fan, J., R. Zhang, W.-K. Tao, and K. I. Mohr, 2008: Effects of aerosol optical properties on deep convective clouds and radiative forcing. *J. Geophys. Res.* **113**, D08209.

Feingold, G., 2003: Modeling of the first indirect effect: analysis of measurement requirements. *Geophys. Res. Lett.* **30**, 1997.

Feingold, G., H. Jiang, and J. Y. Harrington, 2005: On smoke suppression of clouds in Amazonia. *Geophys. Res. Lett.* **32**, L02804.

Ferrier, C., D. MacDonnell, and N. Queruel, 2010: CALIPSO longevity projections. Presentation to the A-Train Mission Operations Working Group, February 2010.

Field, P. R., A. J. Heymsfield, and A. Bansemer, 2006: Shattering and particle interarrival times

measured by optical array probes in ice clouds. *J. Atmos. Oceanic Technol.* **23**, 1357–1371.

Forster, P., and Coauthors, 2007a: Changes in atmospheric constituents and in radiative forcing. In Solomon, S., et al., Eds., *Climate Change 2007: The Physical Science Basis*. Cambridge Univ. Press, Cambridge, UK, pp. 129–234.

Forster, P., G. Hegerl, R. Knutti, V. Ramaswamy, S. Solomon, T. F. Stocker, P. Stott, and F. Zwiers, 2007b: Assessing uncertainty in climate simulations. *Nature Rep. Clim. Change*, doi:10.1038/climate.2007.46a.

Fountoukis, C., and A. Nenes, 2007: ISORROPIA II: a computationally efficient thermodynamic equilibrium model for K^+–Ca^{2+}–Mg^{2+}–NH_4^+–Na^+–SO_4^{2-}–NO_3^-–Cl^-–H_2O aerosols. *Atmos. Chem. Phys*. **7**, 4639–4659.

Fowler, L. D., D. A. Randall, and S. A. Rutledge, 1996: Liquid and ice cloud microphysics in the CSU general circulation model. Part 1: Model description and simulated microphysical processes. *J. Clim.* **9**, 489–529.

Fridlind, A. M., and A. S. Ackerman, 2011: Estimating the sensitivity of radiative impacts of shallow, broken marine clouds to boundary layer aerosol size distribution parameter uncertainties for evaluation of satellite retrieval requirements. *J. Atmos. Oceanic Technol.* **28**, 530–538.

Fridlind, A. M., A. S. Ackerman, E. J. Jensen, A. J. Heymsfield, M. R. Poellot, D. E. Stevens, D. Wang, L. M. Miloshevich, D. Baumgardner, R. P. Lawson, J. C. Wilson, R. C. Flagan, J. H. Seinfeld, H. H. Jonsson, T. M. VanReken, V. Varutbangkul, and T. A. Rissmanet, 2004: Evidence for the predominance of mid-tropospheric aerosols as subtropical anvil cloud nuclei. *Science* **304**, 718–722.

Fu, Q., 2007: A new parameterization of an asymmetry factor of cirrus clouds for climate models. *J. Atmos. Sci.* **64**, 4140–4150.

Gantt, B., N. Meskhidze, M. C. Facchini, M. Rinaldi, D. Ceburnis, and C. O'Dowd, 2011: Wind speed dependent size-resolved parameterization for the organic enrichment of sea spray. *Atmos. Chem. Phys. Discuss*. **11**, 10525–10555.

Gao, B. C., A. F. H. Goetz, and W. J. Wiscombe, 1993: Cirrus cloud detection from airborne imaging spectrometer data using the 1.38 μm water vapor band. *Geophys. Res. Lett.* **20**, 301–304.

Garrett, T. J., H. Gerber, D. G. Baumgardner, C. H. Twohy, and E. M. Weinstock, 2003: Small, highly reflective ice crystals in low-latitude cirrus. *Geophys. Res. Letts*. **30**, 2132–2136.

Gatebe, C. K., M. D. King, S. Tsay, Q. Ji, G. T. Arnold, and J. Y. Li, 2001: Sensitivity of off-nadir zenith angles to correlation between visible and near-infrared reflectance for use in remote sensing of aerosol over land. *IEEE Trans. Geosci. Remote Sens.* **39**, 805–818.

Gayet, J.-F., G. Mioche, V. Shcherbakov, C. Gourbeyre, R. Busen, and A. Minikin, 2011: Optical properties of pristine ice crystals in mid-latitude cirrus clouds: a case study during CIRCLE-2 experiment. *Atmos. Chem. Phys*. **11**, 2537–2544.

Gerber, H., Y. Takano, T. J. Garrett, and P. V. Hobbs, 2000: Nephelometer measurements of the asymmetry parameter, volume extinction coefficient, and backscatter ratio in Arctic clouds. *J. Atmos. Sci.* **57**, 3021–3034.

Ghan, S. J., and S. E. Schwartz, 2007: Aerosol properties and processes: A path from field and laboratory measurements to global climate models. *Bull. Amer. Meteorol. Soc*. **88**, 1059–1083.

Ghan, S. J., and R. A. Zaveri, 2007: Parameterization of optical properties for hydrated internally mixed aerosol. *J. Geophys. Res.* **112**, D10201.

Goloub, P., J. L. Deuzé, M. Herman, and Y. Fouquart, 1994: Analysis of the POLDER polarization measurements performed over cloud covers. *IEEE Trans. Geosci. Remote Sens.* **32,** 78–88.

Goloub, P., M. Herman, H. Chepfer, J. Riedi, G. Brogniez, P. Couvert, and G. Seze, 2000: Cloud thermodynamical phase classification from the POLDER spaceborne instrument. *J. Geophys. Res.* **105**, 14747–14759.

Hair, J. W., C. A. Hostetler, A. L. Cook, D. B. Harper, R. A. Ferrare, T. L. Mack, W. Welch, L. R.

Izquierdo, and F. E. Hovis, 2008: Airborne High Spectral Resolution Lidar for profiling aerosol optical properties. *Appl. Opt.* **47**, 6734–6752.

Hansen, J., and L. D. Travis, 1974: Light scattering in planetary atmospheres. *Space Sci. Rev.* **16**, 527–610.

Hansen, J., A. Lacis, R. Ruedy, and M. Sato, 1992: Potential climate impact of Mount Pinatubo eruption. *Geophys. Res. Lett.* **19**, 215–218.

Hansen, J., M. Sato, and R. Ruedy, 1997: Radiative forcing and climate response. *J. Geophys. Res*. **102**, 6831–6864.

Hansen, J., W. Rossow, B. Carlson, A. Lacis, L. Travis, A. Del Genio, I. Fung, B. Cairns, M. Mishchenko, and M. Sato, 1995: Low-cost long-term monitoring of global climate forcings and feedbacks. *Climatic Change* **31**, 247–271.

Hansen, J., Mki. Sato, A. Lacis, R. Ruedy, I. Tegen, and E. Matthews, 1998: Perspective: climate forcings in the industrial era. *Proc. Natl. Acad. Sci. USA* **95**, 12753–12758.

Hansen, J., L. Nazarenko, R. Ruedy, Mki. Sato, J. Willis, A. Del Genio, D. Koch, A. Lacis, K. Lo, S. Menon, T. Novakov, Ju. Perlwitz, G. Russell, G. A. Schmidt, and N. Tausnev, 2005: Earth's energy imbalance: confirmation and implications. *Science* **308**, 1431–1435.

Hansen, J., R. Ruedy, Mki. Sato, and K. Lo, 2010: Global surface temperature change. *Rev. Geophys.* **48**, RG4004.

Hansen, J., Mki. Sato, P. Kharecha, and K. von Schuckmann, 2011: Earth's energy imbalance and implications. *arXiv.org*, 1105.1140.

Hartmann, D. L., J. R. Holton, and Q. Fu, 2001: The heat balance of the tropical tropopause, cirrus, and stratospheric dehydration. *Geophys. Res. Lett.* **28**, 1969– 1972.

Hasekamp, O. P., 2010: Capability of multi-viewing-angle photo-polarimetric measurements for the simultaneous retrieval of aerosol and cloud properties. *Atmos. Meas. Tech.* **3**, 839–851.

Hasekamp, O. P., and J. Landgraf, 2005a: Retrieval of aerosol properties over the ocean from multispectral single-viewing-angle measurements of intensity and polarization: retrieval approach, information content, and sensitivity study. *J. Geophys. Res.* **110**, D20207.

Hasekamp, O. P., and J. Landgraf, 2005b: Linearization of vector radiative transfer with respect to aerosol properties and its use in satellite remote sensing. *J. Geophys. Res.* **110**, D04203.

Hasekamp, O., and J. Landgraf, 2007: Retrieval of aerosol properties over land surfaces: capabilities of multiple-viewing-angle intensity and polarization measurements. *Appl. Opt.* **46**, 3332–3344.

Hasekamp, O., P. Litvinov, and A. Butz, 2011: Aerosol properties over the ocean from PARASOL multi-angle photopolarimetric measurements. *J. Geophys. Res*., doi:10.1029/ 2010JD015469.

Haywood, J., D. Roberts, A. Slingo, J. Edwards, and K. Shine, 1997: General circulation model calculations of the direct radiative forcing by anthropogenic sulfate and fossil-fuel soot aerosol. *J. Clim.* **10**, 1562–1577.

Hegerl, G. C., and Coauthors, 2007: Understanding and attributing climate change. In Solomon, S., et al., Eds., *Climate Change 2007: The Physical Science Basis*. Cambridge Univ. Press, Cambridge, UK, pp. 663–745.

Herman, M., J.-L. Deuzé, A. Marchant, B. Roger, and P. Lallart, 2005: Aerosol remote sensing from POLDER/ADEOS over the ocean: improved retrieval using a non-spherical particle model. *J. Geophys Res.* **110**, D10S02.

Higurashi, A., and T. Nakajima, 1999: Development of a two-channel aerosol retrieval algorithm on a global scale using NOAA AVHRR. *J. Atmos. Sci.* **56**, 924–941.

Hoff, R., H. Zhang, N. Jordan, A. Prados, J. Engel-Cox, A. Huff, S. Weber, E. Zell, S. Kondragunta, J. Szykman, B. Johns, F. Dimmick, A. Wimmers, J. Al-Saadi, and C. Kittaka, 2009: Application of the Three-Dimensional Air Quality System (3D-AQS) to Western U.S. air quality: IDEA, Smog Blog, Smog Stories, AirQuest, and the Remote Sensing Information Gateway. *J. Air Waste Man-*

age. Assoc. **59**, 980–989.

Holben, B. N., T. F. Eck, I. Slutsker, D. Tanré, J. P. Buis, A. Setzer, E. Vermote, J. A. Reagan, Y. J. Kaufman, T. Nakajima, F. Lavenu, I. Jankowiak, and A. Smirnov, 1998: AERONET – a federated instrument network and data archive for aerosol characterization. *Remote Sens. Environ.* **66**, 1–16.

Holton, J. R., and A. Gettelman, 2001: Horizontal transport and the dehydration of the stratosphere. *Geophys. Res. Lett.* **28**, 2799–2802.

Hoose, C., U. Lohmann, R. Erdin, and I. Tegen, 2008: The global influence of dust mineralogical composition on heterogeneous ice nucleation in mixed-phase clouds. *Environ. Res. Lett.* **3**, 025003.

Hsu, N. C., S.-C. Tsay, M. D. King, and J. R. Herman, 2004: Aerosol properties over bright-reflecting source regions. *IEEE Trans. Geosci. Remote Sens.* **42**, 557–569.

Hu, Y., M. Vaughan, C. McClain, M. Behrenfeld, H. Maring, D. Anderson, S. Sun-Mack, D. Flittner, J. Huang, B. Wielicki, P. Minnis, C. Weimer, C. Trepte, and R. Kuehn, 2007: Global statistics of liquid water content and effective number concentration of water clouds over ocean derived from combined CALIPSO and MODIS measurements. *Atmos. Chem. Phys*. **7**, 3353–3359.

Ichoku, C., L. A. Remer, and T. F. Eck, 2005: Quantitative evaluation and intercomparison of morning and afternoon Moderate Resolution Imaging Spectroradiometer (MODIS) aerosol measurements from Terra and Aqua. *J. Geophys. Res.* **110**, D10S03.

Ignatov, A., and L. Stowe, 2002: Aerosol retrievals from individual AVHRR channels: I. Retrieval algorithm and transition from Dave to 6S radiative transfer model. *J. Atmos. Sci.* **59**, 313–334.

IPCC, 2007: Summary for policymakers. In: Solomon, S., D. Qin, M. Manning, Z. Chen, M. Marquis, K. B. Averyt, M. Tignor, and H. L. Miller, Eds., *Climate Change 2007: The Physical Science Basis*. Cambridge Univ. Press, Cambridge, UK.

Jacob, D. J., J. H. Crawford, H. Maring, A. D. Clarke, J. E. Dibb, L. K. Emmons, R. A. Ferrare, C. A. Hostetler, P. B. Russell, H. B. Singh, A. M. Thompson, G. E. Shaw, E. McCauley, J. R. Pederson, and J. A. Fisher, 2010: The Arctic Research of the Composition of the Troposphere from Aircraft and Satellites (ARCTAS) mission: design, execution, and first results. *Atmos. Chem. Phys*. **10**, 5191–5212.

Jaggard, D. L, C. Hill, R. W. Shorthill, D. Stuart, M. Glantz, F. Rosswog, B. Taggards, and S. Hammond, 1981: Light scattering from particles of regular and irregular shape. *Atmos. Environ.* **15**, 2511–2519.

Jathar, S. H., S. C. Farina, A. L. Robinson, and P. J. Adams, 2011: The influence of semi-volatile and reactive primary emissions on the abundance and properties of global organic aerosol. *Atmos. Chem. Phys. Discuss.* **11**, 5493–5540.

Jensen, E. J., O. B. Toon, H. B. Selkirk, J. D. Spinhirne, and M. R. Schoeberl, 1996a: On the formation and persistence of subvisible cirrus clouds near the tropical tropopause. *J. Geophys. Res.* **101**, 21361–21375.

Jensen, E. J., O. B. Toon, L. Pfister, and H. B. Selkirk, 1996b: Dehydration of the upper troposphere and lower stratosphere by subvisible cirrus clouds near the tropical tropopause. *Geophys. Res. Lett.* **23**, 825–828.

Jensen, E. J., P. Lawson, B. Baker, B. Pilson, Q. Mo, A. J. Heymsfield, A. Bansemer, T. P. Bui, M. McGill, D. Hlavka, G. Heymsfield, S. Platnick, G. T. Arnold, and S. Tanelli, 2009: On the importance of small ice crystals in tropical anvil cirrus. *Atmos. Chem. Phys.* **9**, 5519–5537.

Johnson, B. T., 2005: The semi-direct aerosol effect: comparison of a single-column model with large eddy simulation for marine stratocumulus. *J. Clim.* **18**, 119–130.

Kahn, R., R. Gaitley, J. Martonchik, D. Diner, K. Crean, and B. Holben, 2005: MISR global aerosol optical depth validation based on two years of coincident AERONET observations. *J. Geophys. Res.* **110**, D10S04.

Kahn, R., M. Garay, D. Nelson, K. Yau, M. Bull, B. Gaitley, J. Martonchik, and R. Levy, 2007: Satel-

lite-derived aerosol optical depth over dark water from MISR and MODIS: comparisons with AERONET and implications for climatological studies. *J. Geophys. Res.* **112**, D18205.

Kahn, R., D. Nelson, M. Garay, R. Levy, M. Bull, D. Diner, J. V. Martonchik, S. R. Paradise, E. G. Hansen, and L. A. Remer, 2009: MISR aerosol product attributes and statistical comparisons with MODIS. *IEEE Trans. Geosci. Remote Sens.* **47**, 4095–4114.

Kahn, R., B. Gaitley, M. Garay, D. Diner, T. Eck, A. Smirnov, and B. Holben, 2010: Multiangle imaging spectroradiometer global aerosol product assessment by comparison with the aerosol robotic network. *J. Geophys. Res.* **115**, D23209.

Kalashnikova, O. V., M. J. Garay, A. B. Davis, D. J. Diner, and J. V. Martonchik, 2011: Sensitivity of multi-angle photo-polarimetry to vertical layering and mixing of absorbing aerosols: quantifying measurement uncertainties. *J. Quant. Spectrosc. Radiat. Transfer* **112**, 2149–2163.

Kanakidou, M., K. Tsigaridis, F. J. Dentener, and P. J. Crutzen, 2000: Human-activity-enhanced formation of organic aerosols by biogenic hydrocarbon oxidation. *J. Geophys. Res*. **105**, 9243–9354.

Kato, S., and A. Marshak, 2009: Solar zenith and viewing geometry-dependent errors in satellite retrieved cloud optical thickness: marine stratocumulus case. *J. Geophys. Res.* **114**, D01202.

Kaufman, Y., D. Tanré, L. Remer, E. Vermote, A. Chu, and B. Holben, 1997: Operational remote sensing of tropospheric aerosol over land from EOS moderate resolution imaging spectroradiometer. *J. Geophys. Res.* **102**, 17051–17067.

Kaufman, Y., D. Tanré, and O. Boucher, 2002: A satellite view of aerosols in the climate system. *Nature* **419**, 215–223.

Kawata, Y., 1978: Circular polarization of sunlight reflected by planetary atmospheres. *Icarus* **33**, 217–232.

Kaye, P. H., E. Hirst, R. S. Greenaway, Z. Ulanowski, E. Hesse, P. J. DeMott, C. Saunders, and P. Connolly, 2008: Classifying atmospheric ice crystals by spatial light scattering. *Opt. Lett.* **33,** 1545–1547.

Keene, W. C., H. Maring, J. R. Maben, D. J. Kieber, A. A. P. Pszenny, E. E. Dahl, M. A. Izaguirre, A. J. Davis, M. S. Long, X. Zhou, L. Smoydzin, and R. Sander, 2007: Chemical and physical characteristics of nascent aerosols produced by bursting bubbles at a model air-sea interface. *J. Geophys. Res.* **112**, D21202.

Kiehl, J. T., 2007: Twentieth century climate model response and climate sensitivity. *Geophys. Res. Lett.* **34**, L22710.

Kim, B.-G., M. A. Miller, S. E. Schwartz, Y. Liu, and Q. Min, 2008: The role of adiabaticity in the aerosol first indirect effect. *J Geophys Res* **113**, D05210.

King, M. D., 1987: Determination of the scaled optical thickness of clouds from reflected solar radiation measurements. *J. Atmos. Sci.* **44**, 1734–1751.

King, M. D., W. P. Menzel, Y. J. Kaufman, D. Tanré, B.-C. Gao, S. Platnick, S. A. Ackerman, L. A. Remer, R. Pincus, and P. A. Hubanks, 2003: Cloud and aerosol properties, precipitable water, and profiles of temperature and water vapor from MODIS. *IEEE Trans. Geosci. Remote. Sens.* **41**, 442–458.

Kinne, S., M. Schulz, C. Textor, S. Guibert, Y. Balkanski, S. E. Bauer, T. Berntsen, T. F. Berglen, O. Boucher, M. Chin, W. Collins, F. Dentener, T. Diehl, R. Easter, J. Feichter, D. Fillmore, S. Ghan, P. Ginoux, S. Gong, A. Grini, J. Hendricks, M. Herzog, L. Horowitz, I. Isaksen, T. Iversen, A. Kirkevåg, S. Kloster, D. Koch, J. E. Kristjansson, M. Krol, A. Lauer, J. F. Lamarque, G. Lesins, X. Liu, U. Lohmann, V. Montanaro, G. Myhre, J. Penner, G. Pitari, S. Reddy, O. Seland, P. Stier, T. Takemura, and X. Tie, 2006: An AeroCom initial assessment – optical properties in aerosol component modules of global models. *Atmos. Chem. Phys.* **6**, 1815–1834.

Knap, W. H., L. C.-Labonnote, G. Brogniez, and P. Stammes, 2005: Modeling total and polarized reflectances of ice clouds: evaluation by means of POLDER and ATSR-2 measurements. *Appl. Opt*. **44**, 4060–4073.

Knobelspiesse, K., B. Cairns, C. Schaaf, B. Schmid, and M. Román, 2008: Surface BRDF estimation from an aircraft compared to MODIS and ground estimates at the southern great plains site. *J. Geophys. Res.* **113**, D20105.

Knobelspiesse, K., B. Cairns, J. Redemann, R. W. Bergstrom, and A. Stohl, 2011a: Simultaneous retrieval of aerosol and cloud properties during the MILAGRO field campaign. *Atmos. Chem. Phys.* **11**, 6245–6263.

Knobelspiesse, K., B. Cairns, M. Ottaviani, R. Ferrare, J. Hair, C. Hostetler, M. Obland, R. Rogers, J. Redemann, Y. Shinozuka, A. Clarke, S. Freitag, S. Howell, V. Kapustin, and C. McNaughton, 2011b: Combined retrievals of boreal forest fire aerosol properties with a polarimeter and lidar. *Atmos. Chem. Phys.* **11**, 7045–7067.

Knutti, R., T. F. Stocker, F. Joos, and G.-K. Plattner, 2002: Constraints on radiative forcing and future climate change from observations and climate model ensembles. *Nature* **416**, 719–723.

Koch, D., and A. D. Del Genio, 2010: Black carbon absorption effects on cloud cover: review and synthesis. *Atmos. Chem. Phys.* **10**, 7685–7696.

Kokhanovsky, A. A., and G. de Leeuw, Eds., 2009: *Satellite Aerosol Remote Sensing over Land*. Praxis, Chichester, UK.

Kokhanovsky, A. A., J. L. Deuzé, D. J. Diner, O. Dubovik, F. Ducos, C. Emde, M. J. Garay, R. G. Grainger, A. Heckel, M. Herman, I. L. Katsev, J. Keller, R. Levy, P. R. J. North, A. S. Prikhach, V. V. Rozanov, A. M. Sayer, Y. Ota, D. Tanré, G. E. Thomas, and E. P. Zege, 2010: The inter-comparison of major satellite aerosol retrieval algorithms using simulated intensity and polarization characteristics of reflected light. *Atmos. Meas. Tech*. **3**, 909–932.

Koren, I., Y. J. Kaufman, L. A. Remer, and J. V. Martins, 2004: Measurement of the effect of Amazon smoke on inhibition of cloud formation. *Science* **303**, 1342–1345.

Koren, I., L. Remer, Y. Kaufman, Y. Rudich, and J. V. Martins, 2007: On the twilight zone between clouds and aerosols. *Geophys. Res. Lett.* **34**, L08805.

Koren, I., J. V. Martins, L. A. Remer, and H. Afargan, 2008: Smoke invigoration versus inhibition of clouds over the Amazon. *Science* **321**, 946.

Korolev, A., and G. Isaac, 2003: Roundness and aspect ratio of particles in ice clouds. *J. Atmos. Sci.* **60**, 1795–1808.

Korolev, A., E. F. Emery, J. W. Strapp, S. G. Cober, G. A. Isaac, M. Wasey, and D. Marcotte, 2011: Small ice particles in tropospheric clouds: fact or artifact? Airborne Icing Instrumentation Evaluation Experiment. *Bull. Amer. Meteorol. Soc*., in press.

Koven, C. D., and I. Fung, 2006: Inferring dust composition from wavelength-dependent absorption in Aerosol Robotic Network (AERONET) data. *J. Geophys. Res.* **111**, D14205.

Lawson, R. P., 2011: Effects of ice particles shattering on the 2D-S probe. *Atmos. Meas. Tech.* **4**, 1361–1381.

Lawson, R. P., E. J. Jensen, D. L. Mitchell, B. Baker, Q. Mo, and B. Pilson, 2010: Microphysical and radiative properties of tropical clouds investigated in TC4 and NAMMA. *J. Geophys. Res.* **115**, D00J08.

Lee, J., P. Yang, A. Dessler, B.-C. Gao, and S. Platnick, 2009: Distribution and radiative forcing of tropical thin cirrus clouds. *J. Atmos. Sci.* **66**, 3721–3731.

Levin, Z., and W. Cotton, 2008: *Aerosol Pollution Impact on Precipitation*. Springer, Berlin.

Levy, R. C., 2009: The dark-land MODIS collection 5 aerosol retrieval: algorithm development and product evaluation. In Kokhanovsky, A. A., and G. de Leeuw, Eds., *Satellite Aerosol Remote Sensing over Land*. Praxis, Chichester, UK, pp. 19–68.

Levy, R. C., L. A. Remer, R. G. Kleidman, S. Mattoo, C. Ichoku, R. Kahn, and T. F. Eck, 2010: Global evaluation of the Collection 5 MODIS dark-target aerosol products over land. *Atmos. Chem. Phys*. **10**, 10399–10420.

Lewis, K. A., W. P. Arnott, H. Moosmüller, R. K. Chakrabarty, C. M. Carrico, S. M. Kreidenweis, D. E. Day, W. C. Malm, A. Laskin, J. L. Jimenez, I. M. Ulbrich, J. A. Huffman, T. B. Onasch, A. Trimborn, L. Liu, and M. I. Mishchenko, 2009: Reduction in biomass burning aerosol light absorption upon humidification: roles of inorganically-induced hygroscopicity, particle collapse, and photoacoustic heat and mass transfer. *Atmos. Chem. Phys.* **9**, 8949–8966.

Li, Z., X. Zhao, R. Kahn, M. Mishchenko, L. Remer, K.-H. Lee, M. Wang, I. Laszlo, T. Nakajima, and H. Maring, 2009: Uncertainties in satellite remote sensing of aerosols and impact on monitoring its long-term trend: a review and perspective. *Ann. Geophys.* **27**, 2755–2770.

Liou, K.-N., 2002: *An Introduction to Atmospheric Radiation*. Academic Press, New York.

Litvinov, P., O. Hasekamp, B. Cairns, and M. Mishchenko, 2010: Reflection models for soil and vegetation surfaces from multiple-viewing angle photopolarimetric measurements. *J. Quant. Spectrosc. Radiat. Transfer.* **111**, 529–539.

Liu, Y., and P. H. Daum, 2002: Warming effect from dispersion forcing. *Nature* **419**, 580–581.

Liu, X. H., and J. E. Penner, 2005: Ice nucleation parameterization for global models. *Meteorol. Z.* **14**, 499–514.

Liu, Y., P. Koutrakis, and R. Kahn, 2007a: Estimating fine particulate matter component concentrations and size distributions using satellite retrieved fractional aerosol optical depth: Part 1—Method development. *J. Air Waste Manage. Assoc.* **57**, 1351–1359.

Liu, Y., P. Koutrakis, and R. Kahn, 2007b: Estimating fine particulate matter component concentrations and size distributions using satellite retrieved fractional aerosol optical depth: Part 2—A case study. *J. Air Waste Manage. Assoc.* **57**, 1351–1359.

Liu, X., J. E. Penner, S. J. Ghan, and M. Wang, 2007c: Inclusion of ice microphysics in the NCAR community atmospheric model version 3 (CAM3). *J. Clim.* **20**, 4526–4547.

Liu, X. H., J. E. Penner, and M. H. Wang, 2009: Influence of anthropogenic sulfate and black carbon on upper tropospheric clouds in the NCAR CAM3 model coupled to the IMPACT global aerosol model. *J. Geophys. Res.* **114**, D03204.

Loeb, N. G., and W. Su, 2010: Direct aerosol radiative forcing uncertainty based on a radiative perturbation analysis. *J. Clim.* **23**, 5288–5293.

Lohmann, U., and J. Feichter, 2005: Global indirect aerosol effects: a review. *Atmos. Chem. Phys.* **5**, 715–737.

Lohmann, U., and S. Ferrachat, 2010: Impact of parametric uncertainties on the present-day climate and on the anthropogenic aerosol effect. *Atmos. Chem. Phys.* **10**, 11373–11383.

Lohmann, U., and G. Lesins, 2002: Stronger constraints on the anthropogenic indirect aerosol effect. *Science* **298**, 1012–1025.

Lu, M.-L., and J. H. Seinfeld, 2006: Effect of aerosol number concentration on cloud droplet dispersion: a large-eddy simulation study and implications for aerosol indirect forcing. *J. Geophys. Res.* **111**, D02207.

Lucht, W., C. Schaaf, and A. Strahler, 2000: An algorithm for the retrieval of albedo from space using semiempirical brdf models. *IEEE Trans. Geosci. Remote Sens.* **38**, 977–998.

Maignan, F., F. M. Bréon, E. Feıdelle, and M. Bouvier, 2009: Polarized reflectances of natural surfaces: Spaceborne measurements and analytical modeling. *Remote Sens. Environ*. **113**, 2642–2650.

Mann, G. W., K. S. Carslaw, D. V. Spracklen, D. A. Ridley, P. T. Manktelow, M. P. Chipperfield, S. J. Pickering, and C. E. Johnson, 2010: Description and evaluation of GLOMAP-mode: a modal global aerosol microphysics model for the UKCA composition-climate model. *Geosci. Model Dev.* **3**, 519–551.

Maring, H., D. L. Savoie, M. A. Izaguirre, L. Custals, and J. S. Reid, 2003: Mineral dust aerosol size distribution change during atmospheric transport. *J. Geophys. Res*. **108**, 8592.

Marshak, A., S. Platnick, T. Várnai, G. Wen, and R. F. Cahalan, 2006: Impact of 3D radiative effects

on satellite retrievals of cloud droplet sizes. *J. Geophys. Res.* **111**, D09207.

Martin, R. V., D. J. Jacob, R. M. Yantosca, M. Chin, and P. Ginoux, 2003: Global and regional decreases in tropospheric oxidants from photochemical effects of aerosols. *J. Geophys. Res.* **108**, 4097.

Marshak, A., G. Wen, J. Coakley, L. Remer, N. G. Loeb, and R. F. Cahalan, 2008: A simple model for the cloud adjacency effect and the apparent bluing of aerosols near clouds. *J. Geophys. Res.* **113**, D14S17.

Martonchik, J. V., D. J. Diner, K. A. Crean, and M. A. Bull, 2002: Regional aerosol retrieval results from MISR. *IEEE Trans. Geosci. Remote. Sens.* **40**, 1520–1531.

Martonchik, J. V., R. A. Kahn, and D. J. Diner, 2009: Retrieval of aerosol properties over land using MISR observations. In Kokhanovsky, A. A., and G. de Leeuw, Eds., *Satellite Aerosol Remote Sensing over Land*. Praxis, Chichester, UK, pp. 267–293.

Mayer, B., 2009: Radiative transfer in the cloudy atmosphere. *Eur. Phys. J. Conf.* **1**, 75–99.

Mayer, B., and A. Kylling, 2005: The libRadtran software package for radiative transfer calculations description and examples of use. *Atmos. Chem. Phys.* **5**, 1855–1877.

McFarquhar, G. M., A. J. Heymsfield, J. Spinhirne, and B. Hart, 2000: Thin and sub-visual tropopause tropical cirrus: observations and radiative impacts. *J. Atmos. Sci.* **57**, 1841–1853.

McFarquhar, G. M., and H. Wang, 2006: Effects of aerosols on trade wind cumuli over the Indian Ocean: model simulations. *Q. J. R. Meteorol. Soc.* **132**, 821–843.

McNaughton, C. S., and Coauthors, 2009: Observations of heterogeneous reactions between Asian pollution and mineral dust over the Eastern North Pacific during INTEX-B. *Atmos. Chem. Phys.* **9**, 8283–8308.

Menon, S., A. D. Del Genio, Y. Kaufman, R. Bennartz, D. Koch, N. Loeb, and D. Orlikowski, 2008: Analyzing signatures of aerosol-cloud interactions from satellite retrievals and the GISS GCM to constrain the aerosol indirect effect. *J. Geophys. Res.* **113**, D14S22.

Menzel, W., R. Frey, H. Zhang, D. Wylie, C. Moeller, R. Holz, B. Maddux, B. Baum, K. Strabala, and L. Gumley, 2008: MODIS global cloud-top pressure and amount estimation: Algorithm description and results. *J. Appl. Meteorol. Climatol.* **47**, 1175–1198.

Meskhidze, N., A. Nenes, W. C. Conant, and J. H. Seinfeld, 2005: Evaluation of a new cloud droplet activation parameterization with in situ data from CRYSTAL-FACE and CSTRIPE. *J. Geophys. Res*. **110**, D16202.

Metzger, S., F. Dentener, S. Pandis, and J. Lelieveld, 2002: Gas/aerosol partitioning: 1. A computationally efficient model. *J. Geophys. Res.* **107**, doi:10.1029/2001JD001102.

Meyer, K., and S. Platnick, 2010: Utilizing the MODIS 1.38 μm channel for cirrus cloud optical thickness retrievals: algorithm and retrieval uncertainties. *J. Geophys. Res.* **115**, D24209.

Miller, R. L., R. V. Cakmur, J. Perlwitz, I. V. Geogdzhayev, P. Ginoux, D. Koch, K. E. Kohfeld, C. Prigent, R. Ruedy, G. A. Schmidt, and I. Tegen, 2006: Mineral dust aerosols in the NASA Goddard Institute for Space Sciences ModelE atmospheric general circulation model. *J. Geophys. Res.* **111**, D06208.

Minnis, P., E. Harrison, L. Stowe, G. Gibson, F. Denn, D. Doelling, and W. Smith Jr., 1993: Radiative climate forcing by the Mount Pinatubo eruption. *Science* **259**, 1411–1415.

Mishchenko, M. I., and L. D. Travis, 1997: Satellite retrieval of aerosol properties over the ocean using polarization as well as intensity of reflected sunlight. *J. Geophys. Res.* **102**, 16989–17013.

Mishchenko, M. I., L. D. Travis, W. B. Rossow, B. Cairns, B. E. Carlson, and Q. Han, 1997a: Retrieving CCN column density from single-channel measurements of reflected sunlight over the ocean: a sensitivity study. *Geophys. Res. Lett.* **24**, 2655–2658.

Mishchenko, M. I., L. D. Travis, R. A. Kahn, and R. A. West, 1997b: Modeling phase functions for dustlike tropospheric aerosols using a mixture of randomly oriented polydisperse spheroids. *J.*

Geophys. Res. **102**, 16831–16847.

Mishchenko, M. I., L. D. Travis, and A. A. Lacis, 2002. *Scattering, Absorption, and Emission of Light by Small Particles*. Cambridge Univ. Press, Cambridge, UK.

Mishchenko, M., B. Cairns, J. Hansen, L. Travis, R. Burg, Y. Kaufman, J. Vanderlei Martins, and E. Shettle, 2004: Monitoring of aerosol forcing of climate from space: analysis of measurement requirements. *J. Quant. Spectrosc. Radiat. Transfer* **88**, 149–161.

Mishchenko, M. I., B. Cairns, G. Kopp, C. F. Schueler, B. A. Fafaul, J. E. Hansen, R. J. Hooker, T. Itchkawich, H. B. Maring, and L. D. Travis, 2007a: Accurate monitoring of terrestrial aerosols and total solar irradiance: introducing the Glory Mission. *Bull. Amer. Meteorol. Soc*. **88**, 677–691.

Mishchenko, M. I., I. V. Geogdzhayev, W. B. Rossow, B. Cairns, B. E. Carlson, A. A. Lacis, L. Liu, and L. D. Travis, 2007b: Long-term satellite record reveals likely recent aerosol trend. *Science* **315**, 1543.

Mishchenko, M. I., I. V. Geogdzhayev, L. Liu, A. A. Lacis, B. Cairns, and L. D. Travis, 2009: Toward unified satellite climatology of aerosol properties: what do fully compatible MODIS and MISR aerosol pixels tell us? *J. Quant. Spectrosc. Radiat. Transfer* **110**, 402–408.

Mishchenko, M. I., L. Liu, I. V. Geogdzhayev, L. D. Travis, B. Cairns, and A. A. Lacis, 2010: Toward unified satellite climatology of aerosol properties. 3. MODIS versus MISR versus AERONET. *J. Quant. Spectrosc. Radiat. Transfer* **111**, 540–552.

Mitchell, D. L., 2002: Effective diameter in radiation transfer: general definition, applications and limitations. *J. Atmos. Sci.* **59**, 2330–2346.

Morcrette, J.-J., O. Boucher, L. Jones, D. Salmond, P. Bechtold, A. Beljaars, A. Benedetti, A. Bonet, J. W. Kaiser, M. Razinger, M. Schulz, S. Serrar, A. J. Simmons, M. Sofiev, M. Suttie, A. M. Tompkins, and A. Untch, 2009: Aerosol analysis and forecast in the European Centre for Medium-Range Weather Forecasts Integrated Forecast System: Forward modeling. *J. Geophys. Res.* **114**, D06206.

Moosmüller, H., R. K. Chakrabarty, and W. P. Arnott, 2009: Aerosol light absorption and its measurement: a review. *J. Quant. Spectrosc. Radiat. Transfer* **110**, 844–878.

Morel, A., and S. Maritorena, 2001: Bio-optical properties of oceanic waters: a reappraisal. *J. Geophys. Res.* **106**, 7163–7180.

Myriokefalitakis, S., E. Vignati, K. Tsigaridis, C. Papadimas, J. Sciare, N. Mihalopoulos, M. C. Facchini, M. Rinaldi, F. J. Dentener, D. Ceburnis, N. Hatzianastasiou, C. D. O'Dowd, M. van Weele, and M. Kanakidou, 2010: Global modeling of the oceanic source of organic aerosols. *Adv. Meteorol.* **2010**, 939171.

Myriokefalitakis, S., K. Tsigaridis, N. Mihalopoulos, J. Sciare, A. Nenes, A. Segers, and M. Kanakidou, 2011: In-cloud oxalate formation in the global troposphere: a 3-D modeling study. *Atmos. Chem. Phys. Discuss.* **11**, 485–530.

Nadal, F., and F.-M. Bréon, 1999: Parameterization of surface polarized reflectance derived from polder spaceborne measurements. *IEEE Trans. Geosci. Remote Sens.* **37**, 1709–1718.

Nakajima, T., and M. D. King, 1990: Determination of the optical thickness and effective radius of clouds from reflected solar radiation measurements. Part I: Theory. *J. Atmos. Sci.* **6**, 1878–1893.

Nakajima, T., M. D. King, J. D. Spinhirne, and L. F. Radke, 1991: Determination of the optical thickness and effective particle radius of clouds from reflected solar radiation measurements. Part II: Marine stratocumulus observations. *J. Atmos. Sci.* **48**, 728–751.

Nakićenović, N., and R. Swart, Eds., 2000: *Special Report on Emissions Scenarios*. *A Special Report of Working Group III of the Intergovernmental Panel on Climate Change.* Cambridge Univ. Press, Cambridge, UK.

Nasiri, S. L., and B. H. Kahn, 2008: Limitations of bispectral infrared cloud phase determination and potential for improvement. *J. Appl. Meteorol. Climatol*. **47**, 2895–2910.

Noel, V., and H. Chepfer, 2004: Study of ice crystal orientation in cirrus clouds based on satellite po-

larized radiance measurements. *J. Atmos.Sci.* **61**, 2073–2081.

NPOESS, 2010: VIIRS Aerosol optical thickness (AOT) and particle size parameter algorithm theoretical basis document (ATBD), D43313Rev F, CDRL No. A032.

O'Dowd, C. D., M. C. Facchini, F. Cavalli, D. Ceburnis, M. Mircea, S. Devesare, S. Fuzzi, Y. J. Yoon, and J.-P. Putaud, 2004: Biogenically driven organic contribution to marine aerosol. *Nature* **431**, 676–680.

O'Dowd, C. D., B. Langmann, S. Varghese, C. Scannell, D. Ceburnis, and M. C. Facchini, 2008: A combined organic-inorganic sea-spray source function. *Geophys. Res. Lett.* **35**, L01801.

Odum, J. R., T. Hoffmann, F. Bowman, D. Collins, R. C. Flagan, and J. H. Seinfeld, 1996: Gas/particle partitioning and secondary organic aerosol yields. *Environ. Sci. Technol*. **30**, 2580–2585.

O'Neill, N. T., A. Ignatov, B. N. Holben, and T. F. Eck, 2000: The lognormal distribution as a reference for reporting aerosol optical depth statistics: empirical tests using multi-year, multi-site AERONET sunphotometer data. *Geophys. Res. Lett*. **27**, 3333–3336.

Ortega, J. M., 1988: *Introduction to Parallel and Vector Solution of Linear Systems*. Plenum Press, New York.

Ottaviani, M., B. Cairns, J. Chowdhary, B. Van Diedenhoven, K. Knobelspiesse, C. Hostetler, R. Ferrare, S. Burton, J. Hair, M. Obland, and R. Rogers, 2011: Polarimetric retrievals of surface properties in the region affected by the Deepwater Horizon oil spill. To be submitted to *Remote Sens. Environ.*

Painemal, D., and P. Zuidema, 2011: Assessment of MODIS cloud effective radius and optical thickness retrievals over the Southeast Pacific with VOCALS-Rex *in-situ* measurements. *J. Geophys. Res.*, submitted.

Pankow, J. F., 1994: An absorption model of gas-aerosol partitioning of organic compounds in the atmosphere. *Atmos. Environ.* **28**, 185–188.

Pavolonis, M. J., A. K. Heidinger, and T. Uttal, 2005: Daytime global cloud typing from AVHRR and VIIRS: algorithm description, validation, and comparisons. *J. Appl. Meteorol.* **44**, 804–826.

Pawlowska, H., W. W. Grabowski, and J.-L. Brenguier, 2006: Observations of the width of cloud droplet spectra in stratocumulus. *Geophys. Res. Lett.* **33**, 19810.

Peng, Y., and U. Lohmann, 2003: Sensitivity study of the spectral dispersion of the cloud droplet size distribution on the indirect aerosol effect. *Geophys. Res. Lett.* **30**, 1507.

Penner, J. E., S. Y. Zhang, and C. C. Chuang, 2003: Soot and smoke aerosol may not warm climate. *J. Geophys. Res.* **108**, 4657.

Penner, J. E., L. Xu, and M. Wang, 2011: Satellite methods underestimate indirect climate forcing by aerosols. *Proc. Natl. Acad. Sci.* **108**, 13404–13408.

Persh, S., Y. J. Shaham, O. Benami, B. Cairns, M. I. Mishchenko, J. D. Hein, and B. A. Fafaul, 2010: Ground performance measurements of the Glory Aerosol Polarimetry Sensor. *Proc. SPIE* **7807**, 780703.

Petters, M.D., and S.M. Kreidenweis, 2007: A single parameter representation of hygroscopic growth and CNN activity. *Atmos. Chem. Phys*. **7**, 1961–1971.

Petzold, A., K. Rasp, B. Weinzierl, M. Esselborn, T. Hamburger, A. Dörnbrack, K. Kandler, L. Schütz, P. Knippertz, M. Fiebig, and A. Virkkula, 2009: Saharan dust absorption and refractive index from aircraft-based observations during SAMUM 2006. *Tellus B* **61**, 118–130.

Pham, M., O. Boucher, and D. Hauglustaine, 2005: Changes in atmospheric sulfur burdens and concentrations and resulting radiative forcings under IPCC SRES emission scenarios for 1990–2100. *J. Geophys. Res.* **110**, D06112.

Pilewskie, P., J. Pommier, R. Bergstrom, W. Gore, S. Howard, M. Rabbette, B. Schmid, P. Hobbs, and S. Tsay, 2003: Solar spectral radiative forcing during the southern african regional science initia-

tive. *J. Geophys. Res*. **108**, 8486.

Platnick, S., 2000: Vertical photon transport in cloud remote sensing problems. *J. Geophys. Res.* **105**, 22919–22935.

Platnick, S., and X. Xiong, 2011: Personal communication (5/12/2011).

Platnick, S., M. D. King, S. A. Ackerman, W. P. Menzel, B. A. Baum, and R. A. Frey, 2003: The MODIS cloud products: algorithms and examples from Terra. *IEEE Trans. Geosci. Remote Sens.* **41**, 459–473.

Pollack, J. B., O. B. Toon, and B. N. Khare, 1973: Surface refractive index. *Icarus* **19**, 372–389.

Priestley, M. B., 1981: *Spectral Analysis and Time Series*. Academic Press, London.

Prospero, J. M., 1999: Long-range transport of mineral dust in the global atmosphere: Impact of African dust on the environment of the southeastern United States. *Proc. Natl. Acad. Sci. USA* **96**, 3396–3403.

Pye, H. O. T., and J. H. Seinfeld, 2010: A global perspective on aerosol from low-volatility organic compounds. *Atmos. Chem. Phys*. **10**, 4377–4401.

Quaas, J., and O. Boucher, 2005: Constraining the first aerosol indirect radiative forcing in the LMDZ GCM using POLDER and MODIS satellite data. *Geophys. Res. Lett.* **32**, L17814.

Quaas, J., B. Stevens, P. Stier, and U. Lohmann, 2010: Interpreting the cloud cover – aerosol optical depth relationship found in satellite data using a general circulation model. *Atmos. Chem. Phys.* **10**, 6129–6135.

Ramanathan, V., P. Crutzen, J. Kiehl, and D. Rosenfeld, 2001: Aerosols, climate, and the hydrological cycle. *Science* **294**, 2119–2124.

Ramanathan, V., M. V. Ramana, G. Roberts, D. Kim, C. Corrigan, C. Chung, and D. Winker, 2007: Warming trends in Asia amplified by brown cloud solar absorption. *Nature* **448**, 575–579.

Ramaswamy, V., and Coauthors, 2001: Radiative forcing of climate change. In Houghton, J. T., et al., Eds., *Climate Change 2001: The Scientific Basis.* Cambridge Univ. Press, Cambridge, UK, pp. 349–416.

Redemann, J., Q. Zhang, P. Russell, J. Livingston, and L. Remer, 2009: Case studies of aerosol remote sensing in the vicinity of clouds. *J. Geophys. Res.* **114**, D06209.

Reid, J. S., H. H. Jonsson, H. B. Maring, A. Smirnov, D. L. Savoie, S. S. Cliff, E. A. Reid, J. M. Livingston, M. M. Meier, O. Dubovik, and S.-C. Tsay, 2003: Comparison of size and morphological measurements of coarse mode dust particles from Africa. *J. Geophys. Res*. **108**, 8593.

Remer, L., A. E. Ward, and Y. J. Kaufman, 2001: Angular and seasonal variation of spectral ratios: Implications for the remote sensing of aerosol over land. *IEEE Trans. Geosci. Remote Sens.* **39**, 275–283.

Remer, L., Y. Kaufman, D. Tanré, S. Mattoo, D. Chu, J. Martins, R. Li, C. Ichoku, R. Levy, R. Kleidman, T. Eck, E. Vermote, and B. Holben, 2005: The MODIS aerosol algorithm, products and validation. *J. Atmos. Sci.* **62**, 947–973.

Remer, L., R. G. Kleidman, R. C. Levy, Y. J. Kaufman, D. Tanré, S. Mattoo, J. V. Martins, C. Ichoku, I. Koren, H. Yu, and B. N. Holben, 2008: Global aerosol climatology from the MODIS satellite sensors. *J. Geophys. Res.* **113**, D14S07.

Riedi, J., B. Marchant, S. Platnick, B. A. Baum, F. Thieuleux, C. Oudard, F. Parol, J.-M. Nicolas, and P. Dubuisson, 2010: Cloud thermodynamic phase inferred from MODIS and POLDER. *Atmos. Chem. Phys*. **10**, 11851–11865.

Robinson, A. L., N. M. Donahue, M. K. Shrivastava, E. A. Weitkamp, A. M. Sage, A. P. Grieshop, T. E. Lane, J. R. Pierce, and S. N. Pandis, 2006: Rethinking organic aerosols: semivolatile emissions and photochemical aging. *Science* **315**, 1259–1262.

Rodgers, C. 2000: *Inverse Methods for Atmospheric Sounding: Theory and Practice*. World Scientific, Singapore.

Roesler, E. L., and J. E. Penner, 2010. Can global models ignore the chemical composition of aerosols? *Geophys. Res. Lett*. **37**, L24809.

Rogers, D. C., P. J. DeMott, and S. M. Kreidenweis, 2001: Airborne measurements of tropospheric ice-nucleating aerosol particles in the Arctic spring, *J. Geophys. Res*. **106**, 15053–15063.

Rohen, G. J., W. von Hoyningen-Huene, A. Kokhanovsky, T. Dinter, M. Vountas, and J. P. Burrows, 2011: Retrieval of aerosol mass load (PM_{10}) from MERIS/Envisat top of atmosphere spectral reflectance measurements over Germany. *Atmos. Meas. Tech.* **4**, 523–534.

Rondeaux, G., and M. Herman, 1991: Polarization of light reflected by crop canopies. *Remote Sens. Environ.* **38**, 63–75.

Rosenfeld, D., 2006: Aerosols, clouds, and climate. *Science* **312**, 1323–1324.

Rotstayn, L. D., and Y. Liu, 2003: Sensitivity of the first indirect aerosol effect to an increase of cloud droplet spectral dispersion with droplet number concentration. *J. Clim.* **16**, 3476–3481.

Rotstayn, L. D., and Y. Liu, 2009: Cloud droplet spectral dispersion and the indirect aerosol effect: Comparison of two treatments in a GCM. *Geophys. Res. Lett*. **36**, L10801.

Russell, P., J. Livingston, E. Dutton, R. Pueschel, J. Reagan, T. DeFoor, M. Box, D. Allen, P. Pilewskie, and B. Herman, 1993: Pinatubo and pre-Pinatubo optical-depth spectra: Mauna Loa measurements, comparisons, inferred particle size distributions, radiative effects, and relationship to lidar data. *J. Geophys. Res.* **98**, 22969–22985.

Russell, P. B., R. W. Bergstrom, Y. Shinozuka, A. D. Clarke, P. F. DeCarlo, J. L. Jimenez, J. M. Livingston, J. Redemann, O. Dubovik, and A. Strawa, 2010: Absorption Angstrom Exponent in AERONET and related data as an indicator of aerosol composition. *Atmos. Chem. Phys.* **10**, 1155–1169.

Sassen, K., and B. Cho, 1992: Subvisual-thin cirrus lidar dataset for satellite verification and climatological research. *J. Appl. Meteorol.* **31**, 1275–1285.

Sassen, K., and J. Zhu, 2009: A global survey of CALIPSO linear depolarization ratios in ice clouds: initial findings. *J. Geophys. Res.* **114**, D00H07.

Saunders, P. M., 1967: Shadowing on the ocean and the existence of the horizon. *J. Geophys. Res.* **72**, 4643–4649.

Sayer, A. M., G. E. Thomas, and R. G. Grainger, 2010: A sea surface reflectance model for (A)ATSR, and application to aerosol retrievals. *Atmos. Meas. Tech.* **3**, 813–838.

Schaaf, C. B., F. Gao, A. H. Strahler, W. Lucht, X. Li, T. Tsang, N. C. Strugnell, X. Zhang, Y. Jin, and J. P. Muller, 2002: First operational BRDF, albedo nadir reflectance products from MODIS. *Remote Sens. Environ.* **83**, 135–148.

Schulz, M., C. Textor, S. Kinne, Y. Balkanski, S. Bauer, T. Berntsen, T. Berglen, O. Boucher, F. Dentener, S. Guibert, I. S. A. Isaksen, T. Iversen, D. Koch, A. Kirkevåg, X. Liu, V. Montanaro, G. Myhre, J. E. Penner, G. Pitari, S. Reddy, Ø. Seland, P. Stier, and T. Takemura, 2006: Radiative forcing by aerosols as derived from the AeroCom present-day and pre-industrial simulations. *Atmos. Chem. Phys.* **6**, 5225–5246.

Schuster, G. L., O. Dubovik, B. N. Holben, and E. E. Clothiaux, 2005: Inferring black carbon content and specific absorption from Aerosol Robotic Network (AERONET) aerosol retrievals. *J. Geophys. Res.* **110**, D10S17

Schwartz, S. E., 2004: Uncertainty requirements in radiative forcing of climate change. *J. Air Waste Manage. Assoc*. **54**, 1351–1359.

Schwartz, S. E., and A. Slingo, 1996: Enhanced shortwave cloud radiative forcing due to anthropogenic aerosols. In Crutzen, P. J., and V. Ramanathan, Eds., *Clouds, Chemistry and Climate*. Springer, Berlin, pp. 191–236.

Schwartz, S. E., R. J. Charlson, and H. Rhode, 2007: Quantifying climate change—too rosy a picture? *Nature Rep. Clim. Change* **1**, 23–24.

Segrin, M. S., J. A. Coakley Jr., and W. R. Tahnk, 2007: MODIS observations of ship tracks in summertime stratus off the West coast of the United States. *J. Atmos. Sci.* **64**, 4330–4345.

Seinfeld, J. H., and S. N. Pandis, 2006: *Atmospheric Chemistry and Physics: From Air Pollution to Climate Change.* Wiley, New York.

Seinfeld, J. H., and Coauthors, 1996: *A Plan for a Research Program on Aerosol Radiative Forcing and Climate Change*. National Academy Press, Washington, DC.

Seinfeld, J. H., R. A. Kahn, T. L. Anderson, R. J. Charlson, R. Davies, D. J. Diner, J. A. Ogren, S. E. Schwartz, and B. A. Wielicki, 2004: Scientific objectives, measurement needs, and challenges motivating the PARAGON aerosol initiative. *Bull. Amer. Meteorol. Soc*. **85**, 1503–1509.

Sekiyama, T. T., T. Y. Tanaka, A. Shimizu, and T. Miyoshi, 2010: Data assimilation of CALIPSO aerosol observations. *Atmos. Chem. Phys.* **10**, 39–49.

Shao, Y., M. Ishizuka, M. Mikami, and J. F. Leys, 2011: Parameterization of size-resolved dust emission and validation with measurements. *J. Geophys. Res.* **116**, D08203.

Shi, Y., J. Zhang, J. S. Reid, B. Holben, E. J. Hyer, and C. Curtis, 2011: An analysis of the collection 5 MODIS over-ocean aerosol optical depth product for its implication in aerosol assimilation. *Atmos. Chem. Phys.* **11**, 557–565.

Shindell, D., and G. Faluvegi, 2009: Climate response to regional radiative forcing during the twentieth century. *Nature Geosci.* **2**, 294–300.

Sinyuk, A., O. Torres, and O. Dubovik, 2003: Combined use of satellite and surface observations to infer the imaginary part of refractive index of Saharan dust. *Geophys. Res. Lett.* **30**, GL016189.

Slater, P. N., S. F. Biggar, K. J. Thome, D. I. Gellman, and P. R. Spyak, 1996: Vicarious radiometric calibrations of EOS sensors. *J. Atmos. Oceanic Technol.* **13**, 349–359.

Smith, T. M., T. R. Karl, and R. W. Reynolds, 2002: How accurate are climate simulations? *Science* **296**, 483–484.

Soden, B. J., and I. M. Held, 2006: An assessment of climate feedbacks in coupled ocean-atmosphere models. *J. Clim.* **19**, 3354–3360.

Solomon, S., D. Qin, M. Manning, M. Marquis, K. Averyt, M. M. B. Tignor, H. L. Miller Jr., and Z. Chen, 2007: *Climate Change 2007: The Physical Sciences Basis.* Cambridge Univ. Press, Cambidge, UK.

Sorooshian, A., M.-L. Lu, F. J. Brechtel, H. Jonsson, G. Feingold, R. C. Flagan, and J. H. Seinfeld, 2007: On the source of organic acid aerosol layers above clouds. *Environ. Sci. Technol.* **41**, 4647–4654.

Spinhirne, J. D., S. P. Palm, W. D. Hart, D. L. Hlavka, and E. J. Welton, 2005: Cloud and aerosol measurements from GLAS: overview and initial results. *Geophys. Res. Lett*. **32**, L22S03.

Spracklen, D. V., S. R. Arnold, J. Sciare, K. S. Carslaw, and C. Pio, 2008: Globally significant oceanic source of organic carbon aerosol. *Geophys. Res. Lett.* **35**, L12811.

Spurr, R., K. Stamnes, H. Eide, W. Li, K. Zhang, and J. J. Stamnes, 2007: Simultaneous retrieval of aerosol and ocean color: A classic inverse modeling approach: I. Analytic Jacobians from the linearized CAO-DISORT model. *J. Quant. Spectrosc. Radiat. Transfer* **104**, 428–449.

Stackhouse, P. W. J., and G. L. Stephens, 1991: A theoretical and observational study of the radiative properties of cirrus: results from FIRE 1986. *J. Atmos. Sci.* **48**, 2044–2059.

Stamnes, K., W. Li, B. Yan, H. Eide, A. Barnard, W. S. Pegau, and J. J. Stamnes, 2003: Accurate and self-consistent ocean color algorithm: simultaneous retrieval of aerosol optical properties and chlorophyll concentrations. *App. Opt.* **42**, 939–951.

Stephens, G. L., 1978: Radiation profiles in extended water clouds. II: Parameterization schemes. *J. Atmos. Sci.* **35**, 2123–2132.

Stephens, G. L., 2005: Cloud feedbacks in the climate system: a critical review. *J. Clim.* **18**, 237–273.

Stevens, B., and G. Feingold, 2009: Untangling aerosol effects on clouds and precipitation in a buff-

ered system. *Nature* **461**, 607–613.

Stier, P., 2005: Towards the assessment of the aerosol radiative effects – a global modelling approach. PhD Thesis.

Stier, P., J. H. Seinfeld, S. Kinne, and O. Boucher, 2007: Aerosol absorption and radiative forcing. *Atmos. Chem. Phys.* **7**, 5237–5261.

Takemura, T., T. Nozawa, S. Emori, T. Y. Nakajima, and T. Nakajima, 2005: Simulation of climate response to aerosol direct and indirect effects with aerosol transport-radiation model. *J. Geophys. Res.* **110**, D02202.

Tanré, D., 2010: Derivation of tropospheric aerosol properties from satellite observations. *C. R. Geosci*. **342**, 403–411.

Tanré, D., F. M. Bréon, J. L. Deuzé, O. Dubovik, F. Ducos, P. François, P. Goloub, M. Herman, A. Lifermann, and F. Waquet, 2011: Remote sensing of aerosols by using polarized, directional and spectral measurements within the A-Train: the PARASOL mission. *Atmos. Meas. Tech.* **4**, 1383–1395.

Tie, X., S. Madronich, S. Walters, D. P. Edwards, P. Ginoux, N. Mahowald, R. Y. Zhang, C. Lou, and G. Brasseur, 2005: Assessment of the global impact of aerosols on tropospheric oxidants. *J. Geophys. Res.* **110**, D03204.

Torres, O., P. K. Bhartia, J. R. Herman, A. Sinyuk, P. Ginoux, and B. Holben, 2002a: A long-term record of aerosol optical depth from TOMS observations and comparison to AERONET measurements. *J. Atmos. Sci.* **59**, 398–413.

Torres, O., R. Decae, P. Veefkind, and G. de Leeuw, 2002b: OMI aerosol retrieval algorithm. In Stammes, P., Ed., *OMI Algorithm Theoretical Basis Document*, Vol. 3. Royal Netherlands Meteorological Institute, Utrecht, pp. 47–71.

Travis, L. D., 1992: Remote sensing of aerosols with the Earth Observing Scanning Polarimeter. *Proc. SPIE* **1747**, 154–164.

Trochkine, D., Y. Iwasaka, A. Matsuki, M. Yamada, Y.-S. Kim, T. Nagatani, D. Zhang, G.-Y. Shi, and Z. Shen, 2003: Mineral aerosol particles collected in Dunhuang, China, and their comparison with chemically modified particles collected over Japan. *J. Geophys. Res.* **108**, 8642.

Tsigaridis, K., and M. Kanakidou, 2003: Global modelling of secondary organic aerosol in the troposphere: a sensitivity analysis. *Atmos. Chem. Phys.* **3**, 1849–1869.

Ulanowski, Z., E. Hesse, P. H. Kaye, and A. J. Baran, 2006: Light scattering by complex ice-analogue crystals. *J. Quant. Spectrosc. Radiat. Transfer* **100**, 382–392.

Van Diedenhoven, B., A. M. Fridlind, and A. S. Ackerman, 2011: Influence of humidified aerosol on lidar depolarization measurements below ice-precipitating Arctic stratus. *J. Appl. Meteorol. Climatol*., in press.

Van Zanten, M. C., and Coauthors, 2010: Controls on precipitation and cloudiness in simulations of trade-wind cumulus as observed during RICO. *J. Adv. Model. Earth Syst*. **2**, in press.

Vanderbilt, V. C., and L. Grant, 1985: Plant canopy specular reflectance model. *IEEE Trans. Geosci. Remote Sens.* **23**, 722–730.

Veefkind, J. P., and M. Sneep, 2007: Co-alignment errors: analysis of the effects of clouds for UV-VIS-NIR retrievals. KNMI report TN-CAM-KNMI-014.

Veefkind, J. P., K. F. Boersma, J. Wang, T. P. Kurosu, N. Krotkov, K. Chance, and P. F. Levelt, 2011: Global satellite analysis of the relation between aerosols and short-lived trace gases. *Atmos. Chem. Phys.* **11**, 1255–1267.

Vignati, E., M. C. Facchini, M. Rinaldi, C. Scannell, D. Ceburnis, J. Sciare, M. Kanakidou, S. Myriokefalitakis, F. Dentener, and C. D. O'Dowd, 2010: Global scale emission and distribution of sea-spray aerosol: sea-salt and organic enrichment. *Atmos. Environ.* **44**, 670–677.

Vignati, E., J. Wilson, and P. Stier, 2004: M7: an efficient size-resolved aerosol microphysics module

for large-scale aerosol transport models. *J. Geophys. Res.* **109**, D22202.

Virkkula, A., I. K. Koponen, K. Teinilä, R. Hillamo, V. M. Kerminen, and M. Kulmala, 2006: Effective real refractive index of dry aerosols in the Antarctic boundary layer. *Geophys. Res. Lett.* **33**, L06805.

Vogelmann, A. M., G. M. McFarquhar, J. A. Ogren, D. D. Turner, J. M. Comstock, G. Feingold, C. N. Long, H. Jonsson, A. Bucholtz, D. R. Collins, G. S. Diskin, H. Gerber, P. R. Lawson, R. Woods, J. M. Hubbe, C. Lo, J. M. Tomlinson, B. Schmid, E. Andrews, S. A. McFarlane, and T. Toto, 2011: RACORO extended-term, aircraft observations of boundary layer clouds. *Bull. Amer. Meteorol. Soc.*, submitted.

Volten, H., O. Muñoz, E. Rol, J. F. de Haan, W. Vassen, J. W. Hovenier, K. Muinonen, and T. Nousiainen, 2001: Scattering matrices of mineral particles at 441.6 nm and 632.8 nm. *J. Geophys. Res.* **106**, 17375–17401.

von Hoyningen-Huene, W., J. Yoon, M. Vountas, L. G. Istomina, G. Rohen, T. Dinter, A. A. Kokhanovsky, and J. P. Burrows, 2011: Retrieval of spectral aerosol optical thickness over land using ocean color sensors MERIS and SeaWiFS. *Atmos. Meas. Tech.* **4**, 151–171.

Voss, K. J., and E. S. Fry, 1984: Measurement of the Mueller matrix for ocean water. *Appl. Opt.* **23**, 4427–4439.

Voulgarakis, A., N. H. Savage, O. Wild, G. D. Carver, K. C. Clemitshaw, and J. A. Pyle, 2009: Upgrading photolysis in the p-TOMCAT CTM: model evaluation and assessment of the role of clouds. *Geosci. Model Dev.* **2**, 59–72.

Wang, M., and H. R. Gordon, 1994: Radiance reflected from the ocean-atmosphere system: Synthesis from individual components of the aerosol size distribution. *Appl.Opt.* **33**, 7088–7095.

Wang, M., S. Ghan, M. Ovchinnikov, X. Liu, R. Easter, E. Kassianov, Y. Qian, and H. Morrison, 2011: Aerosol indirect effects in a multi-scale aerosol-climate model PNNL-MMF. *Atmos. Chem. Phys.* **11**, 5431–5455.

Wanner, W., A. H. Strahler, B. Hu, P. Lewis, J. P. Muller, X. Li, C. L. B. Schaaf, and M. J. Barnsley, 1997: Global retrieval of bidirectional reflectance and albedo over land from EOS MODIS and MISR data: theory and algorithm. *J. Geophys. Res*. **102** 17143 – 17161.

Waquet, F., B. Cairns, K. Knobelspiesse, J. Chowdhary, L. Travis, B. Schmid, and M. Mishchenko, 2009a: Polarimetric remote sensing of aerosols over land. *J. Geophys. Res*. **114**, D01206.

Waquet, F., J. Riedi, L. C.-Labonnote, P. Goloub, B. Cairns, J.-L. Deuzé, and D. Tanré, 2009b: Aerosol remote sensing over clouds using A-Train observations. *J. Atmos. Sci.* **66**, 2468–2480.

Waquet, F., J.-F. Léon, B. Cairns, P. Goloub, J.-L. Deuzé, and F. Auriol, 2009c: Analysis of the spectral and angular response of the vegetated surface polarization for the purpose of aerosol remote sensing over land. *Appl. Opt.* **48**, 1228–1236.

Wild, O., X. Zhu, and M. J. Prather, 2000: Fast-J: accurate simulation of in- and below-cloud photolysis in tropospheric chemical models. *J. Atmos. Chem.* **37**, 245–282.

Winker, D. M., J. Pelon, J. A. Coakley Jr., S. A. Ackerman, R. J. Charlson, P. R. Colarco, P. Flamant, Q. Fu, R. M. Hoff, C. Kittaka, T. L. Kubar, H. Le Treut, M. P. McCormick, G. Mégie, L. Poole, K. Powell, C. Trepte, M. A. Vaughan, B. A. Wielicki, 2010: The CALIPSO Mission: a global 3D view of aerosols and clouds. *Bull. Amer. Meteorol. Soc*. **91**, 1211–1229.

Wise, M. E., T. A. Semeniuk, R. Bruintjes, S. T. Martin, L. M. Russel, and P. Buseck, 2007: Hygroscopic behavior of NaCl-bearing natural aerosol particles using environmental transmission electron microscopy. *J. Geophys. Res.* **112**, D10224.

Wood, R., and D. L. Hartmann, 2006: Spatial variability of liquid water path in marine low cloud: The importance of mesoscale cellular convection. *J. Clim.* **19**, 1748–1764.

Xiao, N., T. Shi, C. A. Calder, D. K. Munroe, C. Berrett, S. Wolfinbarger, and D. Li, 2009: Spatial characteristics of the difference between MISR and MODIS aerosol optical depth retrievals over mainland Southeast Asia. *Remote Sens. Environ*. **113**, 1–9.

Xie, X., and X. Liu, 2011: Effects of spectral dispersion on clouds and precipitation in mesoscale convective systems. *J Geophys Res*. **116**, D06202.

Xiong, X. X., B. N. Wenny, and W. L. Barnes, 2009: Overview of NASA Earth Observing Systems Terra and Aqua moderate resolution imaging spectroradiometer instrument calibration algorithms and on-orbit performance. *J. Appl. Remote Sens.* **3**, 32501.

Xiong, X. X., J. Q. Sun, X. B. Xie, W. L. Barnes, and V. V. Salomonson, 2010: On-orbit calibration and performance of Aqua MODIS reflective solar bands. *IEEE Trans. Geosci. Remote Sens.* **48**, 535–546.

Yang, P., and Q. Fu, 2009: Dependence of ice crystal optical properties on particle aspect ratio. *J. Quant. Spectrosc. Radiat. Transfer* **110**, 1604–1614.

Yu, H., P. K. Quinn, G. Feingold, L. A. Remer, R. A. Kahn, M. Chin, and S. E. Schwartz, 2009: Remote sensing and *in situ* measurements of aerosol properties, burdens, and radiative forcing. In Chin, M., R. A. Kahn, and S. E. Schwartz, Eds., *Atmospheric Aerosol Properties and Climate Impacts.* U.S. Climate Change Science Program, Washington, DC.

Zhang, J., and J. S. Reid, 2009: An analysis of clear sky and contextual biases using an operational over ocean MODIS aerosol product. *Geophys. Res. Lett.* **36**, L15824.

Zhang, J., J. S. Reid, D. Westphal, N. Baker, and E. Hyer, 2008: A system for operational aerosol optical depth data assimilation over global oceans. *J. Geophys. Res.* **113**, D10208.

Zhang, Z., P. Yang, G. W. Kattawar, J. Riedi, L. C. Labonnote, B. A. Baum, S. Platnick, and H. L. Huang, 2009a: Influence of ice particle model on satellite ice cloud retrieval: Lessons learned from MODIS and POLDER cloud product comparison. *Atmos. Chem. Phys.* **9**, 7115–7129.

Zhang, H., R. M. Hoff, J. A. Engel-Cox, 2009b: The relation between Moderate Resolution Imaging Spectroradiometer (MODIS) aerosol optical depth and PM2.5 over the United States: a geographical comparison by EPA regions. *J. Air Waste Manage. Assoc.* **59**, 1358–1369.

Zhang, J., J. R. Campbell, J. S. Reid, D. L. Westphal, N. L. Baker, W. F. Campbell, and E. J. Hyer, 2011: Evaluating the impact of assimilating CALIOP-derived aerosol extinction profiles on a global mass transport model. *Geophys. Res. Lett.* **38**, L14801.

Zhao, C., X. Tie, G. Brasseur, K. J. Noone, T. Nakajima, Q. Zhang, R. Zhang, M. Huang, Y. Duan, and G. Li, 2006: Aircraft measurements of cloud droplet spectral dispersion and implications for indirect aerosol radiative forcing. *Geophys. Res. Lett.* **33**, L16809.

Zhao T. X.-P., I. Laszlo, W. Guo, A. Heidinger, C. Cao, A. Jelenak, D. Tarpley, and J. Sullivan, 2008: Study of long-term trend in aerosol optical thickness observed from operational AVHRR satellite instrument. *J. Geophys. Res.* **113**, D07201.

Zinner, T., and B. Mayer, 2006: Remote sensing of stratocumulus clouds: uncertainty and biases due to inhomogeneity. *J. Geophys. Res*. **111**, D14209.

Zinner, T., G. Wind, S. Platnick, and A. S. Ackerman, 2010: Testing remote sensing on artificial observations: impact of drizzle and 3-D cloud structure on effective radius retrievals. *Atmos. Chem. Phys.* **10**, 9535–9549.

Zuidema, P., and K. F. Evans, 1998: On the validity of the independent pixel approximation for boundary layer clouds observed during ASTEX. *J. Geophys. Res.* **103**, 6059–6074.

Appendix A
Specific APS-2 aerosol and cloud retrieval requirements

Table A1. Aerosol optical thickness requirements

Parameter	Science requirement
Horizontal cell size (nadir)	~5 km
Vertical cell size	Total atmospheric column
Measurement range	0 to 5
Measurement accuracy	0.02 or 7% over ocean 0.04 or 10% over land
Measurement precision	0.01 or 5% over ocean 0.03 or 7% over land

Table A2. Aerosol particle size distribution requirements

Parameter	Science requirement
Horizontal cell size (nadir)	~5 km
Vertical cell size	Total atmospheric column
Measurement range	0.1 μm to 5 μm for r_e[1] 0 to 3 for v_e[2]
Measurement accuracy	Greater of 0.1 μm or 10% for r_e Greater of 0.3 or 50% for v_e
Measurement precision	Greater of 0.05 μm or 10% for r_e Greater of 0.2 or 40% for v_e

[1] Effective radius [2] Effective variance

Table A3. Aerosol refractive index and single-scattering albedo requirements

Parameter	Science requirement
Horizontal cell size (nadir)	~5 km
Vertical cell size	Total atmospheric column
Measurement range	1.3 to 1.8 for Re(m)[1] 0 to 1 for SSA
Measurement accuracy	0.02 for Re(m) 0.03 for SSA
Measurement precision	0.01 for Re(m) 0.02 for SSA

[1] Real part of the refractive index

Table A4. Liquid cloud optical thickness requirements

Parameter	Science requirement
Horizontal cell size (nadir)	~5 km
Vertical cell size	Total atmospheric column
Measurement range	0 to 300
Measurement accuracy	Greater of 0.1 or 8%
Measurement precision	Greater of 0.1 or 8%

Table A5. Liquid cloud particle size distribution requirements

Parameter	Science requirement
Horizontal cell size (nadir)	~5 km
Vertical cell size	Total atmospheric column
Measurement range	0.1 to 50 μm for r_e 0 to 2 for v_e
Measurement accuracy	Greater of 1 μm or 10% for r_e Greater of 0.05 or 50% for v_e
Measurement precision	Greater of 0.5 μm or 5% for r_e Greater of 0.04 or 40% for v_e

Appendix B. Measurement characteristics of existing and confirmed passive aerosol sensors

Sensor	Spectral range (# bands / range, nm)[1]	Polarization capability (# bands / range, nm)	Viewing angles (# / range)	Radiometric (polarimetric) accuracy	Reference
AVHRR	2 / 630, 865	–	1 / nadir	5%	Higurashi and Nakajima (1999) Ignatov and Stowe (2002) Mishchenko et al. (2007b)
MODIS	7 / 469–2130[2]	–	1 / nadir	5%[3]	Remer et al. (2005) Xiong et al. (2009, 2010)
MERIS	13 / 410–900	–	1 / nadir	3%	Rohen et al. (2011) von Hoyningen-Huene et al. (2011)
MISR	4 / 440–860	–	9 / ±70.5° along track[4]	3%–4%	Bruegge et al. (2002, 2007) Kahn et al. (2005)
AATSR	4 / 550–1600	–	2 / near nadir and 55° from nadir ahead of satellite	5%	Sayer et al. (2010)
PARASOL	8 / 670–1020	3 / 490, 670, 860	16 / every 9° ±57° along track[4]	3% (1%–2%)	Tanré et al. (2011) Dubovik et al. (2011) Hasekamp (2011)
VIIRS	7 / 410–2250	–	1 / nadir	3%	NPOESS (2010)
APS	8 / 413–2260	8 / 413–2260	~250 / +60°/–80° along track[4]	3% (0.1%–0.2%)	Mishchenko et al. (2007a) Persh et al. (2010)

[1] Number of bands and spectral range used for aerosol retrievals.
[2] 9 / 410–2130 with Deep Blue algorithm.
[3] Radiance-based accuracy; reflectance-based accuracy = 2%.
[4] At the earth.

Appendix C
Flowdown of requisite retrieval requirements into APS-2 measurement characteristics

Requisite retrieval capability	APS-2 measurement characteristic
Particle refractive index	Precise and accurate polarimetry (~0.1%)
Particle size distribution, refractive index, shape	Wide scattering angle range for both intensity and polarization
(i) Particle size distribution, refractive index, shape (ii) Ocean surface roughness	Multiple ($\gtrsim$30) viewing angles for both intensity and polarization
Cloud particle size via rainbow angle	Multiple ($\gtrsim$60) viewing angles for polarization
Aerosol retrievals in cloud-contaminated pixels and above clouds	Multiple ($\gtrsim$30) viewing angles and accurate polarimetry
(i) Separation of submicron and supermicron particles (ii) Spectral refractive index $\Rightarrow$ chemical composition	Wide spectral range (413–2260 nm) for both intensity and polarization
Detection and characterization of thin cirrus clouds and stratospheric aerosols	1376 nm channel for both intensity and polarization; precise and accurate polarimetry (~0.1%)
Accounting for the water-leaving radiance contribution over open oceans	413, 444, 555 nm channels for intensity
Characterization of the land surface contribution at visible wavelengths	2260 nm polarization channel
Column water vapor amount	911 nm channel

Appendix D
Sensitivity analysis

The sensitivity study presented in this work is based upon the Bayesian approach using Gaussian distributions as described in Rodgers (2000). This method estimates retrieval uncertainty given observational configuration and uncertainty with the equation

$$\mathbf{C}_{\mathbf{x}} = (\mathbf{J}^T \mathbf{C}_{\mathbf{o}}^{-1} \mathbf{J})^{-1}, \tag{D1}$$

where $\mathbf{C}_{\mathbf{x}}$ is the retrieval error covariance matrix, $\mathbf{C}_{\mathbf{o}}$ is the observation error covariance matrix, $\mathbf{J}$ is the Jacobian matrix, "T" denotes the matrix transpose, and "–1" denotes the matrix inverse. The observation error covariance matrix represents measurement uncertainty, where the square roots of the standard errors associated with each individual measurement (corresponding to a single view angle, wavelength, and polarization state) are on the main diagonal, while off-diagonal elements represent error correlations. For the sake of simplicity, correlated errors are neglected in this study. $\mathbf{C}_{\mathbf{o}}$ is square with the dimension of the number of measurements made with each observation. The retrieval error covariance matrix, $\mathbf{C}_{\mathbf{x}}$, is similarly structured, but represents the error of the parameters to be retrieved from the data. The Jacobian matrix expresses the sensitivity of the observed scene to changes in the parameters to be retrieved. Radiative transfer simulations, indicated by the function $\mathbf{F}(\mathbf{x})$ (where $\mathbf{x}$ is a vector of aerosol optical parameters), can be used to estimate the Jacobian matrix

$$\mathbf{J}_{ij} = \left. \frac{\partial \mathbf{F}_i(\mathbf{x})}{\partial x_j} \right|_{\mathbf{x}}, \tag{D2}$$

where the partial derivative of the radiative transfer model, $\mathbf{F}(\mathbf{x})$, for the simulated set of parameters, $\mathbf{x}$, is computed for each observation, *i,* and each parameter, *j*. Since $\mathbf{F}(\mathbf{x})$ is nonlinear, it must be assessed for each possible combination of parameters representing a scene. The partial derivative was estimated numerically by perturbing the *j*th element of $\mathbf{x}$ and recalculating the forward model.

The nonlinearity of the radiative transfer model means that the Jacobian matrix is only appropriate for use for the parameter values at which the partial derivatives were assessed. A large number of Jacobians, representing parameters that span the range of what is expected to be observed, must be computed if the sensitivity study is to be broadly applicable. For this study, we used nine aerosol models derived from observations with AERONET sun photometers (Dubovik et al. 2002). Each of these nine was simulated at five AOTs (0.05, 0.1, 0.2, 0.4 and 0.8 at 560 nm), for a total of 45 scenes. Table D1 lists the characteristics of these aerosol classes.

This sensitivity study assesses the simulated retrieval uncertainties that are the square roots of the diagonal terms in the retrieval error covariance matrix. While this method is relatively simple and has been established in the literature as a suitable sensitivity study technique (e.g., Hasekamp and Landgraf 2007; Waquet et al. 2009a; Hasekamp 2010; Knobelspiesse et al. 2011a), it does have limitations. First, the uncertainties express observational sensitivity to parameter change, but they do not show parameter retrievability. This is because it is possible that the system response to change in one parameter is very similar to that for a different parameter, so distinguishing between the two during retrieval would be problematic. The relationships between pairs of parameters are ex-

Table D1. Aerosol classes from AERONET and Dubovik et al. (2002)

Class*	Refractive index	$r_{e,fine}$ (μm)	$v_{e,fine}$	$r_{e,coarse}$ (μm)	$v_{e,coarse}$
Amazon Forest	1.47 – i0.001	0.176	0.174	6.91	0.867
African Savanna	1.51 – i0.021	0.152	0.174	5.95	0.704
Boreal Forest	1.50 – i0.009	0.188	0.203	6.34	0.927
Brazil Cerrado	1.52 – i0.015	0.185	0.247	6.87	0.867
Paris, France	1.40 – i0.009	0.173	0.203	5.39	0.867
Greenbelt, MD, USA	1.40 – i0.003	0.170	0.155	5.52	0.755
Lanai, HI, USA	1.36 – i0.002	0.201	0.259	4.29	0.588
Mexico City, Mexico	1.47 – i0.014	0.165	0.203	4.43	0.487
Maldives	1.44 – i0.011	0.222	0.236	4.96	0.782

*All classes are assumed to be composed of spherical, homogenous particles with a spectrally invariant refractive index. Size is specified bimodally with lognormal distributions.

Table D2. Simulated instrument configurations

Name*	Accuracy		Spectral bands		# viewing angles
	Radiometric	Polarimetric	Radiometric	Polarimetric	
MISR (36)	3%	n/a	4: 440–870 nm	none	9: ± 70°
PARASOL (144)	3%	2%	6: 440–1020 nm	3: 490–870 nm	16: ± 55°
APS-2 (1568)	3%	0.15%	7: 410–2250 nm	7: 410–2250 nm	32: ± 60°

* A value in parentheses is the total number of measurements for each scene location.

pressed by the off-diagonal elements of the retrieval error covariance matrix, and can also be assessed using metrics that describe the information content in an observation (see Rodgers 2000 for more details). For the sake of simplicity, these tests have been omitted from this work. Another important aspect of this sensitivity study is that it does not address modeling approximations or the retrieval algorithm. Essentially, it is assumed that the radiative transfer model used during retrieval is a perfect representation of reality, and that the retrieval algorithm successfully extracts all the information from the data. Uncertainty estimate values should therefore be understood as the best possible uncertainty for a scene, which may degrade if various parameters are difficult to distinguish, if the model is incorrect, or if the retrieval algorithm is unable to successfully exploit the information available in an observation. Nevertheless, this analysis approach can prove very powerful when attempting to compare instrument designs, since it yields a pure expression of the information available with a particular design unaffected by choice of radiative transfer model or retrieval algorithm.

Three types of instruments were compared for this study. Each type is an analog for either a currently operating instrument or the APS-2, with some simplifications to ease comparison. Table D2 lists the simulated instrument types, along with observation accuracies, spectral channels, and numbers of viewing angles (cf. Appendix B). For example, MISR, on the NASA Terra satellite, has a radiometric accuracy of 3%, uses four chan-

nels, has nine viewing angles, and provides no polarization measurements. This simulation treats each spectral band as monochromatic, represented by the effective wavelength. The PARASOL sensor of the French Centre National d'Etudes Spaciales (CNES) is also included in the study, and the reference, of course, is the design of the APS-2. One difference between the actual APS-2 design and this simulation is that far fewer viewing angles (viz., 32) were used, compared to 255 in the design.

Simulations were performed for spherical, bimodal aerosols with a homogeneous vertical distribution in the atmosphere between the surface and an altitude of 1 km. 90% of the total AOT in the simulations is due to the aerosol fine size mode, with the remaining 10% due to the coarse size mode. A solar zenith angle of 45° and relative solar–viewing azimuth angle of 45° were chosen for these simulations, representing the observation geometry of the mid latitudes during spring or fall.

As shown in Table D2, different instrument configurations yield different numbers of measurements. An observation from each instrument is comprised of measurements at various spectral bands, viewing angles, and polarimetric states for a scene location. The uncertainties in these measurements, which are used to form the observation error covariance matrix, are determined as shown in Table D2. Radiometric accuracy is the percent error for observations of the I component of the Stokes polarization vector, expressed in units of reflectance. Polarimetric accuracy is in terms of the degree of linear polarization DoLP = $(Q^2 + U^2)^{1/2} / I$. For simulations of scenes over a body of water, the DoLP is used for the polarimetric channels, as it is compatible with assumptions about ocean reflectance that would be made during operational retrieval of aerosol properties over water. Simulations of aerosol observations over land require a different set of surface reflectance assumptions, which are instead only compatible with the polarized reflectance $R_p = (Q^2 + U^2)^{1/2}$. This situation is slightly less desirable, since the uncertainty in these channels must now be

$$\sigma_{Rp}^2 = (I\sigma_p)^2 + (Q\sigma_I)^2, \tag{D3}$$

where the p and I subscripts indicate the polarimetric and radiometric uncertainties, respectively, while I and Q are components of the Sokes polarization vector in reflectance units. U is minimal and can usually be omitted if the polarization components are defined with respect to the scattering plane.

For each simulation and instrument type, an observation error covariance matrix is created and an appropriate Jacobian matrix is selected, which are used to compute the retrieval error covariance matrix. Because of the large amount of data involved, analysis and visualization may be difficult. In total, ten aerosol parameters and several additional parameters related to surface reflectance are retrieved. In order to condense the presentation of the results, simulated uncertainty values are compared to the measurement accuracy requirements for monitoring of aerosols summarized in Appendix A. For a given instrument and parameter, the percentage of simulated uncertainties meeting that accuracy criterion form the basis of diagrams such as Figs. 10, D2, and D4. One caveat, however, is with the expression of aerosol absorption. Mishchenko et al. (2004) set an accuracy criterion of 0.03 for the SSA. This quantity, however, is not a directly retrieved physical parameter in the radiative transfer model used in this sensitivity study. Aerosol absorption is instead specified by the imaginary part of the refractive index. We therefore chose a somewhat arbitrary accuracy criterion of 0.0025 for the imaginary refractive in-

dex in this study.

Results from this analysis are presented in the following subsections. Because of the differences in observing aerosols over oceans and over land, we performed two separate sets of simulations. APS-2 retrieval capability in the presence of clouds is also discussed, based upon recent simulations for aerosols above clouds (Knobelspiesse et al. 2011a) and mixed cloud and aerosol scenes (Hasekamp 2010). Finally, we address the capability of APS-2 to detect stratospheric aerosols using the channel centered at 1376 nm within a water vapor absorption band.

Aerosol retrievals over the ocean. To test the capability of retrieving aerosol properties over the ocean, nearly fifty simulations were performed for a variety of aerosol classes and AOTs. The ocean reflectance was created for a water body with 0.1 mg m^{-3} of Chlorophyll-a (Chowdhary et al. 2006) and surface roughened by a 5 m s^{-1} wind according to the Cox and Munk (1954) model. In addition to the aerosol parameters, the amount of Chlorophyll-a and the wind speed are also retrieved in this analysis, but since they are considered byproducts of the retrieval algorithm, they are not shown here.

Figure D1 presents the simulated uncertainties as a function of total AOT. Vertical error bars indicate the standard deviation of the set of simulations at that AOT. Dotted lines and shaded yellow areas indicate uncertainties that do not meet the accuracy criteria listed in Appendix A. All of the APS-2 simulated uncertainties, indicated in black, are within the accuracy criteria. Uncertainties from other simulated instruments, such as PARASOL (in red) or MISR (in blue) do not meet the accuracy criteria for many parameters. This figure also shows the relationship between AOT and simulated retrieval accuracy. As AOT increases, simulated uncertainty decreases. This is reasonable considering that the signal from aerosols increases with the total aerosol load. There are upper limits, however, to how much improvement can occur. As the layer of aerosols becomes very thick, simulated uncertainties no longer improve. Since polarization is only sensitive to

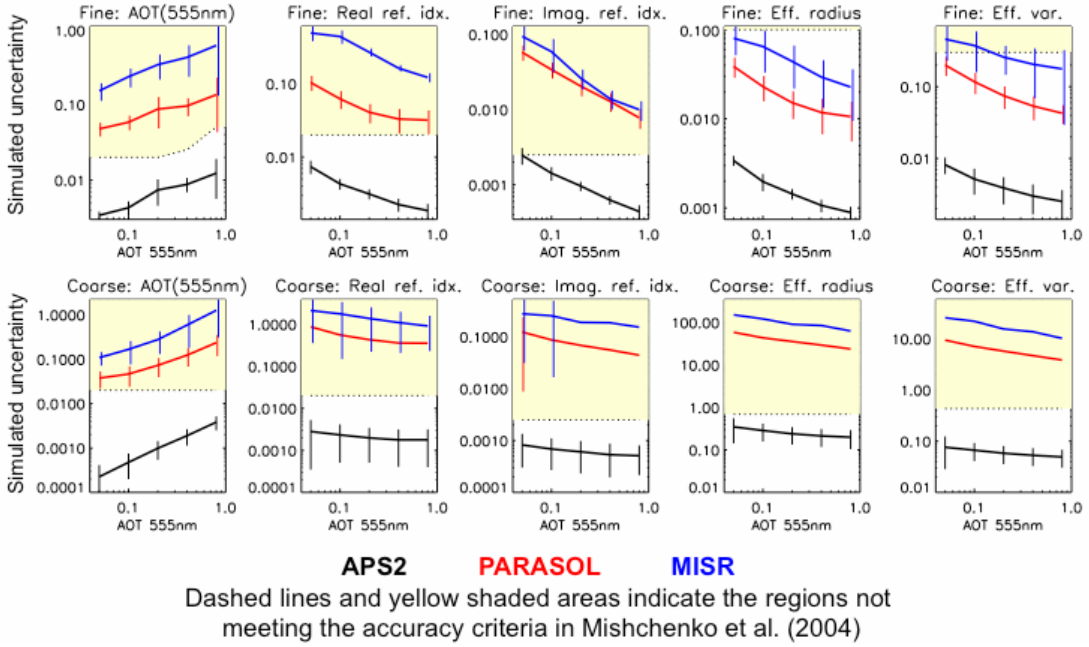

Figure D1. Simulated retrieval uncertainty over the ocean.

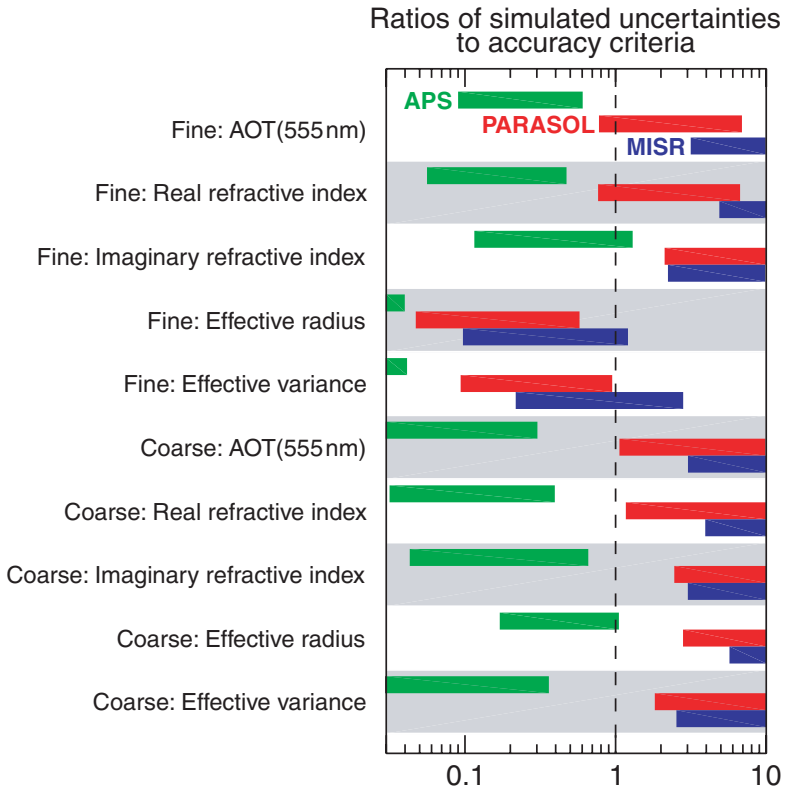

Figure D2. Relative assessment of expected instrument retrieval accuracies for aerosol simulations over an ocean. The ranges of simulated accuracies, normalized by the retrieval requirements described in Mishchenko et al. (2004), are shown for each retrieval parameter and instrument type. Values to the left of the dashed vertical line meet the retrieval requirements, while those to the right exceed them. Very large ratio values indicate a lack of sensitivity to that parameter without prior information.

the top optical depth of one or two in a layer, the polarization signal saturates with large AOT and contains no additional information about aerosol optical properties. The only exceptions to the relationship between AOT and simulated uncertainty are for the simulated uncertainties of AOT. In this representation, the retrieved parameter is changing as a function of AOT, so it is difficult to draw the same sort of conclusions. When the simulated errors are presented as a percentage, this value does decrease as AOT increases.

Figure D2 presents the same information as Fig. D1 but in terms of the ranges of simulated uncertainties for a particular configuration versus the corresponding accuracy criteria in Appendix A. Simulations of APS-2 retrievals meet or exceed the accuracy criteria for all parameters. Other sensors do not perform as well. Essentially, MISR, and PARASOL are only capable of retrieving size parameters for the fine mode within accuracy criteria. PARASOL is somewhat capable of retrieving the coarse-mode AOT within accuracy criteria. This figure makes a strong argument for the use of instruments that can accumulate a large amount of information for a scene, such as the APS-2.

Aerosol retrievals over land. Aerosol retrievals over land were tested for the same aerosol types presented previously using a simulated bright, bare soil surface similar to what was observed in Knobelspiesse et al. (2008) for freshly plowed fields in central Oklahoma. This simulation exploits the kernel-based BRDF models described in Lucht et al. (2000) and used as the basis for surface reflectance observations by MODIS. The polarized surface reflectance was modeled by scaling the Fresnel reflectance coefficient in a similar fashion as Waquet et al. (2009a). Polarized observations are slightly different from the previous study, which used the DoLP as the unit of measure for polarization observations. This study used the polarized reflectance, which is required if the surface is to be characterized with the Fresnel reflectance coefficient. This implies a lower accuracy in

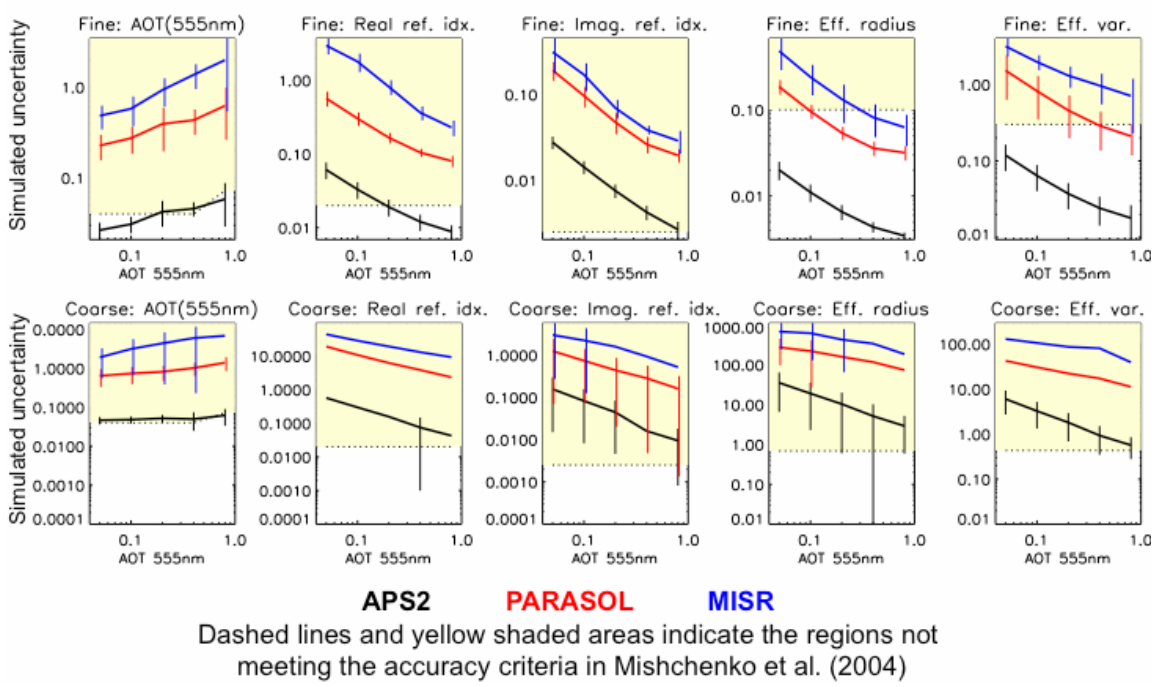

Figure D3. Simulated retrieval uncertainty over land.

these measurements, as described in Eq. (D3). Retrieval of surface parameters is a part of this analysis as well. In total, there are three spectrally invariant parameters retrieved (the Fresnel reflectance coefficient scaling parameter and two kernel parameters describing the shape of the BRDF). An isotropic BRDF kernel must also be retrieved independently for each wavelength. Other than these changes, the aerosol type and vertical distribution, observation geometry, and other factors are all identical to the study of aerosols over water.

Figure D3 presents the uncertainties as a function of simulation total AOT. Most of the APS-2 simulated uncertainties, indicated in black, are within the accuracy criteria. Exceptions are for the imaginary refractive index for the fine mode at low AOTs (although recall that the criterion for imaginary refractive index is arbitrarily chosen) and some of the coarse mode microphysical properties, again for low AOTs. Uncertainties from other simulated instruments, such as PARASOL (in red) or MISR (in blue) are even worse.

Figure D4 presents the same information as Fig. D3 but in terms of the ranges of simulated uncertainties for a particular configuration versus the accuracy criteria in Appendix A. Like in the previous figure, this one shows a reduced capability over land compared to over ocean, which is probably linked to the lower accuracy of observations of the polarized reflectance compared to the DoLP. The differences between the APS-2 and other instruments also confirm the argument for the use of sensors such as the APS-2.

Aerosol retrievals over clouds. The ability of an instrument such as APS-2 to retrieve optical properties of aerosols lofted above clouds was tested by Knobelspiesse et al. (2011a). In that work, observations of pollution and smoke aerosols over a marine stratocumulus cloud were made by the RSP. Prior to performing a retrieval with these observational data, a sensitivity study was completed. This study simulated the retrieval uncer-

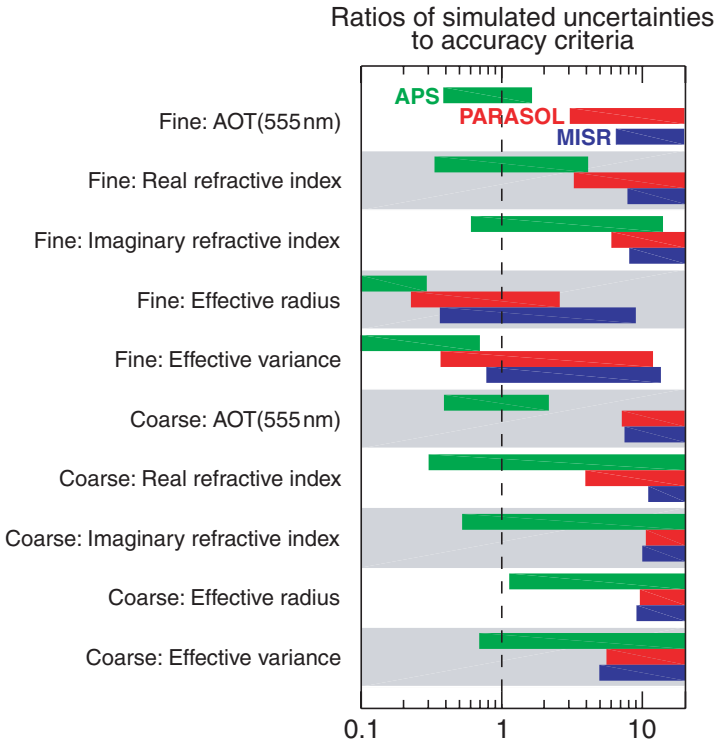

Figure D4. As in Fig. D2, but for simulated retrievals over land.

tainty of various quantities of Mexico City aerosols (see Table D1) lofted above a marine stratocumulus cloud. The results of this study are reproduced here as Fig. D5.

Figure D5 shows that fine and coarse mode AOT, fine mode size distribution, and cloud size distribution can all be retrieved within the accuracy criteria from Appendix A, even though those criteria were intended for aerosols or clouds alone. Refractive index values do not meet the accuracy criteria unless the AOT is very large. Even if the accuracy criteria are not met, retrieval of aerosols optical properties above clouds are quite rare, and any information about this potentially important climate forcing (Schultz et al. 2006) would be very useful. Simultaneous retrieval of aerosol and cloud properties with passive instruments is only possible if the observation includes many measurements with a dense angular sampling. For example, Waquet et al. (2009b) retrieved the AOT and effective radius using PARASOL, but could only do so when aggregating data over a very large area (hundreds of kilometers wide) in order to constrain the cloud droplet size.

Retrieval of aerosol and cloud properties in partially cloudy scenes. A unique feature of the APS-2 design is that it enables the simultaneous retrieval of aerosols and clouds in pixels that contain both. This is a distinct advantage over other passive instrument types, since somewhere between 20% and 30% of global observations at APS-2 spatial resolution will contain both cloud and cloud-free portions (Menzel et al. 2008). Furthermore, the edges of cloud and aerosol-only regions are of particular scientific interest, because of the potential for aerosol impacts on clouds and vice versa (Koren et al. 2007; Redemann et al. 2009). Like the retrieval of aerosols lofted above clouds, retrieval is possible because of the high angular resolution of APS-2 observations. Samples at many viewing angles of the cloud bow provide information about the cloud droplet size distribution, while side scattering angle observations provide information about the aerosols present in the scene.

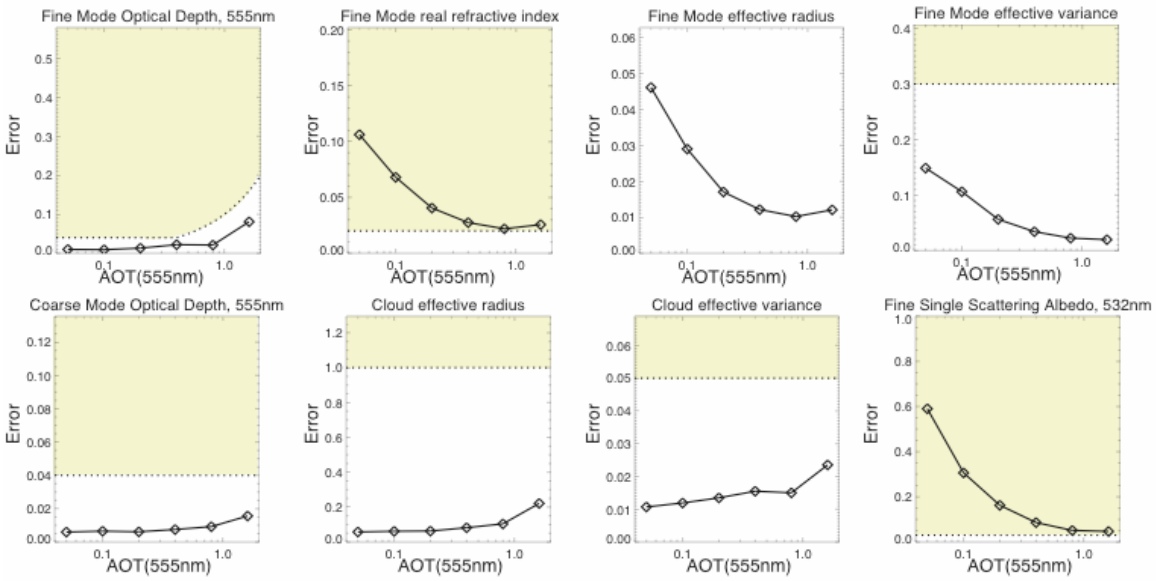

Figure D5. Simulated uncertainties for an urban pollution / biomass burning aerosol lofted above a marine stratocumulus cloud. Shaded yellow areas show where the accuracy criteria from Appendix A are not met.

A sensitivity study for these type of retrievals was performed by Hasekamp (2010). Figure D6, which is reformatted from that paper, shows the simulated uncertainty for a scene where the aerosol portion is composed of biomass burning aerosols with an optical thickness of 0.5 at 550 nm situated between 0 – 2 km, and resides below a cloud located at 2 – 3 km. Uncertainties were similar to those set for APS-2, with a polarimetric accuracy of 0.002 and radiometric accuracy of 2%. Nine wavelength bands were used: 350, 440, 530, 620, 710, 800, 890, 1600, and 2200 nm. Polarimetric measurements were in relative units similar to DoLP. While these characteristics are not identical to those of the APS-2, they are quite similar. The most notable difference is that this study uses a channel further into the UV than the APS-2, and has a coarser angular resolution. Observation geometry is somewhat different than the other tests shown here, since the relative solar–viewing azimuth angle is 0°. These simulations show that retrieval of the aerosol size distribution is obtained within accuracy criteria even for scenes mostly covered with clouds. Other parameters are more difficult to retrieve. For 64 viewing angles, at least half of the scene must be cloud free for AOT and SSA to be retrieved within accuracy criteria, while the scene must be 80% cloud free to retrieve the real refractive index. However, like the aerosol retrievals over clouds, retrievals of this nature cannot be performed with the current or planned set of aerosol observation platforms in orbit. So any information, even if it does not comply fully with the accuracy criteria designed for cloud free scenes, is useful to the scientific community.

Retrieval of stratospheric aerosols with the 1376-nm channel. The APS-2 design includes a dedicated channel centered at 1376 nm. Water vapor has a strong absorption feature at this wavelength (Fig. 8), which means that the resulting measurements will only be sensitive to radiative interactions above the altitudes at which the bulk of water vapor absorption occurs. This implies that the 1376-nm channel is sensitive to aerosols and clouds in the (dry) stratosphere and upper troposphere, but not to aerosols and clouds in

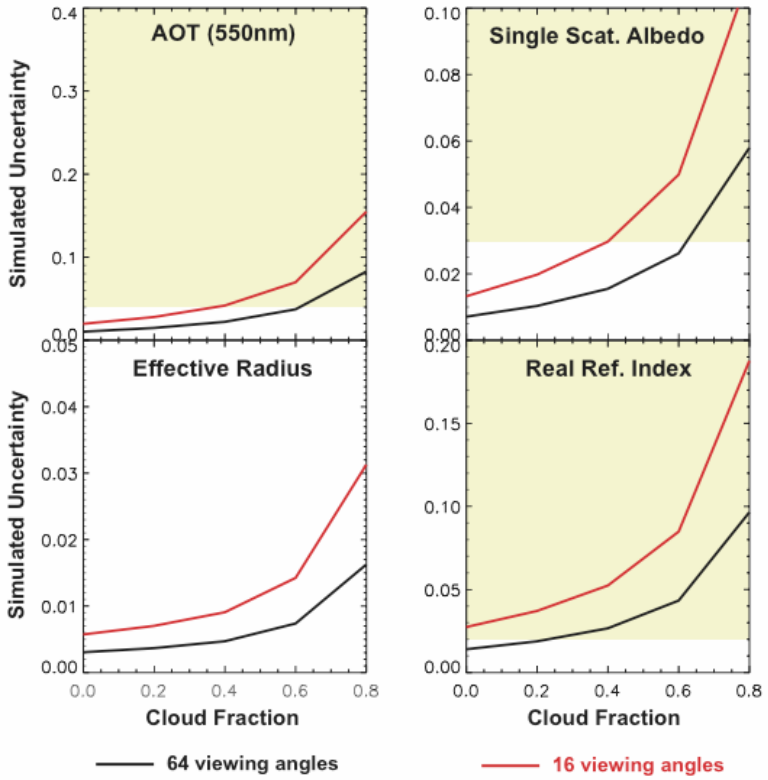

Figure D6. Retrieval capability for partially cloudy scenes. This figure is reformatted from Hasekamp et al. (2010). Red lines indicate simulations using 16 viewing angles, while black lines indicate the use of 64 viewing angles. Shaded yellow areas show where the accuracy criteria from Appendix A are not met.

the lower troposphere. It is therefore ideal for the detection of either high altitude cirrus clouds or stratospheric aerosols. The latter are rare and generally are caused by the injection of volcanic gases into the stratosphere. Once in the stratosphere, these aerosols are less affected by the removal mechanisms affecting tropospheric aerosols, and therefore persist for several years, while exerting a significant cooling radiative forcing (Hansen et al. 1992; Minnis et al. 1993; Russell et al. 1993). While aerosols are infrequently present in the stratosphere (the last major stratospheric injection occurred during the eruption of Mt. Pinatubo in the Philippines in 1991), a means to independently detect and characterize them is essential, both because of their significant climate impact and the interference they could cause in the retrieval of tropospheric aerosol properties.

To test the ability of the 1376-nm channel to detect stratospheric aerosols, various quantities were simulated at an altitude of 18 km. These aerosols were composed of sulfuric acid droplets (refractive index = 1.423 – i0.0000259) with a gamma size distribution having an effective radius of 0.025 μm and effective variance of 0.35. The observation geometry was identical to the previous studies (solar zenith angle = 45° and relative view azimuth angle of 45°), and due to water vapor absorption, was only sensitive down to an altitude of 6 km. The results of this test are shown in Fig. D7, where stratospheric AOT in the range of 0.06 to 0.20 at 555 nm are shown. Simulations were performed using both the total reflectance (I) and either the DoLP or R_p. Clearly, retrievals using the DoLP are more accurate than those that use polarized reflectance. This is especially the case for re-

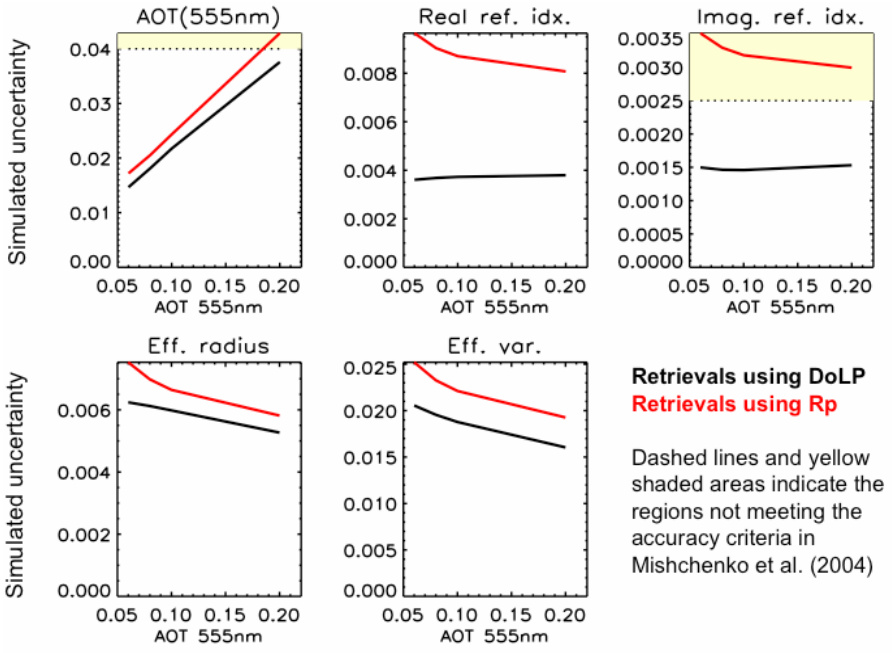

Figure D7. Simulated uncertainty for stratospheric aerosol retrievals.

fractive index. All of the DoLP simulated errors fall within the Appendix A criteria, although the relative error for the AOT is somewhat high. Presumably, errors could be reduced further by constraining the retrieval of refractive index properties, since the chemical composition of stratospheric aerosols would already be known.

Conclusions. This appendix presented a brief sensitivity study for the retrieval of aerosol properties from APS-2 observations in comparison with the capabilities of other passive sensors. The primary philosophy of the APS-2 design is that observations gather a large amount of information for each scene, which can be used to retrieve all the climatically relevant optical properties of atmospheric aerosols. This is in contrast to all of the passive instruments currently in orbit, for which aerosol retrieval is ill-posed. To show this quantitatively, we used a Bayesian statistical approach to link observational characteristics and uncertainties to retrieval uncertainties, when ten aerosol parameters in addition to surface characteristics are simultaneously retrieved. The results of this analysis show that APS-2 is uniquely capable of retrieving these aerosol optical properties to within the accuracy requirements for climate modeling described in Appendix A over oceans, and to a slightly lesser extent, over land. Current instruments, such as MISR and PARASOL, are only capable of meeting the accuracy requirements for the fine size mode aerosol parameters over oceans, and this capability degrades over land. Note that these results also imply that when only AOT is retrieved from measurements of the existing instruments, the results will be significantly influenced by the assumptions made about the other aerosol and surface parameters.

It is important to recognize that our results are a best-case uncertainty scenario, where it is assumed that the radiative transfer model used in a retrieval is a perfect representation of reality, and that the retrieval algorithm is unhindered in its search for the optimal fit between model parameters and observations. Observation errors are highly simplified (accounting for calibration only) and are assumed to be uncorrelated. Calibration errors

are potentially correlated, which is likely to increase certain retrieval uncertainties.

Simulated uncertainties do, however, represent retrievals where all model parameters are determined simultaneously. This would explain why simulations show higher uncertainties for MISR than those reported in the literature (e.g., Kahn et al. 2007, 2010). Because of the underdetermined nature of those observations, retrieval algorithms must utilize predefined models of aerosol properties, which can potentially have a large impact on accuracy. This accuracy degradation is difficult to characterize and quantify. In Kahn et al. (2007), this problem is described as one of the possible explanations for biases between the MODIS and MISR results that are nearly as large as the expected uncertainties based upon AERONET validation. In any case, our results do generally agree with uncertainty assessments for PARASOL (Hasekamp et al. 2010; Dubovik et al. 2011) for algorithms that retrieve all parameters simultaneously. Indeed, similar results have also been found in the simulations by Hasekamp and Landgraf (2007), whose methodology was a template for this study.

We also show the aerosol retrieval capability of an APS type of instrument in scenarios that to date are inaccessible to passive instruments. Specifically, we show that APS-2 observations can be used to retrieve properties of aerosols lofted above clouds, of aerosols in partially cloudy pixels, and of stratospheric aerosols with a specially designed channel at 1376 nm. Not surprisingly, the accuracy of the APS-2 retrievals above clouds and in partially cloudy pixels can be expected to be generally lower than in cloud-free regions, especially for the refractive index. That said, simultaneous cloud–aerosol retrievals of this nature do not exist for current passive instruments, and so we expect them to be of great value to the scientific community.

Appendix E
Examples of Research Scanning Polarimeter retrievals

Research Scanning Polarimeter. Measurements made by RSP are similar to those of APS-2 except for viewing the Earth from 152 angles instead of 255, and for doing this at 410, 469, 550, 670, 865, 962, 1589, 1884, and 2250 nm rather than 413, 444, 555, 674, 866, 911, 1376, 1603, and 2260 nm (Cairns et al. 2003). Note that both the 1884 and 1376 nm bands are extremely effective for screening thin cirrus clouds, but the 1376 nm band APS-2 allows for better detection and characterization of stratospheric aerosols in case of a major volcanic eruption (see Appendix D). The 444 nm band on APS-2 coincides with an absorption peak of Chlorophyll-*a*, which is a photosynthetic pigment found in phytoplankton and can therefore be used as a proxy for the amount of phytoplankton mass.

Aerosol retrievals over the ocean. In this sub-section we describe some case studies of aerosol retrievals over the ocean. These retrievals require a model of scattering by the ocean body that provides consistent simulations of the total and polarized water-leaving radiance. The model uses typical underwater light polarization signatures (e.g., Voss and Fry 1984) to constrain the size and refractive index of marine particulates. We then mix these particulates with clear seawater and determine the scattering and absorption coefficients and the scattering phase matrix of the mixture (e.g., Morel and Maritorena 2001; Chowdhary et al. 2005). This microphysical model for scattering and absorption by the ocean body is then used in a radiative transfer code to calculate the reflection matrix of the ocean body. This approach (Chowdhary et al. 2006; 2011) reproduces the observed

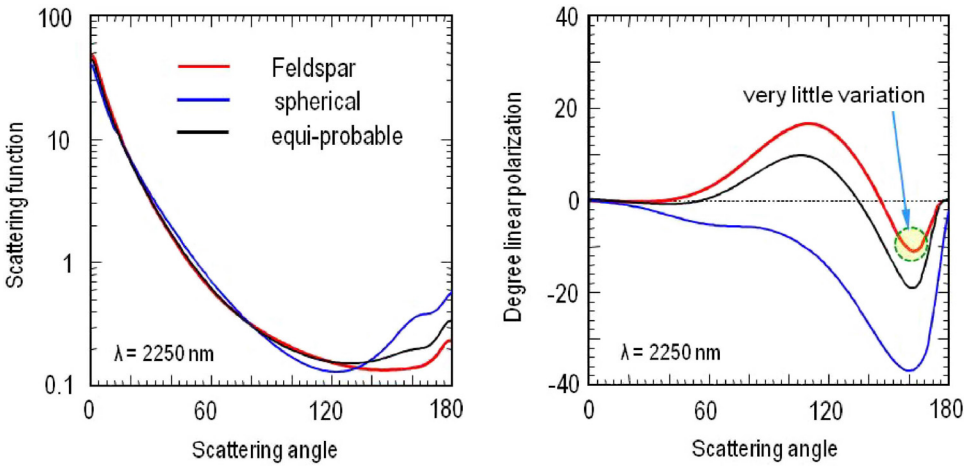

Figure E1. Scattering function (left) and degree of linear polarization (right) for spherical particles and for spheroids with Feldspar-like and equi-probable aspect-ratio distributions. Results are shown for particles with an effective radius of 2 μm, an effective variance of 1, and a refractive index of 1.5. The wavelength of the incident and scattered light is 2250 nm.

variations of the underwater light color with Chlorophyll concentrations [Chl] and provides the total and polarized water-leaving radiance for any viewing geometry.

In early analyses of RSP observations over the ocean in areas that are not noted for having large amounts of dust or soil particles, we found evidence that non-spherical particles were present (Chowdhary et al. 2005). This conclusion was based on the excessively large residual misfit between aerosol retrievals using spherical particles at scattering angles near backscatter and particularly for the longest wavelength bands where the contribution of coarse mode particles dominates. In order to construct a microphysical model for the scattering properties of such randomly oriented non-spherical aerosol particles, we use shape mixtures of randomly oriented spheroids. The shape for a single spheroid can be described by the aspect ratio ε', and a distribution of shapes for an ensemble of such particles by a distribution of aspect ratios ε'. Mishchenko et al. (1997b) show that the flattening of the scattering function at side-scattering angles observed in laboratory measurements for scattering by soil dust (Jaggard et al. 1981) can be reproduced by an ensemble of spheroids. Scattering matrices measured by Volten et al. (2001) show the same featureless behavior in phase functions for a variety of mineral particles including Feldspar, which is a significant component of desert dust. In addition, Volten et al. (2001) found the linear polarization of light scattered by these particles to be similar, with a broad positive maximum at side-scattering angles and a weak negative minimum near the backscattering direction. Dubovik et al. (2006) demonstrated that both features can be reproduced by ensembles of randomly oriented spheroids if $\varepsilon' \geq 1.44$ (Fig. E1), and we will refer to the shape distribution introduced by Dubovik et al. as the Feldspar shape distribution. However, the polarized reflectance observed by RSP often exhibits variations in the polarization minimum near the backscattering direction that can only be reproduced by spheroid ensembles that include $\varepsilon' < 1.44$ and that have salt-like refractive indices. Presumably, such ensembles represent partially hydrated non-spherical salt mixtures with shapes (see e.g. Fig. E2, adapted from Wise et al. 2007) that differ significantly from those of mineral dust. In the following analyses we use the look-up tables computed by Dubovik et al. (2006) for scattering by randomly oriented non-spherical aerosols that in-

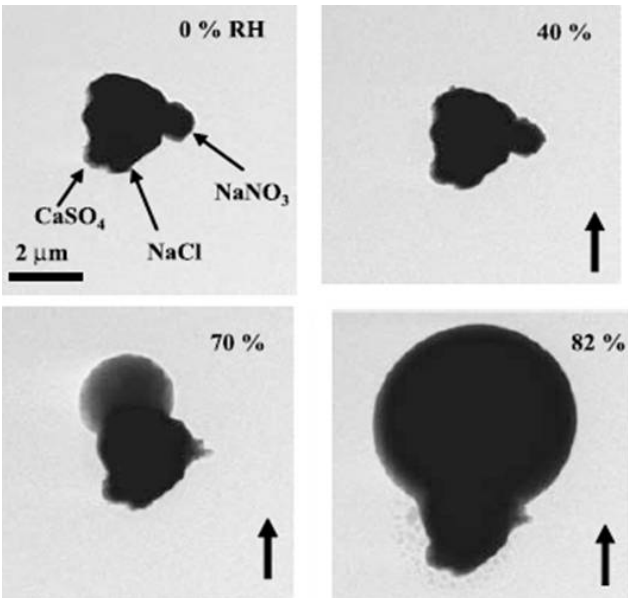

Figure E2. Images of a ~3.6 µm NaCl salt particle with an attached $NaNO_3$ salt crystal collected from polluted maritime air at Scripps Pier in San Diego, CA. The sequence of panels shows change in particle shape as the relative humidity (RH) is increased from 0% to 82% (Wise et al. 2007).

clude wide ranges of refractive index and size and adopt for the aspect ratio the Feldspar and the equi-probable shape distribution for nonspherical-particle mixtures.

Having introduced the microphysical models that are used in the retrieval of aerosol properties, we will now discuss coarse mode aerosol retrievals from RSP measurements obtained during the CLAMS campaign. CLAMS was a shortwave radiative closure experiment that took place during the period from 10 July to 2 August 2001 and involved

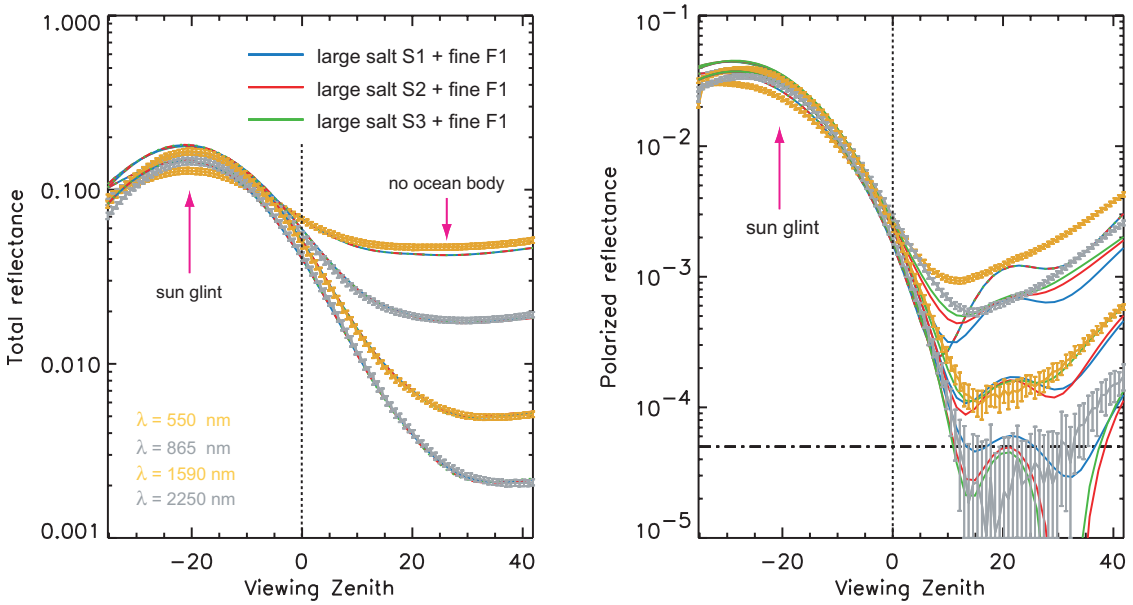

Figure E3. Error bars show total reflectance (left panel) and polarized reflectance (right panel) measured during the CLAMS campaign by the RSP as a function of viewing angle and wavelength λ. The colored curves show fits for the total reflectance measurements assuming spherical shapes for the fine and coarse mode aerosols. The microphysical properties of these aerosols are given in Table E1.

measurements obtained from six research aircraft, several land sites, and the Chesapeake Lighthouse research ocean platform. Here, we focus on data obtained on 17 July 2001 when all the aircraft participating in the CLAMS experiment flew coordinated patterns over the ocean platform site to perform measurements of the upwelling radiation field and aerosol properties (Chowdhary et al. 2005). Figures E3 and E4 show the reflectance and polarized reflectance observations for four wavelengths from 555 to 2264 nm, with the uncertainty in each reflectance measurement indicated by an error bar. The solar zenith and relative azimuth angles for these observations were 22° and 1°, respectively, and the altitude of the aircraft was 3.6 km. The red, green, and blue curves in Fig. E3 show fits to the RSP total reflectance assuming that the coarse mode particles are spherical, in this case, the wet sea salt particles used for MODIS retrievals of aerosols over ocean (Remer et al. 2005 and Table E1). For these fits we omitted the water-leaving radiance, which explains the underestimate for the RSP total reflectance measurements at 555 nm. Note that while the fit for the remaining RSP total reflectance measurements is very good, none of the spherical coarse mode aerosol models (S1, S2, and S3 from Table E1) used for these fits are able to reproduce the corresponding RSP polarized reflectance measurements. In contrast, Fig. E4 shows that using spheroids with an equi-probable aspect ratio distribution for the coarse mode aerosol leads to a fit of both the total and polarized reflectance measured by RSP. The sizes and refractive indices of these spheroids are summarized in Table E1. We note that there is a significant range in the retrieved particle size because the polarized reflectance signal is very small at 2264 nm. Nevertheless, the sizes for the non-spherical coarse mode particles are much larger than for the spherical coarse mode particles in Table E1. Figure E5 shows a comparison of the diffraction peaks calculated for the coarse mode particle size distributions in Table E1 with that

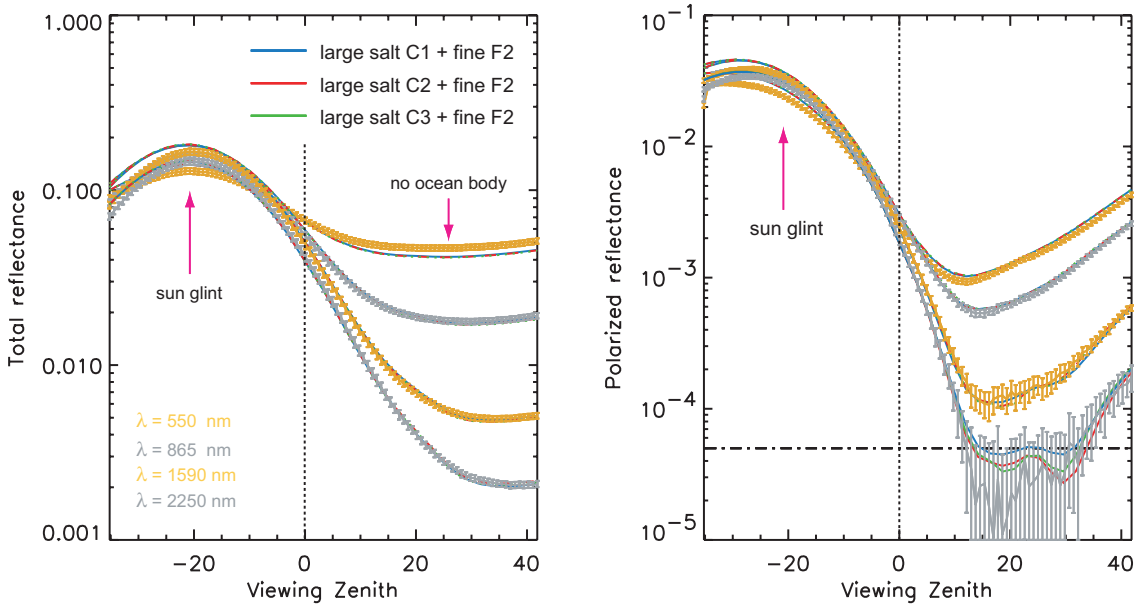

Figure E4. The error bars show the same RSP reflectances as in Fig. E6. The colored curves show fits for the total reflectance measurements assuming randomly oriented spheroids with an equi-probable aspect ratio distribution (cf. Fig. E3b) for the coarse mode aerosols. The microphysical properties of these aerosols are given in Table E2.

Table E1. Aerosol models for analyses of RSP reflectance from the CLAMS field campaign

Aerosol model	r_e [3]	v_e [4]	m ($\lambda \leq 865$nm) [5]	m ($\lambda = 1590$nm) [5]	m ($\lambda = 2250$nm) [5]
Spherical salt (S1) [1]	0.98	0.43	1.45 – i 0.0035	1.43 – i 0.0035	1.43 – i 0.0035
Spherical salt (S2) [1]	1.48	0.43	1.45 – i 0.0035	1.43 – i 0.0035	1.43 – i 0.0035
Spherical salt (S3) [1]	1.98	0.43	1.45 – i 0.0035	1.43 – i 0.0035	1.43 – i 0.0035
Spherical soluble (F1) [1]	0.15	0.43	1.45 – i 0.0035	1.43 – i 0.01	1.4 – i 0.005
Salt-like large (C1) [2]	2	0.5	1.43 – i 0.0005	1.41 – i 0.0005	1.39 – i 0.0005
Salt-like large (C2) [2]	3	0.5	1.47 – i 0.0005	1.43 – i 0.0005	1.41 – i 0.0005
Salt-like large (C3) [2]	4	0.5	1.49 – i 0.0005	1.43 – i 0.0005	1.41 – i 0.0005
Fine mode (F2)	0.15	0.2	≥1.42 – i 0.01	1.41 – i 0.01	1.4 – i 0.01

[1] Source: Remer et al. (2005)

[2] Spheroids with equi-probable aspect-ratio distribution for large salt-like aerosol

[3] Particle size distribution effective radius, in μm

[4] Particle size distribution effective variance

[5] Refractive index

Table E2. Aerosol retrievals using RSP reflectance from the MILAGRO field campaign

Aerosol model [1]	r_e [2]	v_e [3]	m ($\lambda \leq 865$nm) [4]	m ($\lambda = 1590$nm) [4]	m ($\lambda = 2250$nm) [4]
Salt-like large	2	1	≥1.43 – i 0.0005	1.4 – i 0.0005	1.4 – i 0.0005
Fine mode	0.15	0.2	1.46 – i 0.01	1.44 – i 0.01	1.4 – i 0.01

[1] Spheroids with equi-probable aspect ratio distribution for salt-like large aerosol

[2] Particle size distribution effective radius, in μm

[3] Particle size distribution effective variance

[4] Refractive index

measured by an AERONET sun photometer on the Chesapeake Lighthouse platform. Note that such peaks are highly sensitive to particle size but not to particle shape as can be inferred from the solid cyan curve (for spheroids with $r_e = 2$ μm) which overlaps the dashed red curve (for spheres with $r_e \approx 2$ μm). This comparison between the measured diffraction peak and the diffraction peak calculated for the retrieved particle size distribution clearly favors the large particle sizes retrieved with the spheroid coarse mode aerosol models.

Although the aerosol retrievals for CLAMS represent a best fit over the entire spectral range of the RSP observations, the visible part of the spectrum is particularly sensitive to the fine mode aerosol properties. For this part of the spectrum the contribution of water-leaving radiance is always significant at some wavelength, but the wavelength for which the ocean body contribution is largest varies with the type (i.e., coastal versus open) and biological state (i.e., low [Chl] versus high [Chl]) of the ocean. For analyses of total reflectance measurements, this requires that the properties of fine mode aerosols be retrieved simultaneously with those of the ocean. However, the polarization of water-leaving radiance for observations in the principal plane (i.e., the plane containing the vertical axis and the direction of the sun) is always small around the backscattering direction, and relatively small in the sunglint region, such that it can be ignored. For observa-

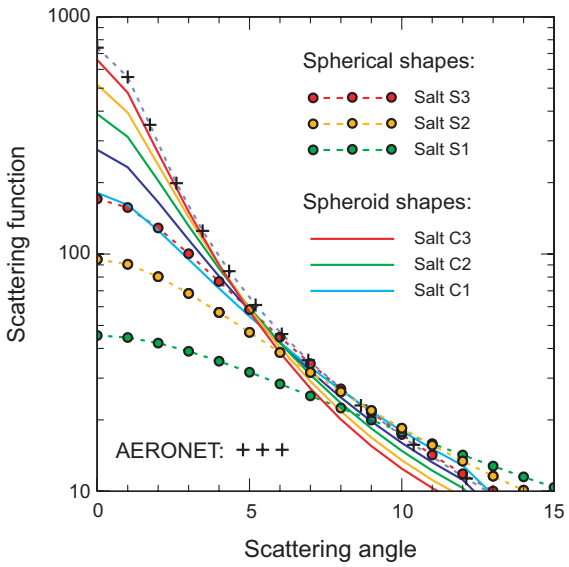

Figure E5. Diffraction peaks for the spherical coarse mode particles in Fig. E3 and Table E1, for the spheroid coarse mode particles in Fig. E4 and Table E1, and for AERONET measurements, at λ = 865 nm.

tions outside the principal plane it exhibits strong angular behavior that is different from the atmospheric scattering contribution. Although the magnitude of the polarization of the water leaving radiance varies with the biological state of the ocean, its relative angular variation is almost independent of [Chl], at least for the open ocean.

Figures E6 and E7 show examples of RSP polarized reflectance observations close to the principal plane and are from the same flight segment used to generate Figs. E3 and E4. The black dashed curves in Fig. E6 show the fit to the RSP polarized reflectance when ignoring the water-leaving radiance contribution, while the cyan solid curves include this contribution, which we computed from *in situ* measurements of underwater light scattering properties. Note that the dashed and solid curves overlap regardless of the wavelength, which implies that the RSP polarized reflectance in Fig. E6 is insensitive to contributions from the ocean body. In contrast, Fig. E7 shows that the polarized reflectance is very sensitive to variations in the fine mode aerosol microphysical model and vertical distribution. The best-fit model is the fine-mode F2 model from Table E1.

The green and blue solid curves in the left-hand panel of Fig. E7 show the sensitivity of the polarized reflectance fit to variations in the real and imaginary refractive index of the fine mode aerosol, respectively. The green and blue solid curves in the right-hand panel show the sensitivity of the polarized reflectance fit to variations in the vertical distribution and in the effective variance of the fine mode aerosol, respectively. The AOT and SSA retrievals generated by fitting a microphysical aerosol model to the total and polarized reflectance are compared with observations made by the Chesapeake Lighthouse AERONET sun photometer in Fig. E8. The range in the fine-mode aerosol imaginary refractive index retrieved from RSP data is caused by the uncertainty in the vertical distribution of the aerosols (Chowdhary et al. 2005). The AOT exhibited substantial temporal and spatial variability on this day, which accounts for the offset in AOT between the RSP and AERONET retrievals (see left-hand panel). Nevertheless, the spectrum of the AOT, which for visible wavelengths is a measure of the fine mode aerosol particle size distribution, is the same for the RSP and AERONET retrievals. In addition, the range in SSA retrieved using the RSP observations is consistent with the SSA range from AERONET (see right-hand panel).

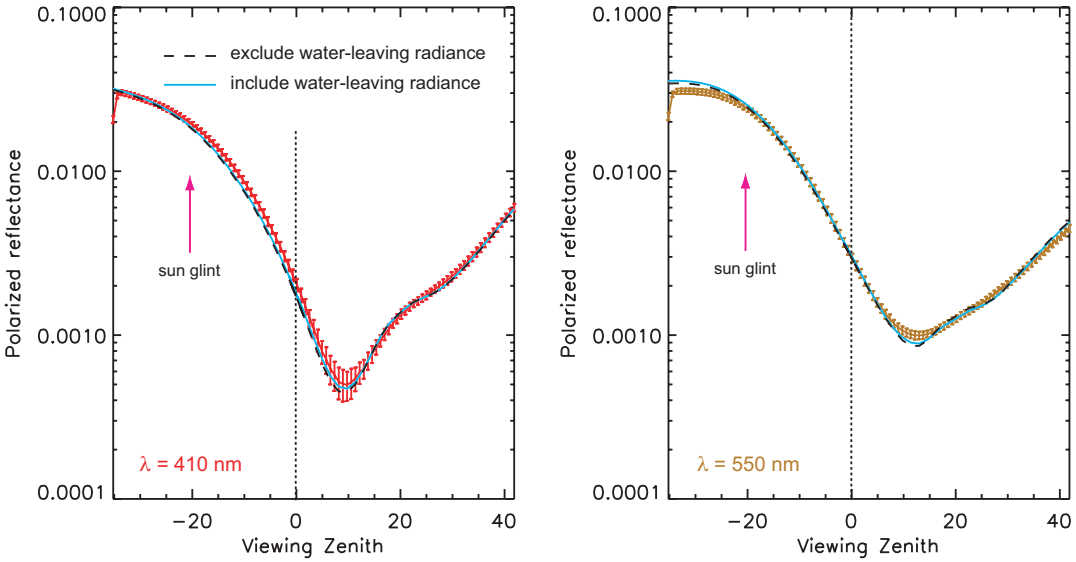

Figure E6. Error bars show polarized reflectance at λ = 410 nm (left-hand panel) and 550 nm (right-hand panel) measured by RSP during the CLAMS campaign as a function of viewing angle. The black dashed curves show fits assuming the F2 fine-mode aerosol from Table E1 and excluding the water-leaving radiance contribution. The cyan solid curves show the same fits except for including the water-leaving radiance contribution (Chowdhary et al. 2005).

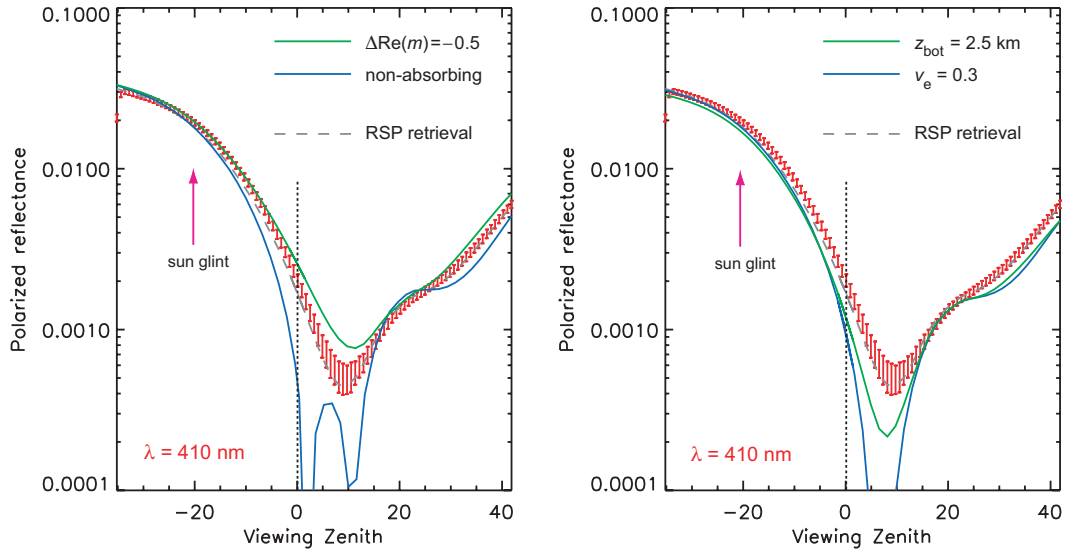

Figure E7. Error bars show polarized reflectance at λ = 410 nm measured by RSP during the CLAMS campaign as a function of viewing angle. The grey dashed curves show fits assuming the aerosol models in Table E2. The green and blue solid curves in the right-hand panel show the sensitivity of the polarized reflectance fit to variations in the vertical distribution (increasing the bottom of the aerosol layer from 0 to 2.5 km) and in the effective variance (increasing v_{eff} by 0.1) of the fine mode aerosol, respectively. The same curves in the left-hand panel show the sensitivity of the polarized reflectance fit to variations in the real refractive index (decreasing m by 0.5) and imaginary refractive index (ignoring absorption) of the fine mode aerosol, respectively.

The only other field experiment, beside CLAMS, for which good quality high and low altitude RSP data were obtained for clear skies over an ocean was phase B of the NASA sponsored Intercontinental Chemical Transport Experiment (INTEX). The INTEX

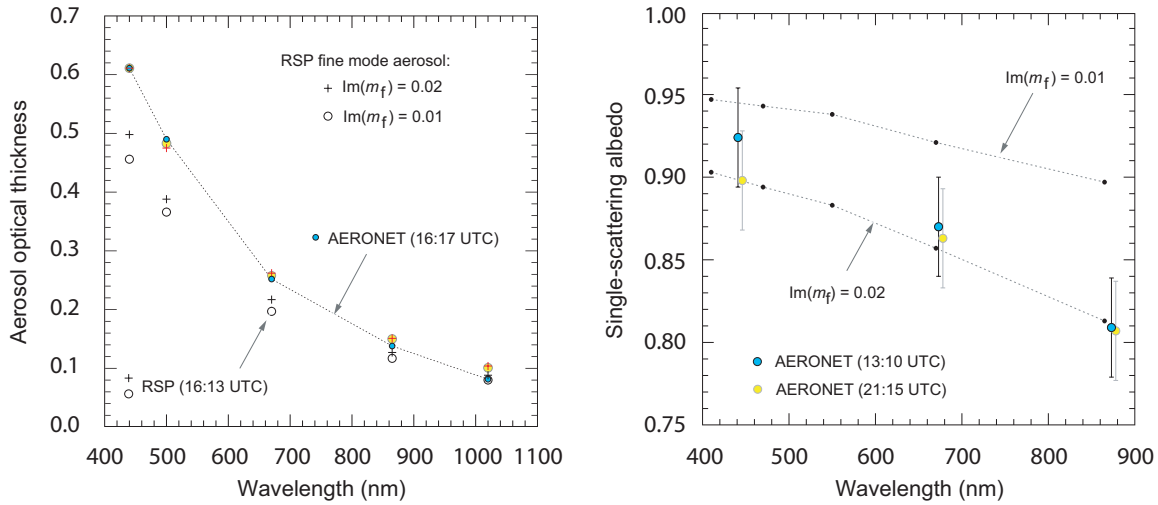

Figure E8. The left-hand panel compares the AOT measured by AERONET (cyan circles) with those retrieved from RSP data with fine mode imaginary refractive index Im(m) = 0.01 (plus symbols) and 0.02 (open circles). The offset between the RSP and AERONET retrievals can be attributed to the spatial and temporal variation of aerosol burden. The yellow circles and red symbols show the spectrum of RSP retrievals when normalizing their AOT to the AERONET AOT at λ = 410 nm. The right-hand panel compares the spectrum of the aerosol SSA retrieved from AERONET (cyan and yellow circles) with those retrieved from RSP data with fine mode imaginary refractive index Im(m) = 0.01 and 0.02.

objectives were to study the transport and evolution of gasses and aerosols at trans- and inter-continental scales, and to assess their impact on air quality and climate. The INTEX-B field study was coordinated with other agencies as part of the MILAGRO campaign, which focused on the flow of pollution out of Mexico City during the March 2006 (Molina et al. 2010). Here, we focus on RSP data obtained on 10 March 2006.

On this day RSP flew over a patch of the Gulf of Mexico identified from SeaWiFS and MODIS/Aqua satellite imagery as case 1 ocean waters, i.e., oceanic waters whose optical properties can be prescribed as a function of [Chl] by the bio-optical model of Morel and Maritorena (2001). The error bars in Fig. E9 show the total reflectance (left-hand panel) and the polarized reflectance at 410 nm (right-hand panel) observed by RSP. The altitude for these observations was very low (68 m), which makes them particularly sensitive to the brightness of the water-leaving radiance. Furthermore, the observations were obtained at a large relative azimuth angle (38°), which makes them sensitive to the polarization properties of the water-leaving radiance.

The black dashed curves in Fig. E9 show the results from multiple-scattering computations in which the water-leaving radiance contributions are ignored. The aerosol properties used for these computations were taken from analyses of RSP data obtained at a high altitude (Table E2, from analyses of Fig. E10). The purple, grey, green, and red colored dashed curves show the results from multiple-scattering computations that include the radiance of light emerging from an open ocean with [Chl] = 0.03, 0.1, 0.3, and 1 mg m^{-3}, respectively. Note that the total and polarized reflectance for these results vary significantly in brightness and bidirectionality, as expected. A good match to the RSP reflectance is found (see cyan solid curve) for underwater light computations with [Chl] = 0.1 mg m^{-3} and slightly elevated amounts of colored dissolved organic matter (CDOM). These retrievals of [Chl] and CDOM are consistent with the MODIS/Aqua retrievals for

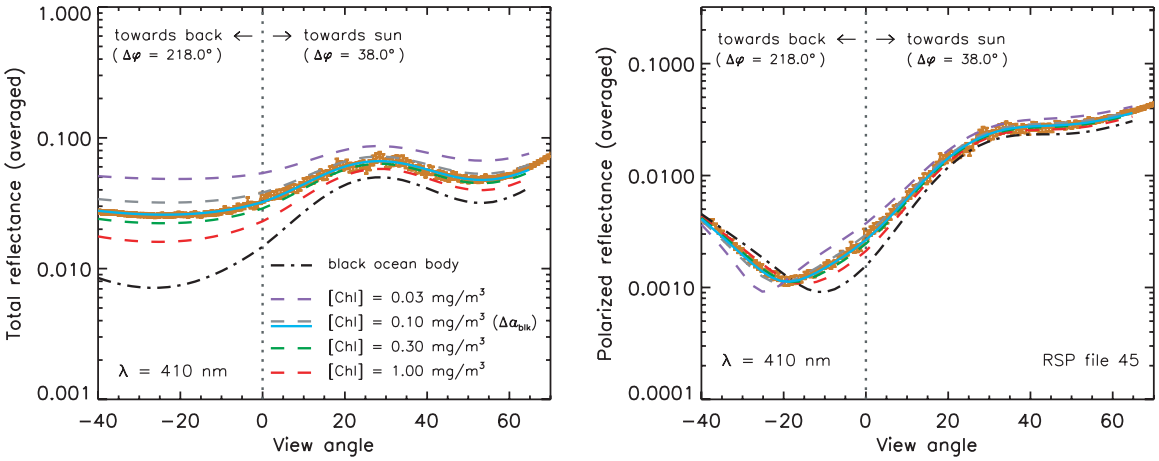

Figure E9. Error bars show total reflectance (left-hand panel) and polarized reflectance (right-hand panel) measured by RSP during the MILAGRO campaign as a function of viewing angle at λ = 410 nm. The altitude for these measurements was 68 m, and the azimuth angle 38°. The black dashed curves show the fits for the total and polarized reflectance measurements when ignoring the water-leaving radiance contribution. The aerosol properties for these fits are given in Table E2. The colored curves show the corresponding fits when including the radiance emerging from an ocean with various [Chl].

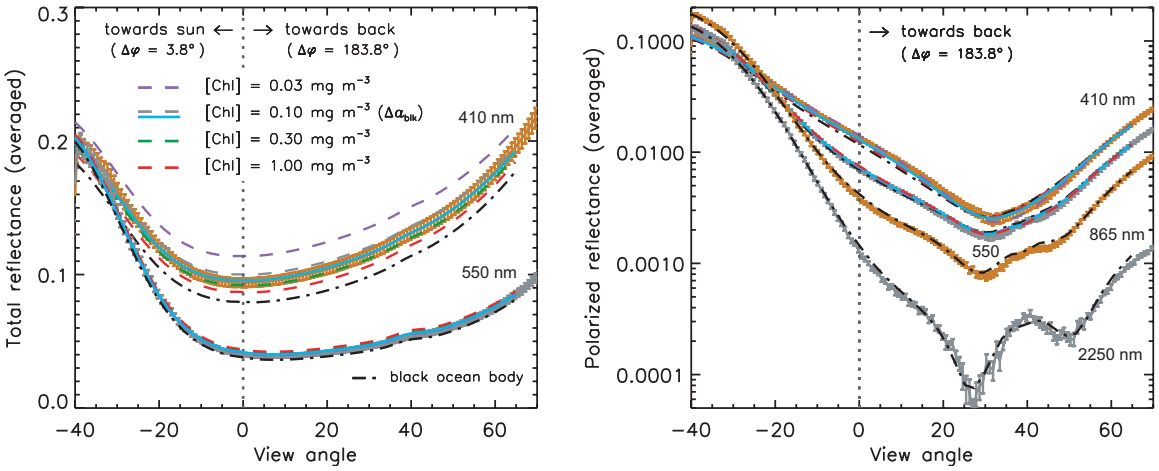

Figure E10. Error bars show total reflectance at λ = 410 and 550 nm (left-hand panel) and polarized reflectance at λ = 410 to 2250 nm (right-hand panel), measured by RSP during the MILAGRO campaign as a function of viewing angle. The altitude and azimuth angle of these measurements was 4.1 km and 3.8°, respectively. The black dashed curves show the reflectance fits when ignoring the water-leaving radiance contribution. The aerosol properties for these fits are given in Table E2. The colored curves show the corresponding fits when including the radiance emerging from an ocean with various [Chl].

this scene. Figure E10 shows RSP measurements (see error bars) obtained at high altitude (4.1 km) and a small relative solar azimuth angle (3.8°). The left- and right-hand panels are for the total reflectance (at λ = 410 and 550 nm) and the polarized reflectance (at λ = 410, 550, 865, and 2250 nm), respectively. The black dashed curves in both panels show fits to the RSP reflectance in which the water-leaving radiance contributions are ignored; whereas the purple, grey, green, and red colored dashed curves show fits that include the radiance of light emerging from an open ocean with [Chl] = 0.03, 0.1, 0.3, and 1 mg m^{-3}, respectively.

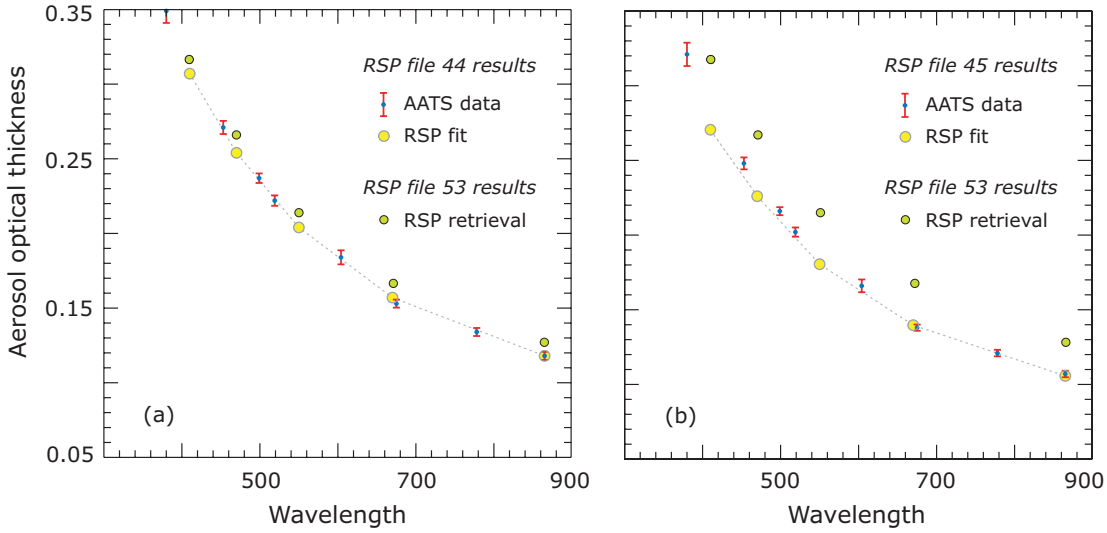

Figure E11. The AOT measured by AATS (red error bars) during low-altitude flights at 19:54 UTC (left-hand panel) and 20:02 UTC (right-hand panel) compared with those retrieved from RSP data (green circles) during a high altitude flight at 20:36 UTC. The offset between the RSP and AERONET retrievals can be attributed to the spatial and temporal variation of aerosol burden. The yellow circles show the spectrum of RSP retrievals when normalizing their AOTs to fit the AATS spectrum.

Note that the calculated total reflectance at 410 nm varies significantly with [Chl], consistent with what is seen in Fig. E9. However, the corresponding polarized reflectance shows no significant variation with [Chl] because the water-leaving radiance is very weakly polarized for viewing planes with small relative solar azimuth angles. This means that the polarized reflectance for such viewing geometries can be used to constrain the fine and coarse mode aerosols regardless of [Chl] or even the type of ocean body. The resulting aerosol retrievals are given in Table E2. We note that the [Chl] and CDOM retrieved from the total reflectance in Fig. E10 are again consistent with the MODIS/Aqua retrievals for this scene.

In Fig. E11, we compare the AOT retrieved from the high-altitude RSP reflectance observations that were shown in Fig. E10 with the AOT measured by the NASA AATS (Redemann et al. 2009) during low-altitude RSP flights. The left- and right-hand panels show AATS results for different flight segments (the AOT measurements in the right-hand panel were obtained during the same segment as the RSP total and polarized reflectance shown in Fig. E9). The offset in each panel between the measured and retrieved AOTs is consistent with the temporal and spatial variation of aerosol burden for this scene (e.g., see change in AATS data between left- and right-hand panels); however, the yellow circles show that the AOT spectra from the AATS data can be reproduced by scaling the AOT from the RSP retrievals.

Aerosol retrievals over land. One of the main beauties of the Earth when viewed in remote sensing measurements from space, or aircraft, is its bright, many hued, underlying surface. This also presents one of the main difficulties in retrieving the AOT and aerosol microphysical model using passive remote sensing measurements of the intensity over land surfaces since the background is brighter than our object of interest, the aerosols in the atmosphere. Although the polarized reflectance of the land surface at visible wavelengths is typically smaller than the signal from aerosols, it is clear that in order to use

polarization measurements to provide an accurate determination of the type and amount of aerosols present in the atmosphere we need a quantitative understanding of the polarization properties of the land surface. The polarizing properties of natural surfaces as understood from ground and aircraft-based measurements and observations from several space shuttle flights have been summarized by Coulson (1988). This summary is still an excellent reference to the historical measurements that have been made of the polarizing properties of mineral and vegetated surfaces, although the tendency to present linear polarization measurements in terms of the degree of linear polarization (DoLP) makes some of this information difficult to use. This is because the DoLP, which is a ratio, mixes the effects of the polarization properties of the surface (numerator) and the reflection properties of the surface (denominator) that are to a large extent caused by the different mechanisms of surface and volume scattering, respectively. There has also been a significant number of satellite measurements provided by POLDER flown on the ADEOS-I, -II and PARASOL missions, and airborne measurements made by RSP since Coulson's review was published. We will therefore briefly summarize here the present understanding of the polarizing properties of the surface.

It is generally believed that the polarization of surfaces is primarily generated by external reflections off the facets of soil grains, or the cuticles of leaves. The rationale for such a model is observations of minerals and the surface cuticles of vegetation (Vanderbilt et al. 1985; Rondeaux and Herman 1991) that show the polarized reflectance to be grey. This has also been observed in macroscopic measurements of natural scenes such as forests, bare soils, agricultural fields and even urban landscapes over the spectral range from the deep blue to IR (Waquet et al. 2009c). If surface polarization is generated by external reflections then its magnitude will tend to be spectrally neutral as long as variations in the real refractive index of the surface are relatively small. This is generally true of both the waxy cuticles of vegetation and minerals (Pollack et al. 1973). Thus, although the surface reflectance is both colorful and spatially variable, the surface polarized reflectance is spatially variable but spectrally grey. It is this feature of the surface polarized reflectance that makes polarization measurements such a useful tool for aerosol retrievals over land. The key remaining questions regarding the surface polarized reflectance, if we are to use polarization for remote sensing of aerosols, are the predictability of its absolute value, for a particular surface, and its angular distribution.

Measurements taken with RSP over agricultural land containing bare soil and a range of different crops that are grown near Oxnard, CA (broccoli, peppers, etc.) are shown in Fig. E12a. These measurements, which were obtained with the RSP installed in a small survey plane flying at an altitude of 3000 m, have been atmospherically corrected using simultaneous, collocated sun-photometer measurements These measurements show that if a long-wavelength measurement (e.g., 2264 nm) that is only weakly affected by the aerosol and molecular scattering is available then this can be used to characterize the polarized reflectance across the entire solar spectrum. The only limiting factor in using a long wavelength measurement to characterize the surface is whether the observational viewing geometry is sufficient to predict the behavior of the surface polarization for other viewing geometries. This is primarily of concern for short wavelengths, where the molecular and aerosol scattering is sufficiently strong that diffuse surface-atmosphere interactions have to be modeled. This is why a model of the surface is necessary for accurate forward modeling of the polarized reflectance at short wavelengths.

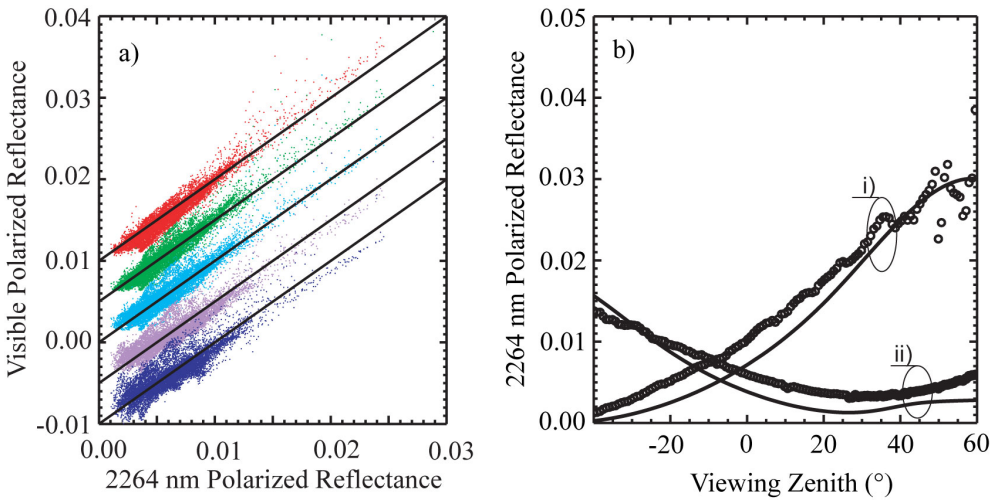

Figure E12. (a) Polarized reflectance measurements taken with RSP mounted on a small survey plane over agricultural land near Oxnard, CA at an altitude of 3000 m. The visible polarized reflectances at 410, 469, 555, 670, and 865 nm are plotted against that at 2264 nm in blue, mauve, turquoise, green and red respectively. The bands are offset by 0.005 from one another to allow any spectral differences in behaviour to be identified. The solid 1:1 lines show what is expected if the surface has a grey polarized reflectance. (b) Atmospherically corrected polarized reflectance measurements at 2264 nm with the data taken in meridional planes (i) close to the principal plane and (ii) at 45° to the principal plane.

Figure E12b shows observations in the solar principal plane (the plane that contains the local vertical and the sun) that are used to estimate the parameters in a simple Fresnel model of the surface polarized reflectance (Cairns et al. 2009b) and predict the polarized reflectance for a different viewing geometry. It can be seen that the model prediction of the polarized reflectance for a different viewing geometry to that used to estimate the model is in good agreement with the observations in this other scan plane. The conclusion we draw is that a simple Fresnel model, fitted to observations of the surface (or long wavelength observations), is sufficient to predict the angular variation of the surface polarized reflectance at all view angles that are not close to the backscatter direction.

Once a simple model of the surface polarized reflectance is available it is relatively straightforward to estimate the surface model, the AOT, and an aerosol microphysical model using an optimal estimation method (Waquet et al. 2009a; Cairns et al. 2009a; Dubovik et al. 2011; Hasekamp et al. 2011). Examples of aerosol retrievals that were made using such a model during the Aerosol Lidar Validation Experiment (ALIVE) and INTEX-B are presented in Fig. E13. Figures E13a and b show measurements performed on 16 and 19 September 2005 during the ALIVE experiment, close to the AERONET station are shown. The spikes in these scans, which are correlated across all spectral bands most obviously in Fig. E13a, are the result of different view angles seeing different surface types, since the data have not been re-organized to view the same point on the ground. Nonetheless the residuals of the model fit to the data are $\sim 10^{-3}$ because such surface heterogeneity can be accommodated by the retrieval algorithm. Figure E13c shows data acquired on the 15 March 2006 around 1800 UT during the MILAGRO experiment over a ground site in the center of Mexico City. For this analysis the data are reorganized so that each part of the scan sees the same target at the ground, as would be the case for observations taken from satellites. The retrieved AOT is equal to 0.3 at 670 nm and gives

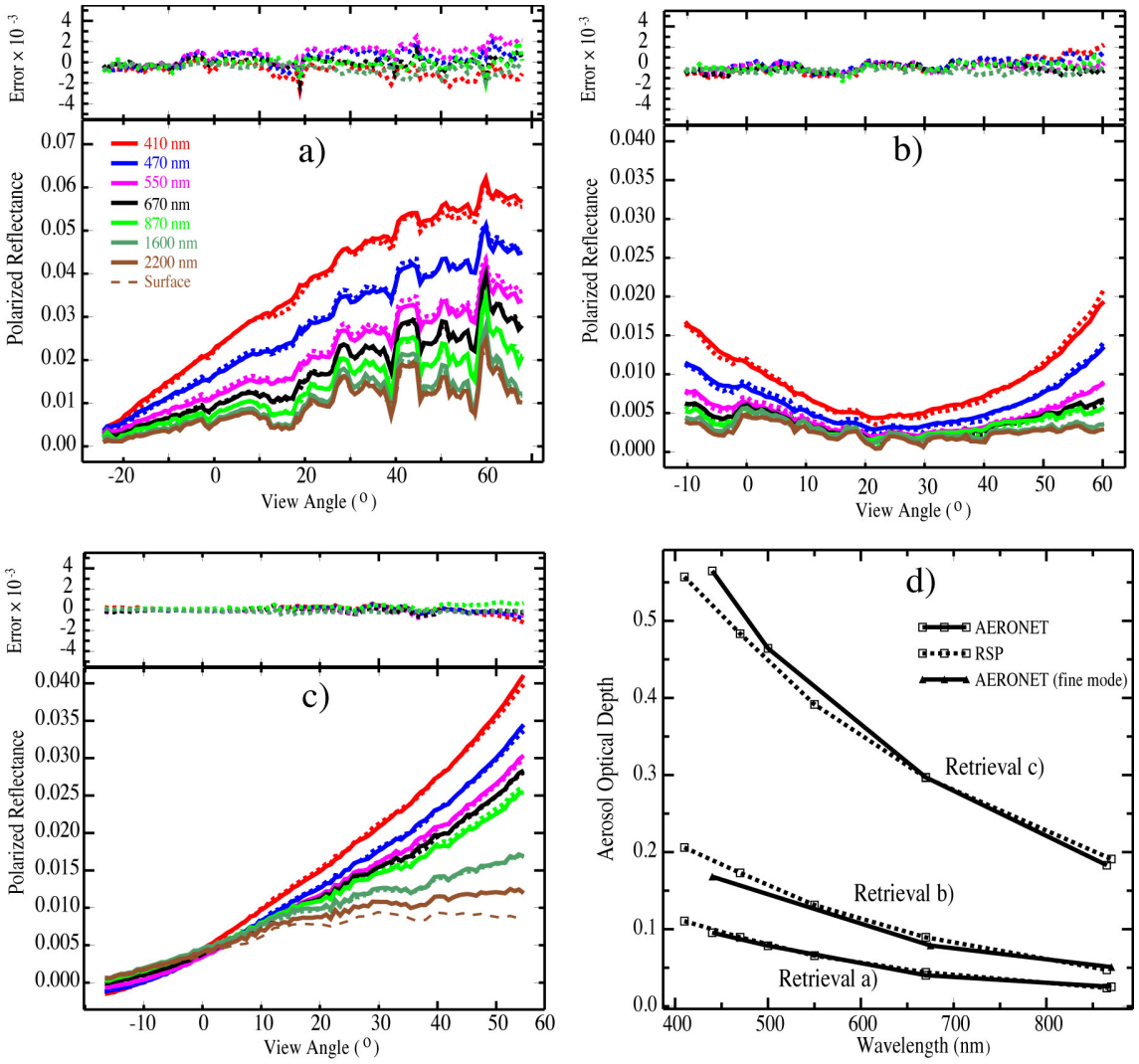

Figure E13. (a–c). Polarized reflectance measured at the aircraft level (solid curves) and simulated polarized reflectance (dashed curves) as a function of the viewing angle. The wavelengths are 410, 470, 555, 670, 865, 1600, and 2250 nm, respectively, in red, blue, magenta, black, green, dark green, and brown. The dashed brown curve corresponds to the direct surface contribution (measurements at 2250 nm corrected from the atmospheric effects). The error is the difference between the simulated and measured polarized reflectances and is shown at the top of the figures. Scans (a) and (b) were obtained on 09/16/05 and 09/19/05 during the ALIVE experiment (southern Great Plains, USA). Scan (c) was obtained over Mexico City on 03/15/06 during the MILAGRO experiment. (d) AOT retrieved by the RSP instrument from the measurements shown in (a–c) and coincident AERONET measurements (or retrievals when the fine mode AOT is reported) as a function of the wavelength.

an example of the performance of the AOT retrieval for higher aerosol loads than were present during ALIVE. Figure E13d compares the spectral AOT retrieved from the RSP measurements and the AOT measured by AERONET and shows good agreement for both the spectral variation and the absolute magnitude of the AOT.

A thick smoke plume that was observed during the Arctic Research of the Composition of the Troposphere from Aircraft and Satellites (ARCTAS) field campaign (Jacob et al. 2009) has recently been used to validate the retrievals obtained using the optimal estimation method applied to RSP measurements (Knobelspiesse et al. 2011b). In Fig. E14

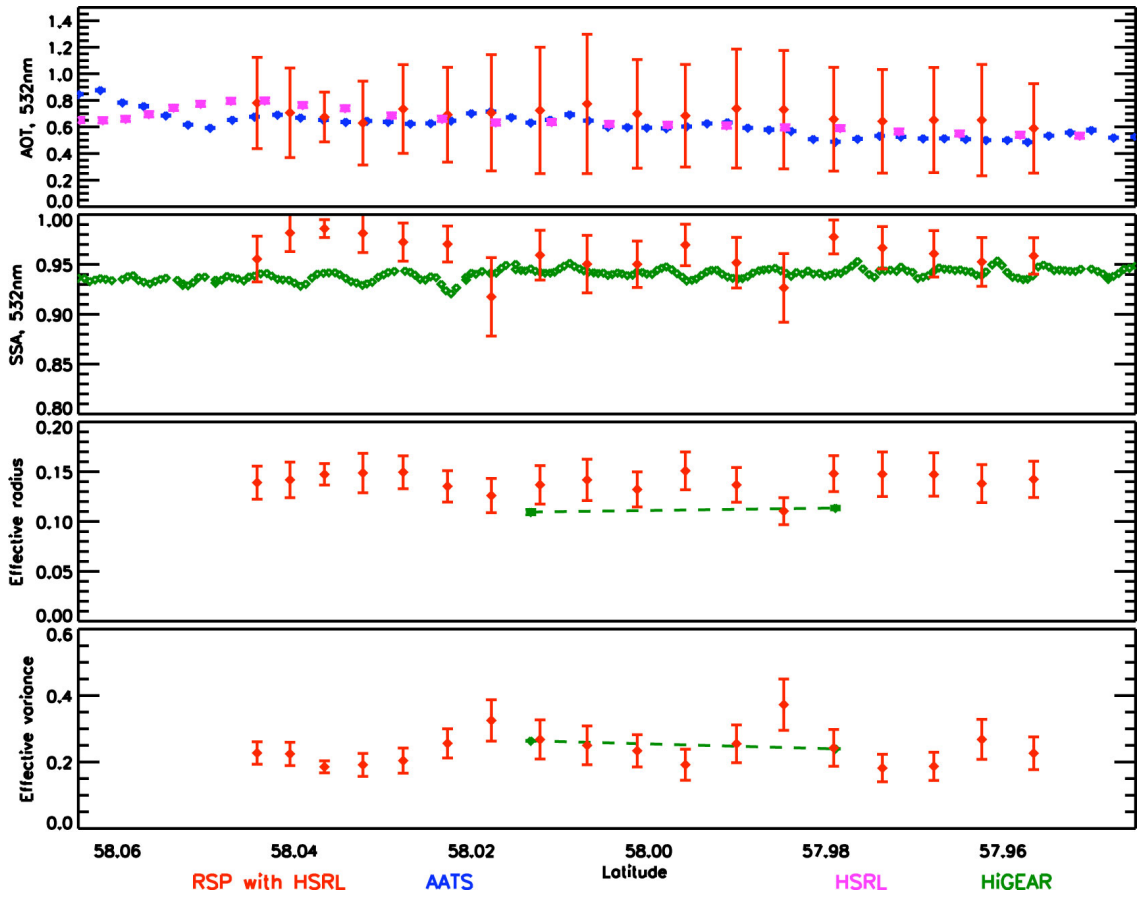

Figure E14. RSP, HSRL, AATS, and HiGEAR data are plotted with respect to latitude (aircraft were flying to the South). The top panel is the total AOT at 532nm for RSP retrievals with HSRL data (red) compared to estimates from AATS-14 (blue) and HSRL (magenta). That color scheme is maintained for the rest of the panels, with green indicating HiGEAR data in the second, third and fourth panels (SSA, effective radius and effective variance, respectively).

retrievals of the total AOT are compared with estimates of the AOT from the AATS-14 (Redeman et al. 2009) and the HSRL (Hair et al. 2008). The fine mode SSA, effective radius, and effective variance across the smoke plume are also compared with *in situ* measurements from the HiGEAR suite (Clarke et al. 2007; McNaughton et al. 2009). We note that the retrievals shown here use the HSRL to condition the retrieval by providing the first guess number concentration of aerosols and that the error bars on the AOT retrieved from the RSP observations are much larger than the sample to sample retrieval variations. This suggests that even though the retrieval errors are estimated using error propagation and the retrieval covariance matrix (Hasekamp et al. 2007; Knobelspiesse et al. 2011b) they are in fact overestimated.

Finally it is interesting to note that these airborne observations suffer from the same issue of different view angles seeing different scenes as is a concern for APS-2 observations, because the aircraft is yawing by 20° or more and the different RSP views are therefore looking at scenes ±3 km from the aircraft ground-track. Although this heterogeneity effect is included in the measurement uncertainties, a much larger contributor to the measurement uncertainty for these observations was the attitude of the aircraft, which

was caused by the very large yaw and a relatively low quality inertial navigation system that has since been replaced with a more accurate model.

Droplet size distribution retrievals. To have a controlled test of the capability to retrieve cloud droplet size distributions from polarized reflectance measurements over the scattering angle range of the rainbow, the radiative transfer model MYSTIC (Monte Carlo code for the phYSically correct Tracing of photons In Cloudy atmospheres; Mayer 2009) was used to compute 3D radiation fields that simulate RSP measurements. MYSTIC is one of several radiative transfer solvers of the libRadtran radiative transfer package (Mayer and Kylling 2005), and the simulations presented here used the backward ray-tracing mode (Emde and Mayer 2007) to simulate the polarized radiation field (Emde et al. 2010) to include polarized radiation due to scattering by randomly oriented particles, i.e., clouds, aerosols, and molecules.

The radiative transfer model was applied to a realistic cloud field obtained from large-eddy simulations (LES) of shallow, maritime convection. The LES model used (Ackerman et al. 2004) treats 3D fluid dynamics of the atmosphere and incorporates a bin microphysics model that resolves the size distributions of aerosol and cloud droplets in

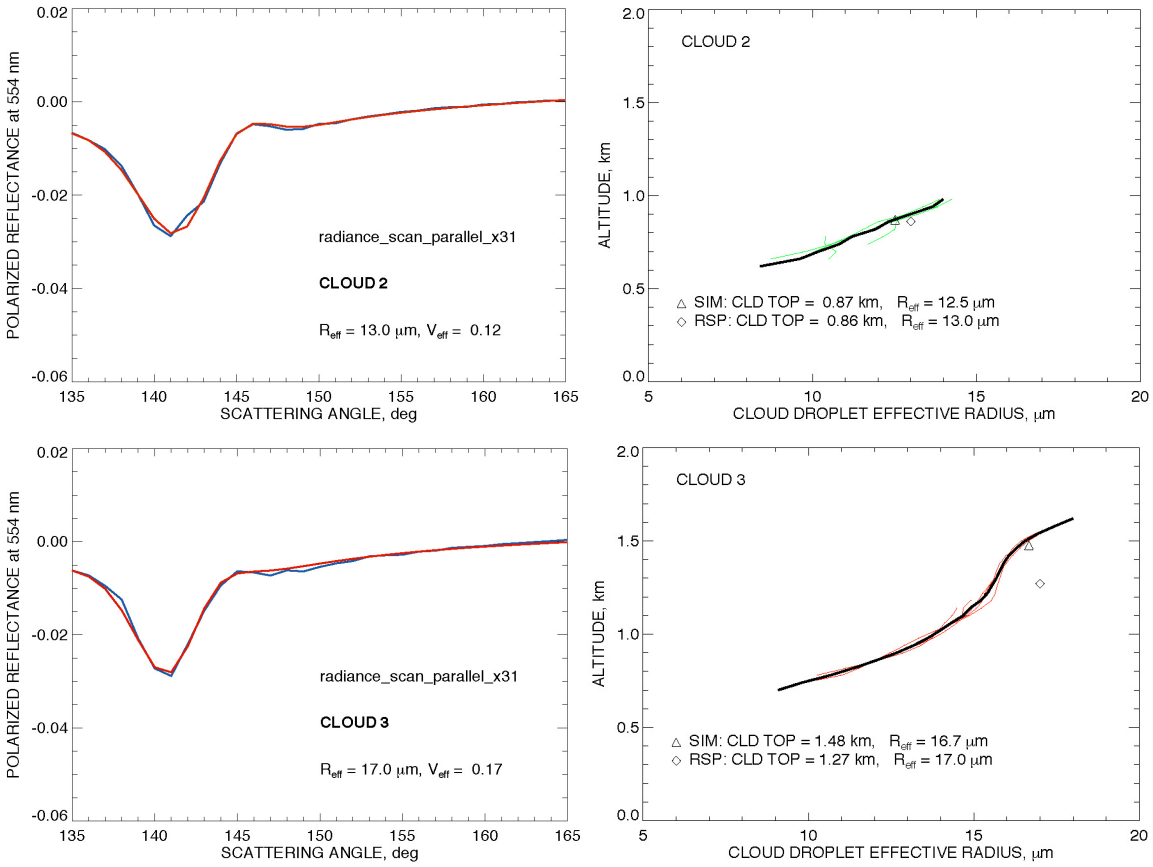

Figure E15. RSP-type retrievals of cloud droplet size from radiation fields simulated for realistic clouds using 3D Monte Carlo radiative transfer model. Left: fits (red) to simulated polarized reflectances (blue) for 2 cumulus clouds. Right: comparison between retrieved cloud droplet sizes (12.5–17 μm) and cloud top heights (diamonds) with those obtained from the original microphysical model by averaging of vertical profiles with transmission-like weighting function (triangles).

each grid cell. It also includes a two-stream radiative transfer model that treats the vertical transport of radiation in each model column. The LES dataset used in this study is based on idealizations of measurements obtained during the Rain in Cumulus over the Ocean project (RICO; van Zanten et al. 2010). The examples shown here are generated using the LES model bin microphysical outputs as inputs to MYSTIC for a wavelength of 555 nm with a solar zenith angle of 40° and a relative solar azimuth of 0° to simulate the multi-angle RSP observations at an altitude of 2.4 km. Retrievals of the cloud droplet sizes (12.5 – 17 μm) from the simulated polarized radiation field are consistent with those calculated from the original bin microphysical model at the corresponding cloud top heights (860 – 1270 m). Figure E15 shows the RSP fits to the polarized reflectance simulated for two cumulus clouds. The comparison in size is between RSP retrievals of effective radius and an exponentially weighted average over the corresponding profiles from the microphysical model.

Comparison of the 3D simulations with plane parallel calculations for the same cloud profile showed that 3D effects do exist, however they do not affect the structure of the rainbow. An example of this is shown in Fig. E16, where the polarized reflectance from the 3D Monte Carlo calculation (red curve) is almost identical to the black curve, which is the result of a plane parallel calculation. However the plane parallel calculation has been scaled by a factor of 1.5. The reason that the droplet size retrievals are not affected is that they are using the structure of the rainbow that is present in the P_{12} phase matrix element not the absolute magnitude of the polarized reflectance.

The first cloud droplet size distribution retrievals using RSP data were performed for the Coastal STRatocumulus Imposed Perturbation Experiment (CSTRIPE; cf. Meskhidze et al. 2005), which was designed to quantify the effect aerosol has on the microphysics, precipitation and dynamics of marine stratocumulus. The Center for Interdisciplinary Remotely Piloted Aircraft Studies (CIRPAS) Twin Otter aircraft was deployed in a three-week mission off the coast of Monterey, California in July 2003. During this campaign RSP was deployed onboard a Cessna 310 aircraft and made measurements during 5 research flights. The Forward Scattering Spectrometer Probe (FSSP; cf. Brenguier et al.

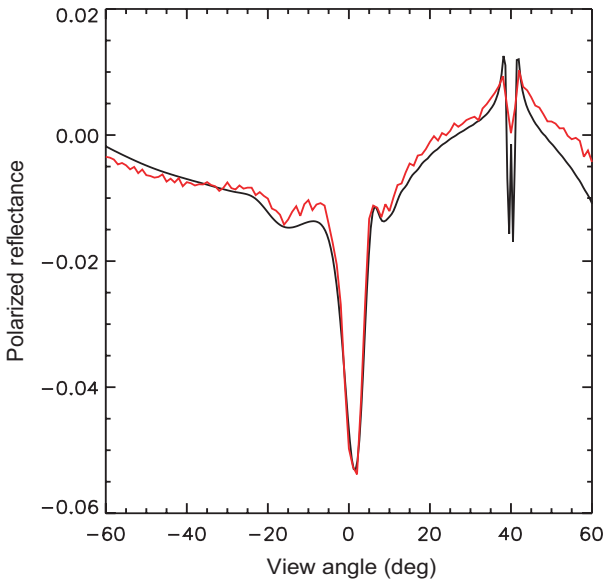

Figure E16. Comparison of the polarized reflectance from 3D Monte Carlo calculations (red) with the result of a plane parallel calculation scaled by the factor of 1.5 (black) for the same vertical column profile of droplet number and size distribution.

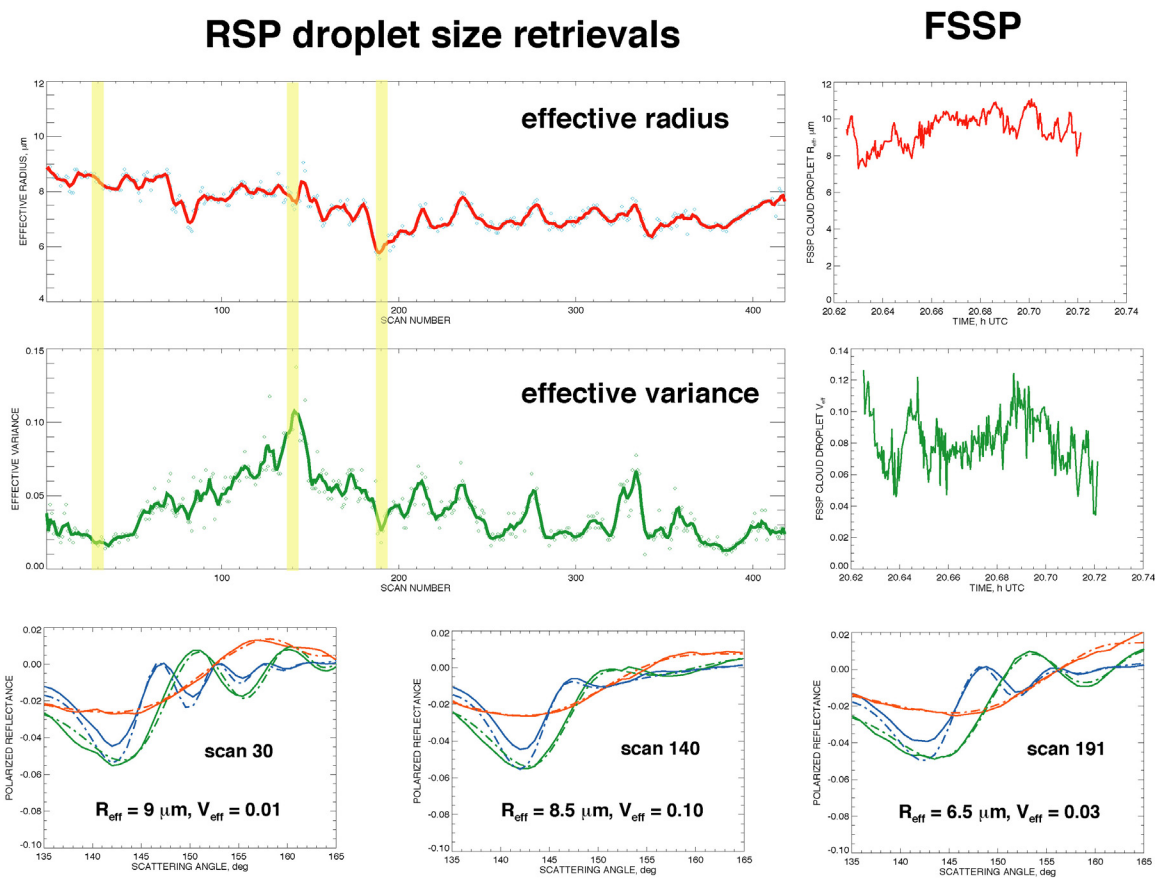

Figure E17. Top: time series of cloud droplet effective radius and variance retrieved from RSP (left) and *in situ* FSSP (right) measurements made on 22 June 2003 (RSP segment 19). Bottom: fit of polarized rainbow in RSP measurements (solid curves) using Mie theory (dashed curves) for specific cloud size distributions (blue – 410 nm RSP channel, green – 865 nm, red – 2264 nm).

1998) onboard the Twin Otter aircraft is an optical particle counter, suitable for counting and sizing particles in the size range of 0.5–47 μm diameter (20 channels), that was used to validate the RSP size distribution retrievals.

An example of RSP and correlative FSSP droplet size retrievals for the stratocumulus cloud field observed on 22 July 22 2003 is presented in Fig. E17. At the time of the measurements the Twin Otter aircraft was near cloud top. Minimal distance between the two planes was 5 km at 20.64 h UTC. Despite some lack of collocation between RSP and *in situ* FSSP measurements, a good agreement is observed in the cloud droplet size retrievals, especially at the RSP scan 140, when the distance between the two planes was the smallest. Both instruments show 8–9 μm droplet effective radius, while the effective variance is around 0.1.

The second field experiment for which RSP measurements were coordinated with *in situ* observations was organized by the ARM Aerial Facility (AAF), the Routine AAF Clouds with Low OpticalWater Depths Optical Radiative Observations field campaign (RACORO; Vogelman et al. 2011), which conducted long-term, systematic flights in boundary layer, liquid-water clouds over the ARM Southern Great Plains (SGP) site between 22 January and 30 June 2009. This campaign also used the CIRPAS Twin Otter and the *in situ* measurements used for comparison with the RSP size retrievals were again

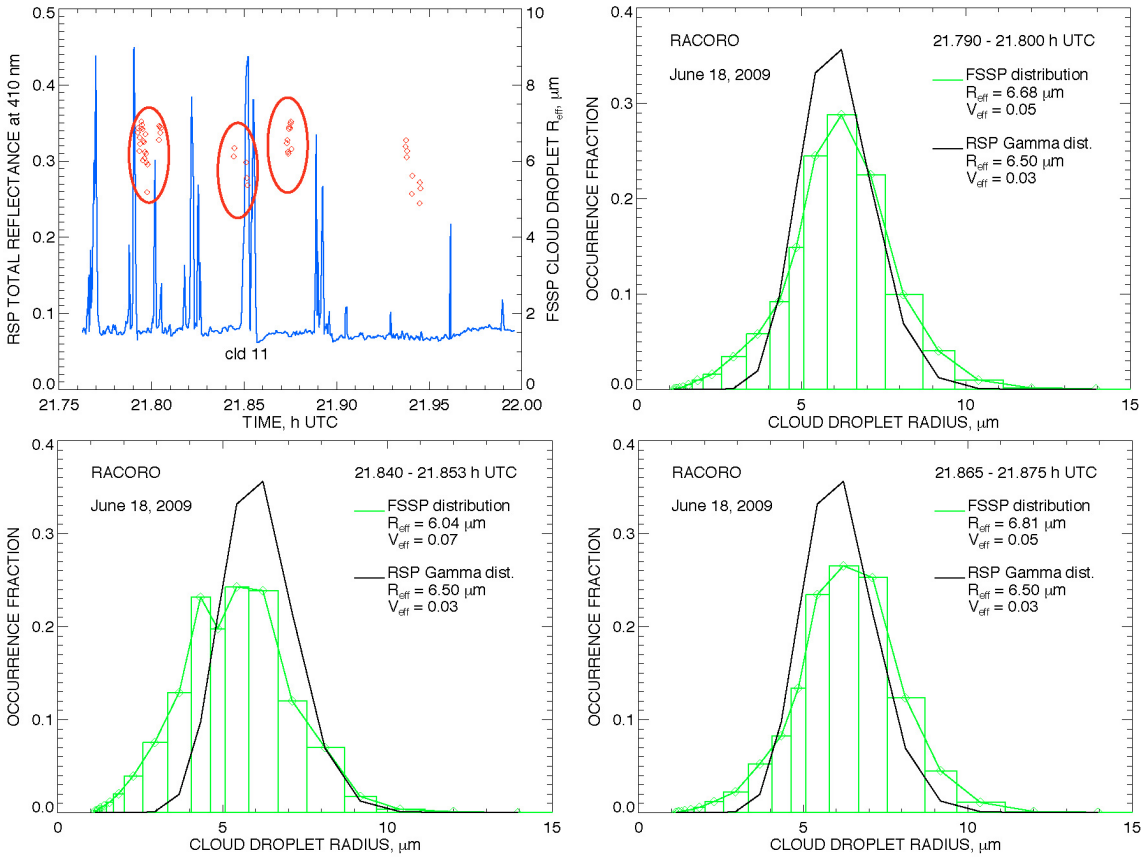

Figure E18. Top left: RSP-measured total reflectances (solid blue curve) and FSSP-derived droplet sizes (red diamonds) in the vicinity of cloud 11. Other plots: droplet size distributions obtained from FSSP measurements (green) for 3 clouds near cloud 11 (circled in the top left plot) compared to the gamma distribution (black) with the effective radius and variance values from RSP retrievals.

from the FSSP. The RSP was deployed in June 2009 onboard the NASA B200 aircraft together with the HSRL and was based in Ponca City, OK. This aircraft performed 19 science flights including 15 flights coordinated with the CIRPAS Twin Otter aircraft.

Figure E18 presents an example of droplet size distribution retrievals from the data obtained during the flight on 18 June 2009 (RSP segment 16). The scene was a popcorn cumulus cloud field typical for the SGP in summer. During the time of measurement the Twin Otter aircraft was flying near cloud top, it was over-passed by the B200 at 21.84 h UTC in the vicinity of "cloud 11". While in the case of small cumulus clouds perfect collocation of the measurements from the two planes for the same cloud is practically impossible, we see that the RSP retrievals for a cumulus cloud 11 (effective radius 6.5 μm, effective variance 0.03) are in good agreement with *in situ* measurements (effective radius 6–6.8 μm, effective variance 0.05–0.07) from clouds nearby that were crossed by the Twin Otter. The FSSP histograms confirm that the gamma distribution is an adequate model of the cloud droplet size distribution for these non-precipitating clouds.

Aerosols above clouds. In addition to determining the droplet size distribution near cloud top from polarimetric remote sensing measurements, it is also possible to detect and characterize aerosols above clouds (AAC). AAC are a potentially important component of the

positive forcing of climate, since absorbing AAC can significantly reduce a high underlying cloud albedo (Haywood et al. 1997). However, reliable estimates of the global prevalence and anthropogenic component of this type of forcing are limited by a lack of appropriate observations, especially since the climate forcing is strongly dependent on the aerosol SSA (Hansen et al. 1997). Furthermore, AAC can interfere with the ability of intensity only observations to accurately determine cloud optical thickness and droplet effective radii (Coddington et al. 2010).

Several approaches have been developed recently to observe AAC, but they are limited in their ability to distinguish aerosol types because of the significant assumptions required by their retrieval algorithms. Chand et al. (2008) used the active observations with CALIPSO to determine AAC AOT at two wavelengths. The ratio of the AOT spectral pair suggests the aerosol particle size. This method is therefore somewhat limited in its ability to determine the climate forcing from AAC, although this type of analysis shows considerable promise for combined retrievals with passive remote sensing data. Another method uses passive spectrometer observations at ultra-violet wavelengths from instruments such as the Scanning Imaging Absorption Spectrometer for Atmospheric Chartography (SCIAMACHY). De Graaf et al. (2007) fit simulations of biomass burning (smoke) AAC to SCIAMACHY observations to determine the aerosol total and absorbing optical thickness.

The technique we demonstrate here is to use multi-angle, multi-spectral, passive observations of polarized reflectance to simultaneously determine cloud and AAC optical properties. In Fig. E19 we show that for side-scattering angles the polarized reflectance is more sensitive to aerosols, while in the rainbow scattering angle range the polarized reflectance is sensitive to cloud droplet size (structure and location of the rainbow) and also aerosols (magnitude of the rainbow). In a similar approach Waquet et al. (2009b) used MODIS retrievals of cloud top height and POLDER polarized observations at a variety of scattering angles to determine the AOT of biomass burning AAC in the South Atlantic

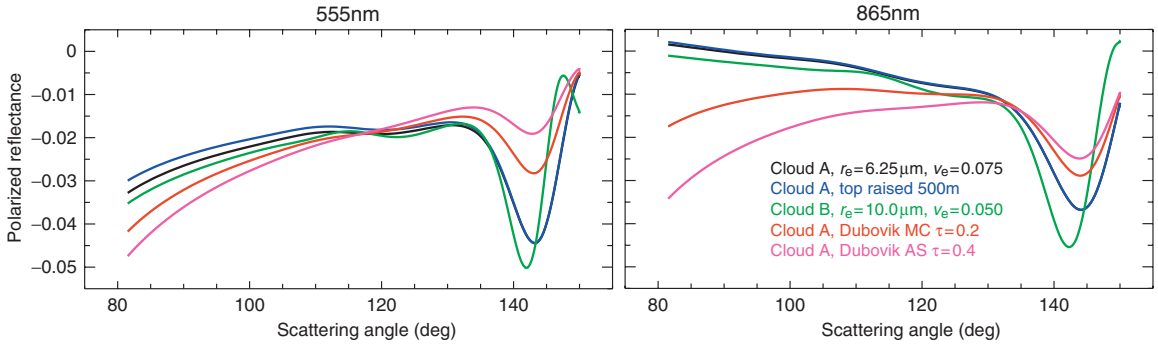

Figure E19. The sensitivity of the polarized reflectance to cloud and aerosol optical properties is demonstrated in this figure. Black curves are for a simulated cloud (type A) with an optical thickness of 20.0 and a vertically uniform droplet size distribution from the ground to 480 m with an effective radius of 6.25 µm and an effective variance of 0.075. The left-hand panel illustrates the polarized reflectance at 555 nm while the right-hand panel is for the polarized reflectance at 865 nm. Blue curves show the effect of raising the cloud top by 500 m. Green curves show the polarized reflectance of a cloud containing different droplet sizes with an effective radius of 10 µm and an effective variance of 0.05. Red and magenta curves indicate the reflectance of a cloud with aerosols above, the former for "Mexico City" type urban aerosols with an AOT of 0.2 and the latter for "African Savann" biomass burning aerosols with an AOT of 0.4 (Dubovik et al. 2002). All scenes are simulated with a solar zenith angle of 45° and a relative azimuth angle of 45°.

Ocean. This required assumptions about the aerosol size and refractive index, since a single POLDER band at 865 nm and a single scattering model were used.

The RSP measurement set is much larger than that available from POLDER and has a much greater angular density. Since the polarized reflectance generated by stratiform clouds does not depend on the cloud optical thickness once it is larger than ~3, it is possible to perform an optimal estimate of the cloud droplet size distribution with a fixed cloud optical thickness of 5 together with an estimate of the aerosol microphysical model and AOT where only the polarized reflectance observations are used in the retrieval.

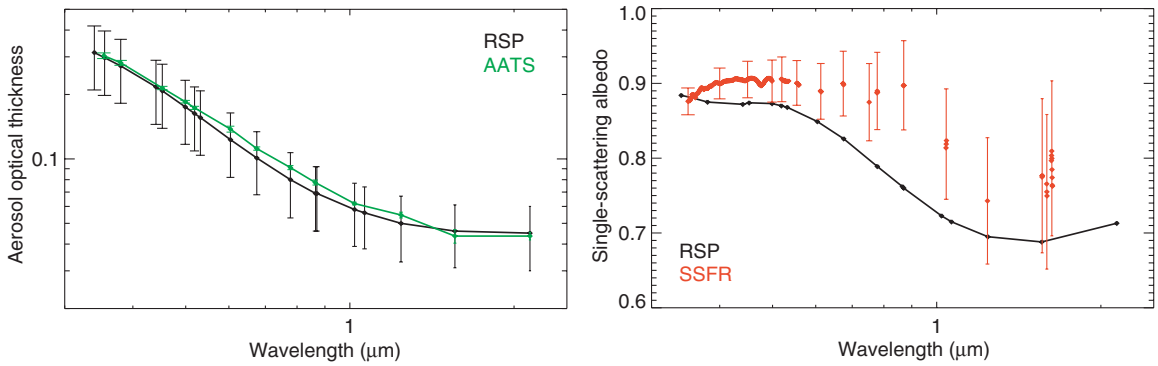

Figure E20. The left-hand panel shows the spectral dependence of RSP-retrieved total AOT (black curve) and the AATS observation (green curve) at an altitude of 480 m during the downward spiral that occurred shortly after the RSP observations were acquired. The right-hand panel is the spectral dependence of the total SSA. The black curve is for the RSP retrieval and the red curve is the SSFR estimate as described in Bergstrom et al. (2010).

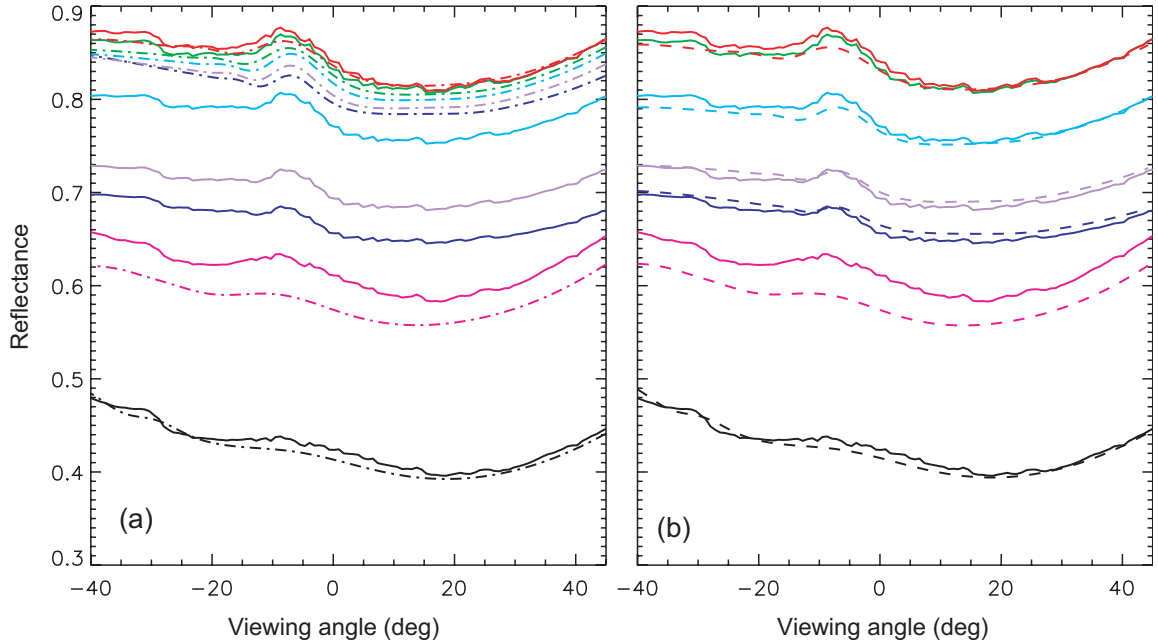

Figure E21. (a) Total reflectance at 410, 469, 555, 670, 865, 1589, and 2264 nm shown as blue, mauve, turquoise, green, red, fuschia, and black respectively. Solid curves represent RSP observations and dot-dashed curves are model calculations for an atmosphere with no aerosols above the cloud. (b) As in (a) but with aerosols above cloud included and model calculations shown as dashed curves.

This was done for AAC over the Gulf of Mexico during the INTEX-B field experiment on 13 March 2006. The AATS-14 (Redeman et al. 2009) made observations of the spectral AOT in a cloud free region about 125 km northwest of the cloudy scene observed by RSP, and aerosol absorption was also estimated in this area using observations made by the Solar Spectral Flux Radiometer (SSFR) (Pilewskie et al. 2003; Bergstrom et al. 2010). The results from the RSP optimal estimate are compared in Fig. E20 to the AATS-14 and SSFR measurements. The AOT we retrieved agrees very well with AATS observations from an altitude of 480 m, which was the cloud top height in our AAC scene. At wavelengths less than 800 nm, the majority of total AOT is determined by the fine mode, and AATS-14 measurements at these wavelengths agree with the RSP retrieved values to well within the retrieval uncertainties.

The SSA that is retrieved using only the polarized reflectance has a very large uncertainty (Knobelspiesse et al. 2011a). However, comparisons with SSFR observations show some degree of similarity, at least for the shorter wavelengths of the spectrum, and more recent analyses that included the total reflectance in the optimal estimate have substantially smaller uncertainties in the retrieved imaginary index because of the large effect aerosol absorption has on the short wavelength spectral bands as shown in Fig. E21. Figure E21a depicts observations of the same AAC scene as presented by Knobelspiesse et al. (2011a) together with calculations for a two layer cloud with no aerosols above it. The cloud optical thickness of the top and bottom layer are 10 and 40, respectively, and the effective radii are 7.02 μm and 5.5 μm, respectively, with the top layer having an effective variance of 0.029. This cloud model was estimated using the polarized reflectance at 410, 865 and 2264 nm and the total reflectance at 2264 nm and the discrepancy between the model and observations at 1588 nm indicates that the two layer model for the vertical profile of cloud droplet sizes is probably inadequate since this spectral band is sensitive to droplet size deeper into the cloud than the 2264 nm band.

The results of a cloud and aerosol retrieval using the total and polarized reflectance with the two-layer cloud are presented in Fig. E21b, where it can be seen that the total AOT of 0.15 has a huge effect on the 410 and 469 nm total reflectance because of the relatively low SSA (cf. Fig. E20b). The use of these total reflectance measurements in the retrieval algorithm therefore reduces the estimated uncertainty in the imaginary refractive index retrieval to ~10%, which improves substantially on the results we previously presented for the case where only the polarized reflectance was used.

Detection and characterization of thin cirrus clouds. Observations in spectral bands that are centered on strong water vapor features allow for the detection of thin cirrus clouds by suppressing the contribution from clouds lower in the atmosphere and the surface (Gao et al. 1993). The RSP and APS-2 instruments provide measurements in such bands (1884 and 1376 nm, respectively) and have the additional capability to obtain multi-angle polarization observations of thin cirrus clouds. This allows the crystal habit and particle roughness to be estimated and provides effective constraints on the asymmetry parameter of the scattering phase function and therefore the radiative behavior of the clouds.

Figure E22 shows the angular behavior of the RSP total and polarized reflectance at 1884 nm averaged over 5 scans at 18.74 UTC on 11 May 2010. The flight trajectory was oriented only 8° away from the principal plane, so that RSP viewing angles of −20° and 20° correspond to directions very close to specular reflection and backscatter, respectively, as indicated by the label on the top x-axis. The peak in total reflectance (partially

recognizable also in the polarized reflectance) was attributed to reflection from a small fraction of horizontally oriented ice crystals (Chepfer et al. 1999; Bréon and Dubrulle

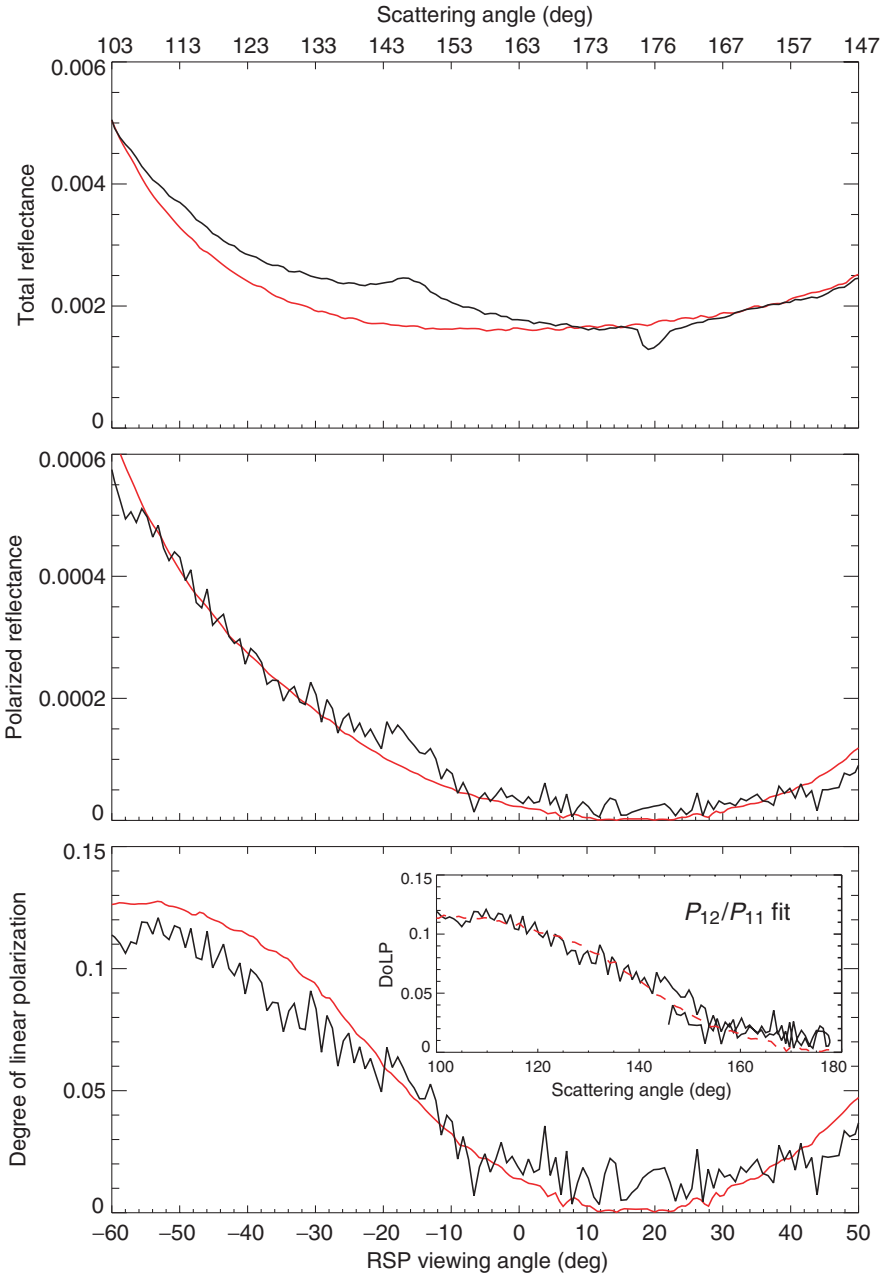

Figure E22. Data from the RSP channel at 1884 nm (black lines), usually very dark, reveals the presence of cirrus beneath the aircraft. Top panel: the peak in total reflectance around the direction of specular reflection (scattering angle ~140°) is an indication of horizontally oriented ice crystals. The dip near backscatter is the aircraft shadow. Lower panels: polarized reflectance and degree of linear polarization. The red curves are the RT simulations for a cirrus immediately below the aircraft totaling 0.08 in optical depth, and composed of small ice plates with an effective radius of 9 μm, an aspect ratio of 0.25 and roughness parameter of 0.55. This particle class was selected by minimizing the residuals between the measured DoLP and the P_{21}/P_{11} elements of phase matrices computed with a ray-tracing method (inset in the lowest panel).

2004; Noel and Chepfer, 2004). The small dip near backscatter is caused by the shadow of the airplane, which is unavoidable when flying very close to a target, and that does not carry any polarization signature.

The scattering properties of the cirrus away from the specular and backscatter directions were further investigated in order to estimate its crystal habit and optical thickness (Ottaviani et al. 2011). We used geometric optics (Macke et al. 1996) to construct a database with optical properties of plates and columns with varying sizes, aspect ratios, and small-scale roughness parameters (cf. definition in Macke et al. 1996). Plate aspect ratios were varied between 0.1 and 1 with a step size of 0.05 (with corresponding reciprocal values used for columns). Roughness parameters were varied from 0.2 to 0.8 with a step size of 0.05. Small and large particles with effective radii of about 9 and 30 μm, respectively, were included. From this database, the particle class was first selected for which the ratio of phase matrix elements P_{21}/P_{11} best matched the degree of linear polarization at 1884 nm (see inset in the lowest panel of Fig. E22). The DoLP is a convenient modeling choice because it is independent of the optical thickness, at least within the single-scattering approximation, which should apply for thin cirrus at this wavelength, and can thus be directly compared to the P_{21}/P_{11} elements of a modeled phase matrix.

At scattering angles larger than about 100°, typical of RSP measurements, distinctive features that facilitate the discrimination among different ice crystal models are an inversion in the sign of polarization near backscatter, and a more or less pronounced modulation at side-scattering angles. These structures are suppressed in the presence of irregular crystal habits, small-scale surface roughness, or by inclusion of air bubbles (Baran 2009). A change in the sign of the polarization would manifest itself as a discontinuity at the minimum of the DoLP, but such a feature is absent near backscatter, where the signal smoothly declines toward zero. This fact, together with the smooth increase toward side-scattering angles, indicates that the cirrus particles are not pristine crystals.

The optimal fit was obtained for small ice plates (effective radius ~9 μm) characterized by an aspect ratio of 0.25 and a roughness parameter of 0.55. This roughness parameter is close to values generally found from analysis of global POLDER data (Knap et al. 2005; Baran and Labonnote 2006). The optical thickness required to simultaneously fit the total reflectance was then estimated using the ice crystal model that had been determined using the polarization measurements and was found to be 0.08. This magnitude of optical thickness places the observed cirrus in the threshold-visible category (Sassen and Cho 1992), where actual visibility depends on illumination conditions and that in this case did not make the cloud perceivable to the naked eye. This provides an example of the unique capability of polarization observations in water vapor absorption bands (1884 nm for RSP and 1376 nm for APS-2) to detect and characterize thin cirrus clouds that are suspected to have significant effects on climate (McFarquhar et al. 2000).

Appendix F
Assessment of APS-2 sampling

The APS-2 sensor would provide retrievals along the satellite ground track with a horizontal spatial sample similar to that provided by CALIPSO for any of the acceptable sun synchronous orbit options. Existing uncertainties in the radiative forcing by aerosols appear to be primarily driven by uncertainties in the fractional absorption (single-scattering co-albedo) and vertical distribution, especially the partitioning between above and below cloud, of aerosols (Chung et al. 2005; Loeb and Su 2010). However, one of the most variable aerosol fields is the AOT, and it is therefore important to understand what the limitations of the sample of this field obtained by an APS-2 would be. We show here that APS-2 sampling uncertainties for the geometric mean AOT at a 10°×10° monthly mean scale are less than the accuracy requirements given in Table A1 between 80% and 95% of the time. In the following we provide a description of the data sources and analysis on which these conclusions are based. The geometric mean and log standard deviation are the primary summary statistics used to evaluate the APS-2 sampling in this Appendix since these appear to be the appropriate statistics for the evaluation of an AOT field that is log normally distributed (O'Neill et al. 2000) and we show that the AOT data sources we use are consistent with a log-normal sampling distribution.

In order to motivate some of the figures presented in the remainder of this Appendix we briefly summarize the properties of a log normal distribution. We introduce the definition of a log-normal distribution viz.,

$$p_l(\ln\tau)\,\mathrm{d}\ln\tau = \frac{1}{\sqrt{2\pi\sigma^2}}\exp\left(-\frac{\ln(\tau/\tau_g)^2}{2\sigma^2}\right)\mathrm{d}\ln\tau, \tag{F1}$$

where τ_g is the geometric mean and σ is the log standard deviation. We note that the moments of this distribution are given by the expression

$$\langle\tau^m\rangle = \tau_g^m \exp\left(\frac{(m\sigma)^2}{2}\right). \tag{F2}$$

The first two log moments are

$$\begin{aligned}\langle\ln\tau\rangle &= \ln\tau_g,\\ \langle(\ln\tau)^2\rangle &= \sigma^2 + (\ln\tau_g)^2,\end{aligned} \tag{F3}$$

where σ^2 is the log variance. An additional statistic that provides a simple consistency check as to whether a quantity is log normally distributed is the log difference, which we define to be,

$$\ln\langle\tau\rangle = \langle\ln\tau\rangle - \frac{\sigma^2}{2}. \tag{F4}$$

If a sample is log normally distributed then the mean and standard deviation should be correlated but with considerable scatter if the log standard deviation is not a constant, which is clearly true of AOT fields. In contrast the log difference and the log variance should be strongly correlated with a 2:1 regression line independent of the geometric

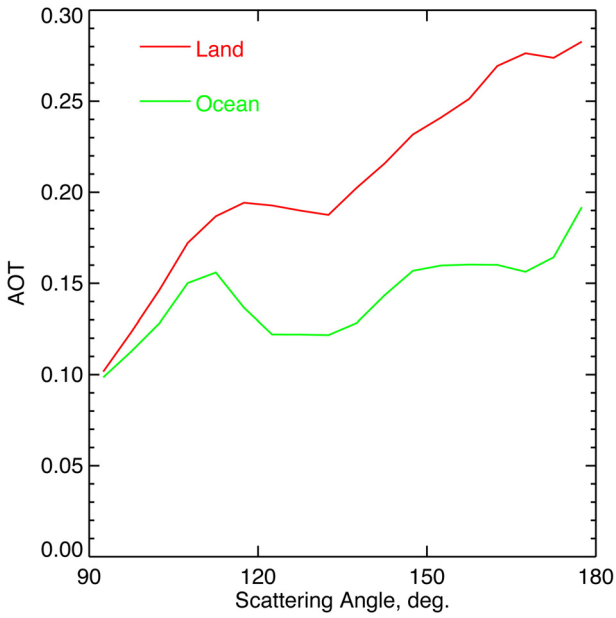

Figure F1. Variation of AOT at 550 nm with scattering angle.

mean optical thickness if the AOT is log normally distributed. We note in passing that a χ^2-similarity test can be used to verify the hypothesis that the observed distributions are log-normally distributed, but for the AOT data used here the probability of rejecting that hypothesis is extremely small (< 0.01%) and we therefore present below (in Fig. F5) scatter plots that provide a more illuminating, albeit subjective, indicator of the plausibility of a log normal distribution for the data.

There are two sources of AOT fields that can be used in assessing the sampling properties of an APS-2 sensor. Global imagers such as MODIS provide aerosol retrievals over both ocean and land and have been validated against AERONET (Remer et al. 2005; Remer et al. 2008; Levy et al. 2009; Levy et al. 2010). General Circulation Models (GCMs) have an increasing level of fidelity in their simulations of aerosols and their output fields are readily available (Schulz et al. 2006).

The advantage of using the daily pixel level aerosol retrievals from MODIS to assess APS-2 sampling is that limitations caused by the presence of clouds are implicit in the sample and the seasonal and regional variations of such cloud effects are captured coherently. The only problem with using an imager to assess a ground-track only sample is that if there are any view angle biases in the aerosol product then these biases will increase the apparent error in the ground-track only sample. In Fig. F1 we show the variation of the MODIS AOT with scattering angle for the seven year period of the sample that we are using. We note that some of the variations of AOT with scattering angle shown in Fig. F1 may be real. However, scattering and view angle biases caused by using inappropriate aerosol and surface models in the retrieval algorithm are expected and are likely to have land surface type, regional, and seasonal dependencies (Remer et al. 2001; Gatebe et al. 2001; Herman et al. 2005) that make their diagnosis and disentanglement from sampling effects difficult.

GCMs are available that provide AOT fields with a daily temporal sampling and a spatial sampling that is finer (1.125°) than the equator ground track spacing of the A-Train (1.6°). Re-sampling the model AOT field does not have the problem of view angle dependencies and the quality and availability of the AOT field is the same over land and

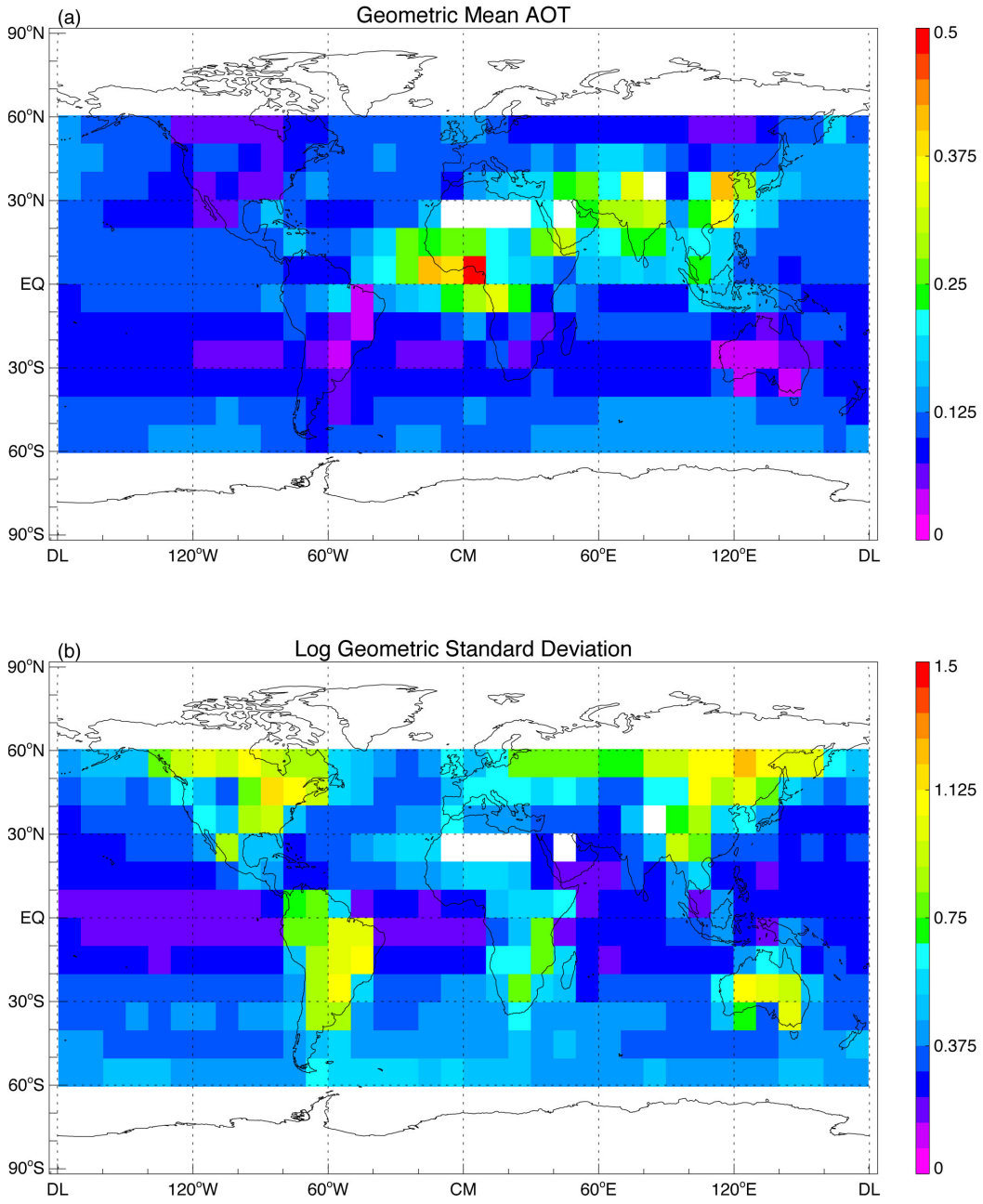

Figure F2. 10°×10° monthly mean median values for 1/2001–12/2007 of the geometric average and log standard deviation of the MODIS AOT at 550 nm.

ocean. However a model AOT field with a 1.125° resolution will not provide a realistic test of the reduction in the sample caused by clouds.

MODIS and GCM AOT fields are therefore highly complementary in assessing the sampling provided by APS-2. Re-sampling the MODIS AOT field to get an APS-2 like sample will, with its potential view angle dependencies, tend to overestimate sampling errors. Re-sampling a GCM AOT field using the CALIPSO ground-track with no cloud effects included will tend to underestimate sampling errors. The MODIS and GCM AOT fields can therefore be used to provide an upper and lower bound respectively on the

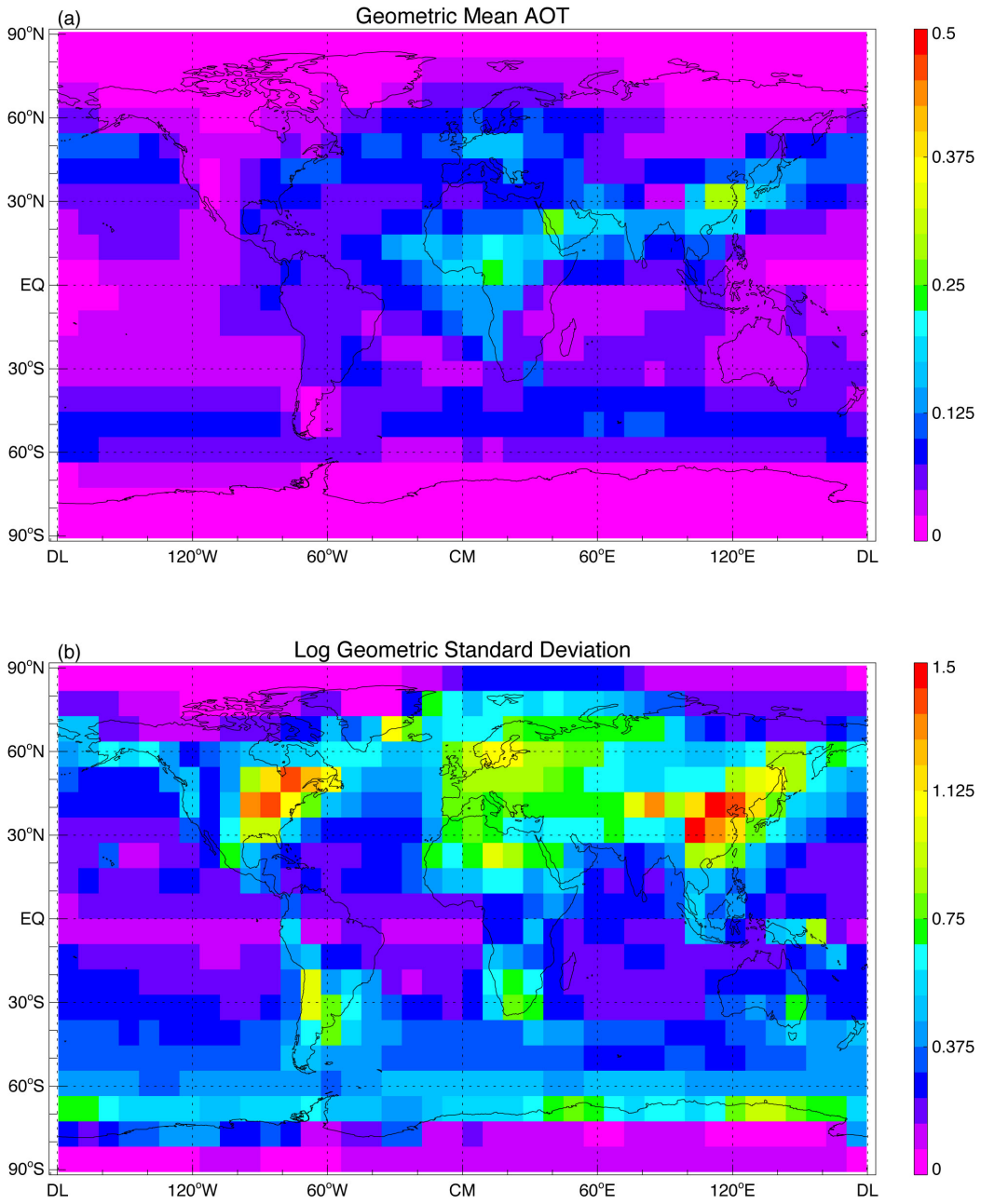

Figure F3. 9°×9° monthly mean median values for 1/2000—12/2008 of the geometric average and log standard deviation of the SPRINTARS AOT at 550 nm.

sampling errors of an APS-2 sensor. In the following we use daily MODIS level 2 AOT retrievals from the Terra satellite for the period 1 January 2001 to 31 December 2007 and the daily AOT field from the SPRINTARS GCM (Takemura et al. 2005) for the period 1 January 2000 to 31 December 2008. The geometric mean and log geometric standard deviation for the complete MODIS and SPRINTARS AOT fields at 10° and 9° resolution respectively are shown in Figs. F2 and F3. These figures show that the basic structure of the two fields is similar: highest variability over land where the largest sources are and largest values over central Africa as well as South and East Asia.

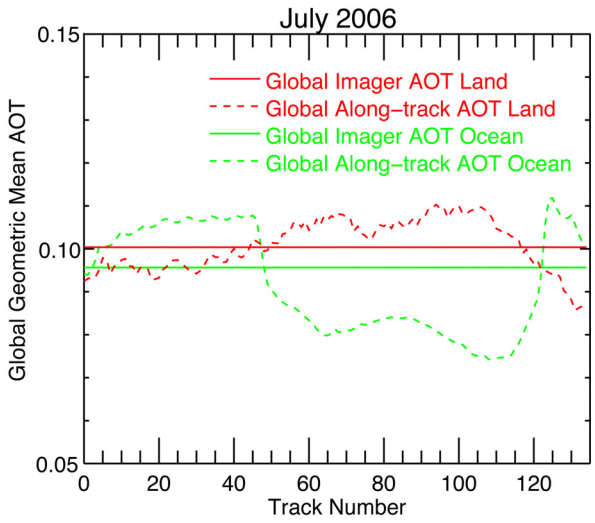

Figure F4. Variation of global geometric mean AOT at 550 nm with cross-track sample for July 2006.

The MODIS data have a native resolution of 10 km both along and cross track with 135 cross track samples and can therefore be averaged to any grid spacing coarser than 10 km. A 10° grid was chosen here to yield a regional spatial average (cf. Kinne et al. 2006) that is sufficient to provide a radiative forcing with adequate spatial resolution (Shindell and Faluvegi 2009) and statistics are calculated using all the MODIS retrievals over ocean and all MODIS high quality (QC = 3) retrievals over land for the monthly time averages. Over oceans an APS-2 like sub-sample was obtained by using the 50th MODIS cross track sample since this reduces sun glint artifacts. Over land the 67th cross track sample was used since it is close to nadir. An example of the variation of the global geometric mean AOT as a function of the selected cross track sample is shown in Fig. F4 for July 2006. Other months and years have similar magnitude variations, although the pattern of AOT variation with cross track sample changes.

The SPRINTARS AOT field is calculated on a 1.125° grid, and in order not to introduce any artifacts from interpolation it was averaged onto a 9° grid, rather than the 10° grid used for the MODIS data, and statistics were again calculated for monthly time averages. The CALIPSO ground track pattern was used to sample the SPRINTARS AOT field with a horizontal spacing of 10 km along the ground track, and this APS-2 subsample is restricted to ground pixels that have a solar zenith angle of less than 70°. The 10°×10° and 9°×9° monthly mean AOT fields that use all the data will henceforth be referred to as the complete AOT fields and the APS-2 samples as the sub-sampled AOT fields.

In Fig. F5 we show scatter plots of the standard deviation of AOT against the arithmetic mean value and the difference between the log-difference and the log variance for the SPRINTARS, MODIS over ocean, and MODIS over land complete AOT fields. These figures show that the standard deviation of the AOT is indeed proportional to its mean value, although with considerable scatter, which is expected for AOT samples. These figures also show that the log-difference is close to half of the log variance and shows substantially less scatter which, as noted above, is a useful subjective indicator that a quantity is indeed log normally distributed.

As a measure against which to test the adequacy with which the APS-2 sub-samples capture the complete AOT statistics we will use the AOT accuracy requirements given in

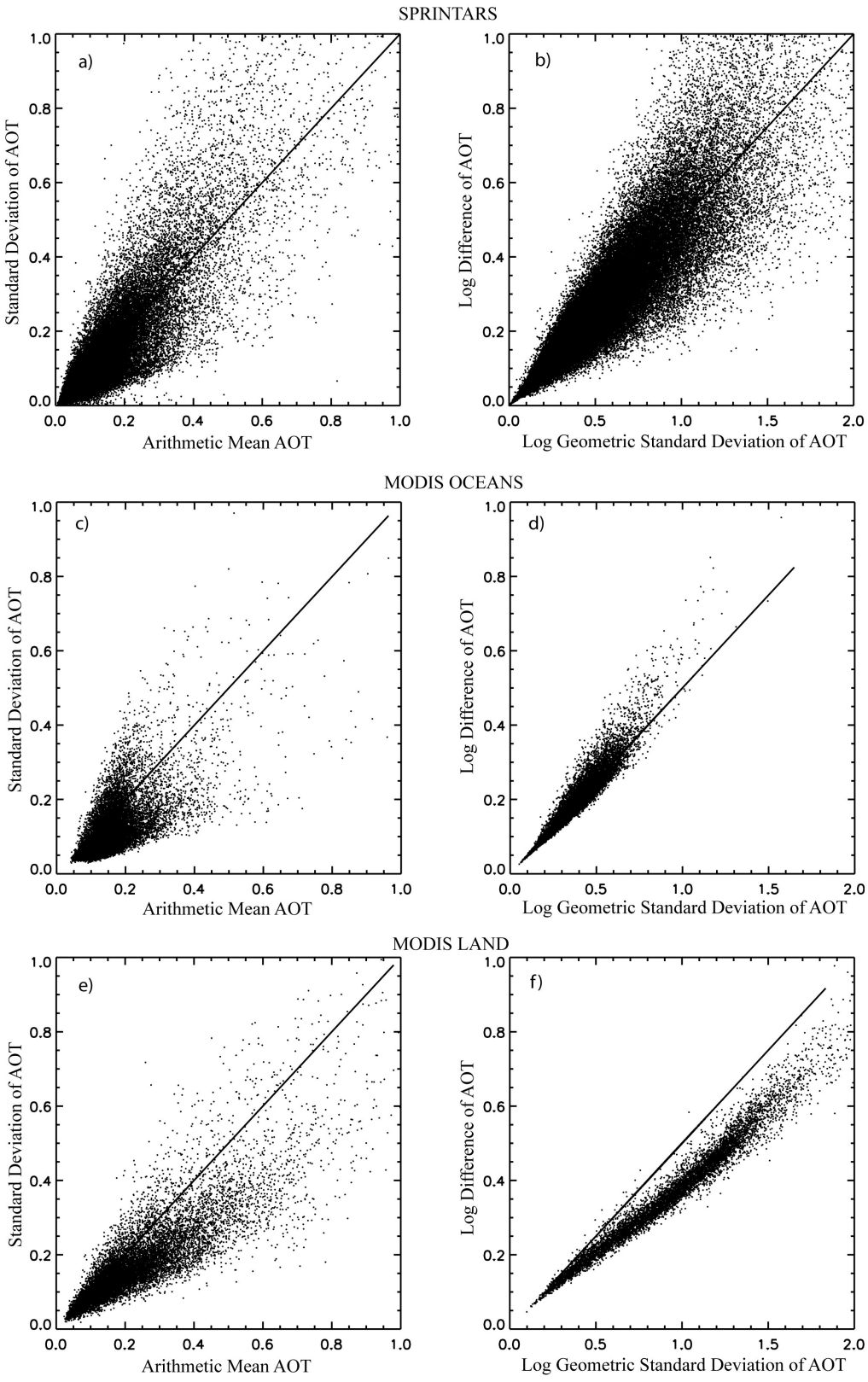

Figure F5. Scatter plots of standard deviation against mean and log-difference against log variance for the SPRINTARS complete AOT field (a) and (b), the MODIS oceans AOT field (c) and (d), and the MODIS land AOT field (e) and (f).

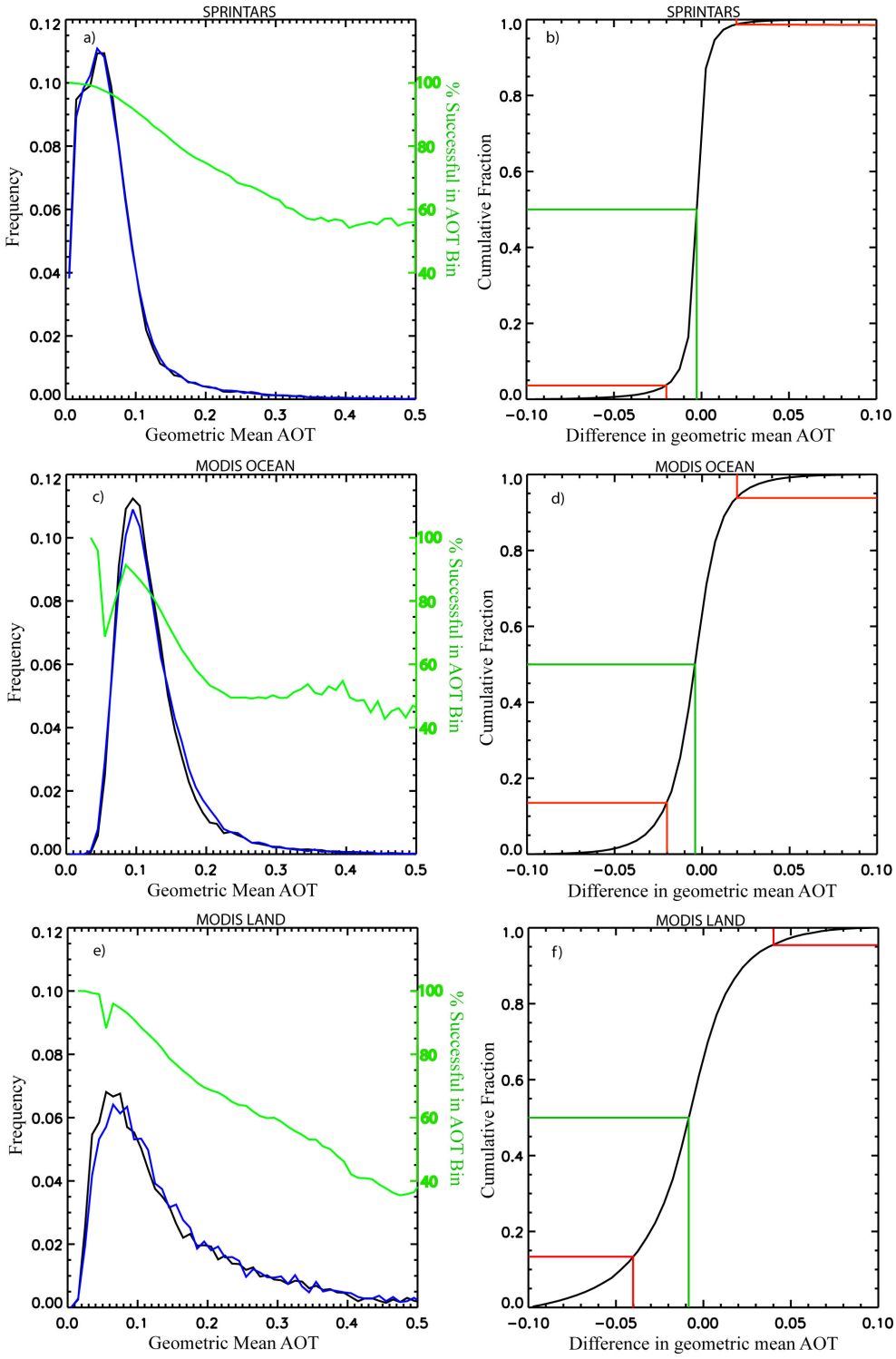

Figure F6. (a, c, e) Comparisons of complete (black curve) and sub-sampled (blue curve) geometric mean AOT probability distributions. The green curve shows, for each AOT, the frequency for which the sampling errors are smaller than the accuracy requirements specified in Table A1 for oceans (a, c) and land (e). (b, d, f) Cumulative histograms of the differences between the complete and sub-sampled geometric mean AOTs. Green lines indicate any biases in the median values while the red lines are construction lines to indicate what the factional coverage is for a confidence interval of ±0.02 (b, d) or ±0.04 (f) and whether the confidence interval is symmetric.

Table A1. The accuracy of retrievals for a sensor that provides a sufficient number of measurements to make the retrieval well posed (Hasekamp et al. 2010; Dubovik et al. 2011) is determined primarily by instrumental accuracy. Averaging is not expected to reduce accuracy errors and will be present in long-term, large-scale statistics. In order for sampling effects not to dominate the uncertainty in the AOT retrievals they should therefore be comparable to, or smaller than, the accuracy requirements. Figure F6a shows the frequency distribution of the monthly mean 9°×9° geometric mean AOT generated from the complete SPRINTARS AOT sample, the APS-2 sub-sample, and for each AOT bin (0.01 width) the frequency with which the difference between the complete sample and the APS-2 sub-sample is less than the oceanic accuracy requirement. The cumulative distribution of the differences between the complete and sub-sampled SPRINTARS geometric mean AOT fields are shown in Fig. F6b. A total of 95% of all monthly mean sub-sampled AOTs match the complete sample within the requirement for accuracy over ocean specified in Table A1. We note that if the requirement is applied to the arithmetic mean AOT then 91% of the sub-sampled AOTs match the complete sample and in the following the performance for the arithmetic mean is given in parentheses following each geometric mean comparison.

Figures F6c−f show the same analysis as presented in Figs. 6a and 6b, but for MODIS over ocean and MODIS over land. The agreement between the complete and sub-samples is within the accuracy requirement 82% (77%) of the time over ocean and 81% (72%) over land. The median geometric mean AOT bias is in all three cases less than 0.01 and the sampling uncertainties increase (frequency with which accuracy requirement is met decreases) with mean AOT. Figure F7 shows the same analysis as Fig. F6 for log standard deviation statistics. The complete and sub-sampled log standard deviations are within ±0.1 of one another 85% of the time for the SPRINTARS AOT field and 77% of the time for the MODIS AOT field over the ocean. The variability of the MODIS AOT field is substantially larger over land (mode of log standard deviation of 0.9) than over the ocean (mode of log standard deviation of 0.55). In Fig. 7f we therefore show the fraction of samples for which the difference in log standard deviations is less than ±0.2, which is 90%, and note there is also a bias of −0.03 for the sub-sampled estimate of the log standard deviation compared to the complete sample.

The sub-sample has larger uncertainties at higher AOTs because the standard deviation of the underlying AOT distribution is larger (see Figs. F2 and F3) and also because the spatial scales of the AOT field that contribute at a monthly mean time scale are larger for areas with high AOTs. Figure F8 shows the temporal and spatial correlations calculated from the MODIS AOT field to demonstrate what is seen observationally in a cloud screened data set. In Fig. F9 we use the SPRINTARS AOT field to evaluate the space-time correlations of the AOT field since the absence of missing data makes the reliability of such an evaluation somewhat simpler. Figure 9a shows the estimate of the time in days at which the correlation of the SPRINTARS AOT field at different times would be reduced to 0.7. We note that the MODIS and SPRINTARS estimates of this critical correlation time are both less than one day (the temporal spacing of the samples for both fields). In Fig. F9b the distance between SPRINTARS 1.125° grid boxes at which the correlation is reduced to 0.7 is shown. This distance is the root-mean-square of the meridional and zonal distances at which the correlation is reduced to 0.7 and is also consistent at a large-scale with the spatial correlation lengths estimated using the MODIS data.

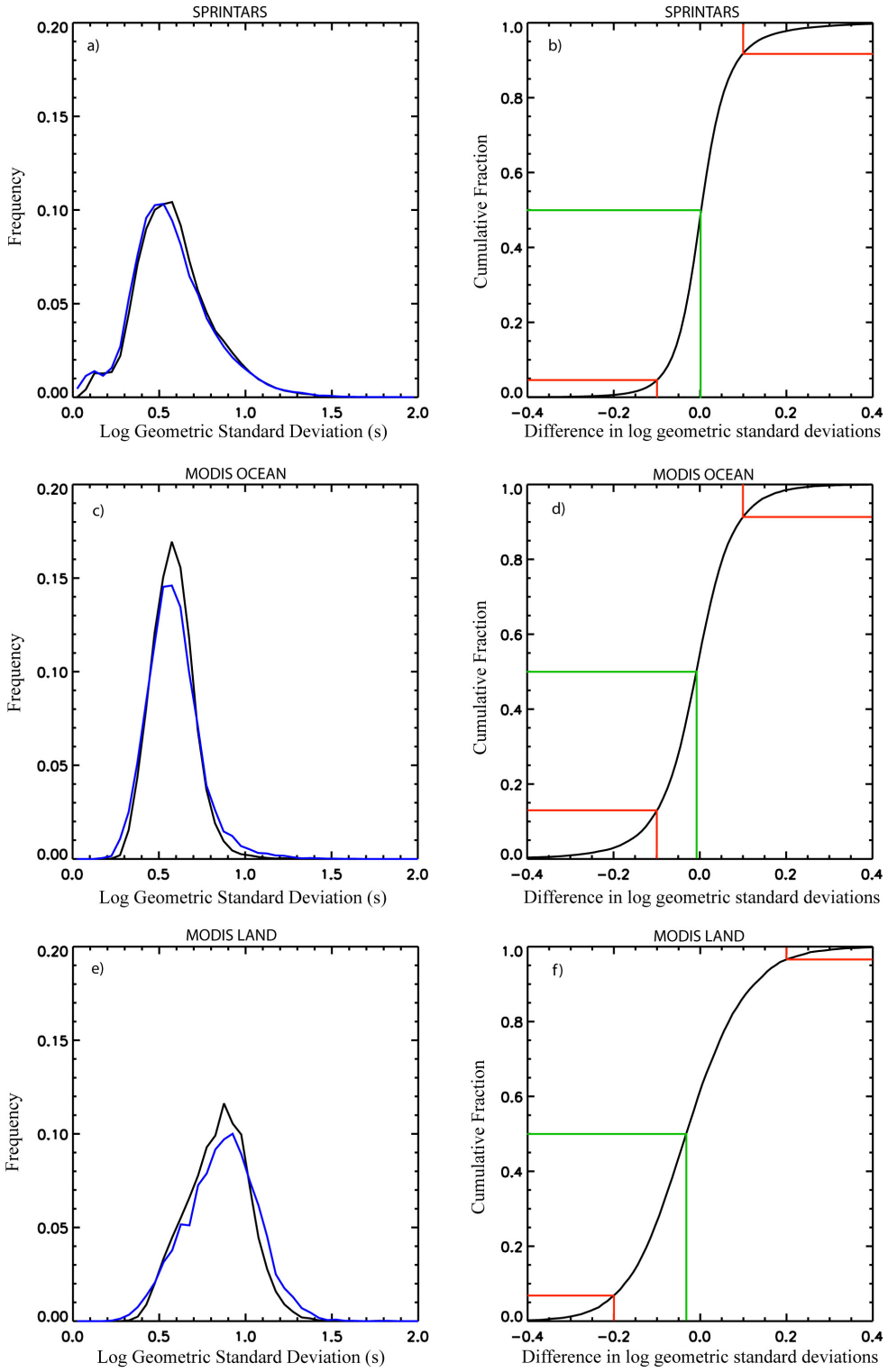

Figure F7. (a, c, e) Comparisons of complete (black curve) and sub-sampled (blue curve) log geometric standard deviation of the AOT probability distributions. (b, d, f) Cumulative histograms of the differences between the complete and sub-sampled log geometric standard deviations of the AOT. Green lines indicate any biases in the median values while the red lines are construction lines to indicate what the factional coverage is for a confidence interval of ±0.1 (b, d) or ±0.2 (f) and whether the confidence interval is symmetric.

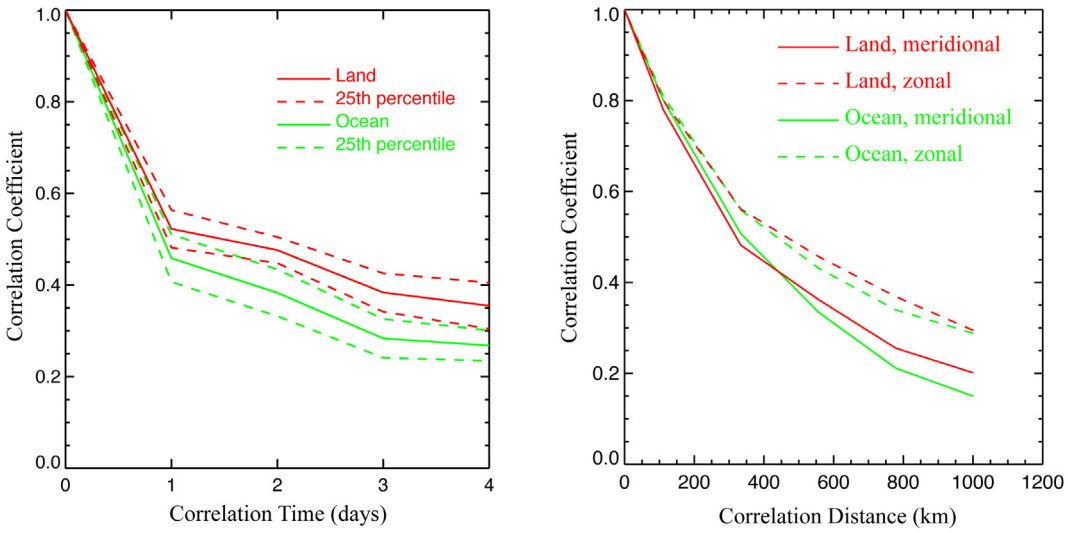

Figure F8. Global average temporal and spatial correlation functions for the MODIS Terra AOT field for land only (red) and MODIS ocean only (green). The 50% confidence interval for this function is indicated by dashed lines of the appropriate color for each surface type.

The long correlation lengths associated with errors that have a high AOT mean that the ~100 observations for a CALIPSO ground track crossing of a grid box of ~1000 km size in reality only yield 1–2 independent measurements. The number of independent measurements acquired over a month will therefore be ~25 (13 days × 2 spatial samples), which limits the reduction in sampling uncertainties and is the reason for the poorer performance of the sub-sample at higher AOTs. Indeed, even the 1350 km wide MODIS sample is only providing ~120 (30 days × 4 spatial samples) independent measurements for a 10° grid box if the correlation length is ~500 km which is not uncommon in the tropics. Since sampling uncertainties are reduced by the square root of the number of independent samples the sampling uncertainty for a single MODIS instrument observing the Saharan dust plume is therefore half that of the APS-2 sub-sample for a 10°×10° monthly mean average.

In summary, based on this analysis we expect that large-scale (10°×10°) long-term (monthly-mean) averages provided by an APS-2 sensor will be affected by random sampling errors at a level that is substantially less than the bias errors caused by calibration errors. These bias errors are themselves substantially less than the cited uncertainties in AOT retrievals from sensors that are currently on orbit and moreover the purpose of APS-2 is to provide measurements of aerosols that are far more informative than the AOT alone.

Appendix G
Glossary of acronyms

3D	three-dimensional
AAC	aerosols above clouds
AATS	Ames Airborne Tracking Sunphotometer (http://geo.arc.nasa.gov/sgg/AATS-website)

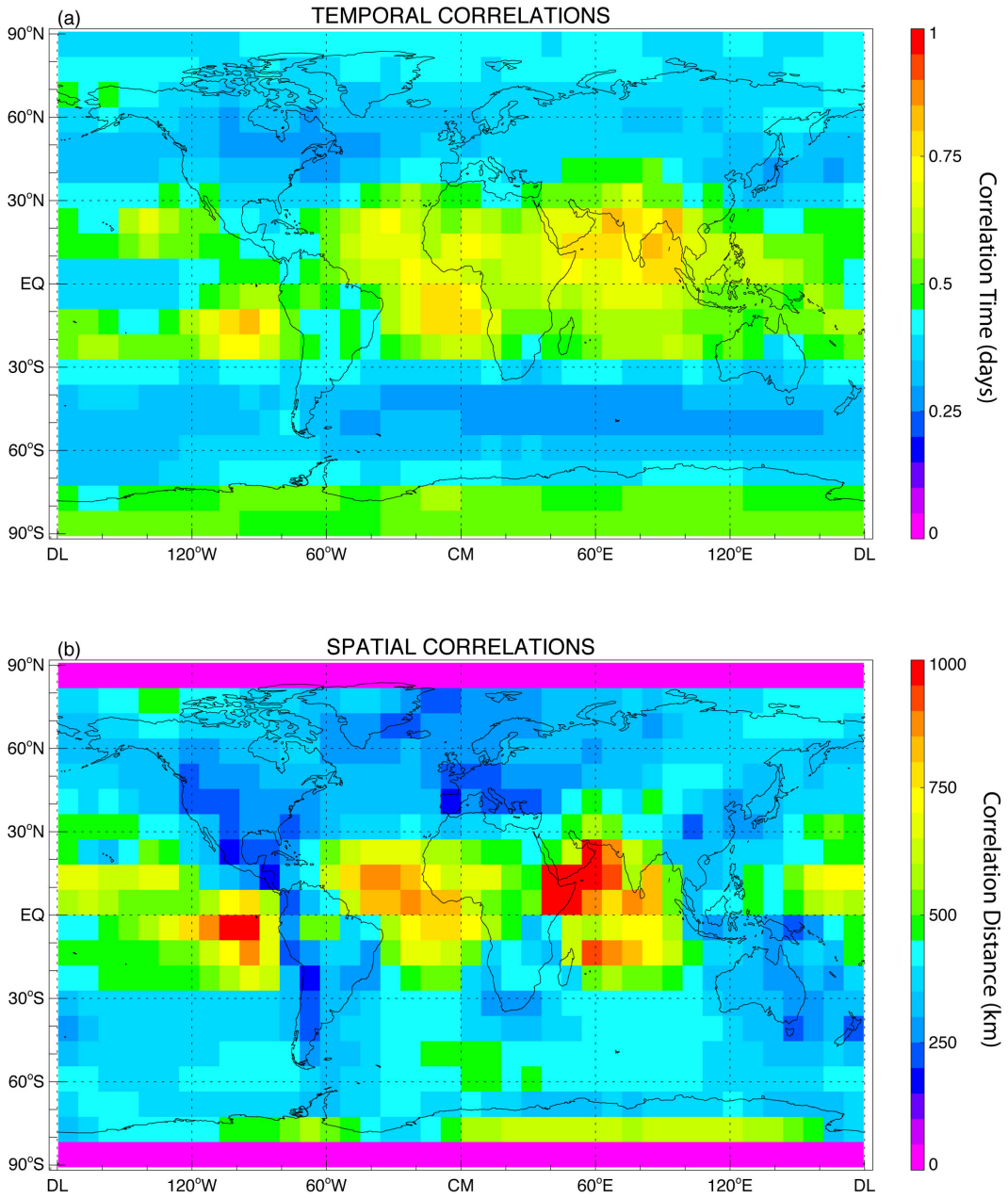

Figure F9. (a) Global distribution of the median time at which the temporal correlation is reduced to 0.7 calculated from the SRINTARS native resolution (1.125° resolution, daily) AOT field. (b) As in (a) but for the RMS distance at which the correlation is reduced to 0.7.

ACE	Aerosol–Cloud–Ecosystems Decadal Survey Mission (http://dsm.gsfc.nasa.gov/ace/index.html)
AERONET	AErosol RObotic NETwork (http://aeronet.gsfc.nasa.gov)
AIRS	Atmospheric InfraRed Sounder (http://airs.jpl.nasa.gov)
ALIVE	Aerosol Lidar Validation Experiment
AMBRALS	Algorithm for Modeling[MODIS] Bidirectional Reflectance Anisotropies of the Land Surface

AOT	aerosol optical thickness
APS	Aerosol Polarimetry Sensor (http://glory.giss.nasa.gov/aps)
ARCTAS	Arctic Research of the Composition of the Troposphere from Aircraft and Satellites
AVHRR	Advanced Very High Resolution Radiometer
BRDF	bidirectional reflectance distribution function
CALIOP	Cloud–Aerosol LIdar with Orthogonal Polarisation
CALIPSO	Cloud–AerosoL and Infrared Pathfinder Satellite Observation
CCN	cloud condensation nuclei
CDOM	colored dissolved organic matter
CIRPAS	Center for Interdisciplinary Remotely Piloted Aircraft Studies
CLAMS	Chesapeake Lighthouse Airborne Measurements for Satellites
CNES	Centre National d'Etudes Spaciales (http://www.cnes.fr)
CPI	cloud particle imager
CrIS	Cross-track Infrared Sounder (http://jointmission.gsfc.nasa.gov/cris.html)
CRM	cloud-resolving model
CSTRIPE	Coastal STRatocumulus Imposed Perturbation Experiment
DARF	direct aerosol radiative forcing
DoLP	degree of linear polarization
ESA	European Space Agency (http://www.esa.int/esaCP/index.html)
FSSP	Forward Scattering Spectrometer Probe
GCM	General Circulation Model
GHG	greenhouse gas
GLAS	Geoscience Laser Altimeter System
HSRL	High Spectral Resolution Lidar
IFOV	instantaneous field of view
INTEX	Intercontinental Chemical Transport Experiment
IPCC	Intergovernmental Panel on Climate Change
IR	infrared
LES	large-eddy simulations
MILAGRO	Megacity Initiative: Local And Global Research Observations
MISR	Multi-angle Imaging SpectroRadiometer (http://www-misr.jpl.nasa.gov)
MODIS	MODerate resolution Imaging Spectroradiometer (http://modis.gsfc.nasa.gov)
MYSTIC	Monte Carlo code for the phYSically correct Tracing of photons In Cloudy atmospheres
NASA	National Aeronautics and Space Administration (http://www.nasa.gov)
NIST	National Institute of Standards and Technology (http://www.nist.gov)
NOAA	National Oceanic and Atmospheric Administration (http://www.noaa.gov)
NPP	NPOESS Preparatory Project (http://jointmission.gsfc.nasa.gov)
OMI	Ozone Monitoring Instrument
PARASOL	Polarization and Anisotropy of Reflectances for Atmospheric Sciences coupled with Observations from a Lidar (http://smsc.cnes.fr/PARASOL)
POLDER	POLarization and Directionality of the Earth's Reflectances instrument
RACORO	Routine ARM Aerial Facility (AAF) Clouds with Low Liquid Water Depths (CLOWD) Optical Radiative Observations (field campaign)

RICO	Rain In Cumulus over the Ocean project
RSP	Research Scanning Polarimeter (http://data.giss.nasa.gov/rsp_air)
SCIAMACHY	SCanning Imaging Absorption spectroMeter for Atmospheric ChartograpHY
SGP	Southern Great Plains
SPRINTARS	Spectral Radiation-Transport Model for Aerosol Species
SSA	single-scattering albedo
SSFR	Solar Spectral Flux Radiometer
SWIR	short-wave infrared
TES	Tropospheric Emission Spectrometer (http://tes.jpl.nasa.gov)
TOMS	Total Ozone Mapping Spectrometer
TROPOMI	TROPOspheric Monitoring Instrument (http://www.tropomi.eu/TROPOMI/me.html)
UV	ultraviolet
VIIRS	Visible Infrared Imaging Radiometer Suite (http://jointmission.gsfc.nasa.gov/viirs.html)
VNIR	visible and near-infrared